Prediction of specific psychiatric symptoms based on electrophysiological measurements in an animal model

(Vorhersage spezifischer psychiatrischer Symptome auf Grundlage elektrophysiologischer Messungen im Tiermodell)

Inaugural-Dissertation
to obtain the academic degree
Doctor rerum naturalium (Dr. rer. nat.)
submitted to the Department of Biology, Chemistry and Pharmacy
of Freie Universität Berlin
by
Cristian Alexandru Tătărău
2019

Die Arbeit wurde angefertigt im Zeitraum 2015-2018 unter der Leitung von Prof. Dr. Christine Winter an der Charité Berlin.

1. Gutachter: Prof. Dr. Christine Winter

2. Gutachter: Prof. Dr. Mathias Wernet

Disputation am 11.7.2019

CONTENTS

LIST OF FIGURES

LIST OF TABLES

ABSTRACT

The dopaminergic system modulates motor control, motivational and cognitive functions. Its dysfunction is related to many neuropsychiatric conditions, among them Tourette's syndrome, Parkinsonism and other tic and movement disorders. One regulatory element in the dopaminergic action chain is the dopamine transporter, whose role in repetitive motor disease has until now remained obscure. This study is focused on a mutant overexpressing the dopamine transporter (DAT-transgenic (DAT-tg) rat), which is showing easy to induce stereotypic movements. Its electrophysiological characteristics are being studied here. Non invasive electric brain stimulation methods have been recently on the rise as therapy for tic disorders, being able to modulate brain activity without the risks of invasive brain surgery. The exact working mechanisms are still under inquiry, but therapeutic results are encouraging. This work reveals, for the first time, how transcranial direct current stimulation (tDCS) is affecting functional connectivity in electrophysiologically recorded rat local field potentials, in both the nonmanipulated wild-type animal as well as in DAT-tg. The findings are that (i) DAT-tg electrophysiologic activity is less adaptive than in wild-types (ii) the caudate putamen is linked to motor stereotypy, (iii) functional connectivity is reduced in DAT-tg, (iv) tDCS is affecting the centromedian/parafascicular complex in both genotypes and (v) tDCS is affecting functional connectivity of the centromedian/parafascicular complex in a genotype dependent way.

ÜBERSICHT

Das dopaminerge System moduliert motorische Funktionen, Motivation sowie Kognition. Dysfunktionen sind mit vielen neuropsychiatrischen Erkrankungen verbunden, wie Tourette Syndrom, Parkinson-Syndrom und anderen Motor- und Ticstörungen. Der Dopamin Transporter ist ein Element des dopaminergen Systems, dessen Rolle in Ticstörungen bisher wenig untersucht wurde. Vorliegende Arbeit befasst sich mit einer Dopamintransporter überexprimierenden Mutante (DAT-tg Ratte), welche leicht induzierbare Stereotypien zeigt. Hier werden ihre elektrophysiologischen Charakteristiken untersucht. In den letzten Jahren wurde nicht-invasive elektrische Hirnstimulation (tDCS) immer interessanter für die klinische Anwendung, wegen ihrer neuromodulatorischen Wirkung ohne die Risiken eines operativen Eingriffes ins Gehirn. Die genauen Wirkmechanismen sind zum Teil noch unbekannt, aber therapeutische Ergebnisse erwecken bereits Hoffnung. Die vorliegende Studie zeigt zum ersten Mal mit elektrophysiologischen Mitteln, wie tDCS die funktionelle Konnektivität beeinflußt, sowohl im nicht manipulierten Wildtyp Tier, als auch in DAT-tg. Die Ergebnisse deuten darauf hin, dass (i) DAT-tg weniger Adaptation der elektrischen Feldpotentiale zeigt, (ii) ein Zusammenhang besteht zwischen Caudate Putamen und motorischen Stereotypien, (iii) die funktionelle Konnektivität in DAT-tg reduziert ist, (iv) tDCS in beiden Genotypen auf den centromedialen Kernkomplex wirkt, (v) tDCS im centromedialen Kernkomplex eine Genotyp-spezifische Wirkung hat.

1 INTRODUCTION

Dysfunctions of the basal ganglia and of the dopaminergic signaling system are currently thought to be involved in various motor disorders, such as Parkinson's and Tourette's syndrome (TS). The comorbidities found in TS patients suggest that this disorder might share a common pathophysiology with the obsessive-compulsive (OCD) and attention-deficit hyperactivity disorder (ADHD) [1] [2].

Tic disorders are characterized by "sudden, rapid, recurrent, nonrhythmic motor movement or vocalization" [3]. Tics are involuntary events, but patients are able to suppress them for brief periods of time. Additionally, patients may have a premonitory sensation (premonitory urge) which foreshadows tic onset [1]. These premonitory urges are experienced by the majority of patients and are described as intrusive feelings, driving the patient towards the execution of the movement or vocalization, which brings relief once performed [4].

Tics can be classified as simple and complex, both lacking a purpose. Simple tics are brief, complex tics are more prolonged and may be coordinated sequences or combinations of simple tics. This can result in facial or body contortions, clapping or hopping and also include verbal tics. [5] [3].

Some factors allow a prognosis of tic severity and give hints about its pathophysiology. Stress, excitement, anxiety and exhaustion worsen, while focused activities reduce tic severity. Observing specific gestures or sounds in other people can trigger tics. Common comorbidities are ADHD and OCD [3]. While evidence for genetic inheritance has been identified, a clear pattern of transmission remains dim [1].

THE ROLE OF DOPAMINE IN PSYCHIATRIC DISORDERS

Current research in TS, and generally in repetitive disorders, focuses on the neurotransmitter dopamine. The main anatom-

ical hypotheses involve the cortical - basal ganglia - thalamo - cortical loop (CBGTC).

TS can be treated pharmacologically by using dopamine antagonists like risperidon or haloperidol, with good results [5] [6]. An alternative medication are $\alpha 2$ adrenergic agonists like clonidine, which has less severe side effects than antipsychotics (dopamine antagonists) [7], which cause other motor dysfunctions (dyskinesia). Conversely, amphetamine and other stimulants, which increase the synaptic release of dopamine, are worsening tics in TS patients [7]. This is a strong evidence for a dopaminergic involvement in repetitive symptoms.

Another evidence is the role of D_1 and D_2 receptors in the transition from goal-directed to habitual behaviors, to which tics belong [6]. Exposure to amphetamine results in faster habit formation. This effect is reversed by D_1 receptor antagonists and enhanced by D_2 receptor antagonists [8], which are discussed as potential mechanisms for pathophysiology.

Given this clear effect of dopaminergic antagonists and amphetamine, it is intriguing that l-dopa reduces motor tic severity, while being known to increase dopaminergic signaling [9]. Similarly intriguing is that atypical antipsychotics such as risperidone are found to induce OCD symptoms in patients which did not show them before treatment (de novo emergence) [10]. We can therefore conclude that repetitive symptoms cannot be explained by an unidimensional high or low level of dopamine. A more elaborate model is needed.

The hypothesis of tonic-phasic imbalance

The hypothesis of the tonic-phasic imbalance proposes that the dopaminergic system can process two types of signals: a fast, phasic one, and a slow and spatially diffuse one. The phasic signal is limited to the synapse and occurs on synaptic transmission. For example, bursting dopaminergic neurons can provide a fast response to rewarding events on a short time scale, providing feedback information about the outcome of an action and therefore regulating behavior. The tonic signal is mediated by dopamine leaking into extrasynaptic space and affecting a larger number of neighboring neurons. Its concentration changes slower than the phasic signal and is about an order of magnitude lower than during a synaptic phasic event. Its role is assumed to be mediating the reactivity, motivation or

preparedness of the organism. A reduced tonic concentration leads to a lower dopamine autoreceptor feedback at the presynapse, which in turn results into an overstimulation on phasic events [11] [12] [13]. This model has been proposed as potential TS pathology [14] [1] [5]. One mechanism is supposed to be an overexpression of the dopamine transporter (DAT). A metaanalysis found that 6 out of 12 studies report an increased DAT level in TS patients as compared to healthy controls [15]. We can therefore assume that DAT plays a role in TS pathophysiology, even if other factors may also be relevant.

The hyperinnervation hypothesis

Several other competing theories regarding the pathophysiology of repetitive disorders are currently debated in the scientific community. A notable example is the hypothesis of dopaminergic hyperinnervation. It postulates an increased number of dopaminergic terminals in the striatum, which causes an increase in both tonic and phasic dopamine. The role of phasic dopamine release is to reinforce behavior by coding a prediction error [16] [17]. Exaggerated phasic release could reinforce in a maladaptive way, helping to translate tics to persistent behavior. This corresponds to the "Go" pathway of the basal ganglia. Tonic dopamine increases the probability of action. Elevated tonic release could therefore raise the probability of expressing previously learned behavior, including maladaptive ones, such as tics. This corresponds to an inhibited "NoGo" pathway. The dopamine receptors D_1 and D_2 are thought to be responsible for these effects [18] [15]. D_1 receptors have a low, D_2 receptors a high affinity to dopamine. The classical understanding is that D_1R is excitatory and D_2R is inhibitory [19].

Manipulating the dopamine transporter

DAT regulates the removal of dopamine from the synaptic gap [20]. Its density is dynamic, as DAT can be internalized, in a process which is dependent on the membrane potential. Membrane depolarisation leads to a reduction of DAT levels [21].

A nearby experimental approach is therefore to over- or down-regulate DAT. A mouse with DAT KD (knock-down) mutation was created and it shows an opposite behavior as observed in

DAT-tg. The DAT KD mouse exhibits excessive sequential stereotypy (super-stereotypy) in which sequences of behavioral patterns are hard to interrupt and get increasingly rigid. After disruption, the animals return to the place in the syntactic grooming chain where they were interrupted [22]. Super-stereotypy is indeed found in TS and OCD, but resembles only partly to simple or complex tics because super-stereotypy does serve a purpose and because it consists of a large number of distinct movements which are combined into phases to form the pattern. This is different from the most complex tics observed in TS. In DAT-tg, the stereotypy consists of short episodes and broken and restarted chains of grooming (personal observations). Anyway, the tic expression can take multiple forms, from simple to complex, vocal tics may or may not be prevalent, comorbidities can or cannot occur. The repetitive phenotype is very different in both DAT models discussed in this paragraph, and the scientific debate over the similarity to TS tics goes on.

Conversely, DAT overexpression leads to stronger amphetamine-induced learning and to a weaker responsiveness to natural rewards [23]. The response to natural rewards is reduced due to the normal dopamine reuptake via DAT. The amphetamine-induced dopamine release occurs through DAT reverse transport (additionally to vesicular release), a higher DAT expression leading therefore to a higher release [24].

Therefore, manipulation of DAT is a valuable tool for the dissection of the dopaminergic system.

THE DAT TRANSGENIC MODEL

Based on the tonic-phasic imbalance hypothesis and on the lack of data about the behavioral relevance of DAT, the lab created the DAT-tg rat model. A useful animal model needs to be valid with respect to phenotype, pathologic model and therapy.

DAT-tg was created by pronuclear microinjection of the DAT gene, leading to overexpression of the DAT protein. After injection of 2.0 mg/kg body weight of amphetamine, DAT-tg rats show stereotypic behavior emerging at 80 - 120 min later. At this amphetamine concentration, wild-type (wt) shows increased locomotion but no stereotypy. wt rats are exhibiting stereotypy only at a higher concentration of around 5 mg/kg [25] to 6 mg/kg [26] amphetamine. The effects of clonidine and fluox-

etine on DAT-tg strengthen the links to TS. Clonidine, used as TS medication in humans, reduces stereotypy, while fluoxetine, used in OCD patients, does not [27].

One relevant characteristic of the DAT-tg for this study is the amphetamine induced stereotypy. However, the model shows several other distinctive traits. In the morris water maze, DAT-tg rats do not use effective spatial search strategies, while wt rats are using hippocampus dependent egocentric and allocentric search. In the discrimination reversal test, DAT-tg need more trials and some animals are not able to complete the task. Those which complete the task are learning the reversal just as wt rats do. Locomotor and exploratory activity are reduced in DAT-tg in the radial maze with food reward and in open field tests [28]. This results are in line with previous findings about anhedonia [27]. Furthermore, they show learning deficits and very simple and stereotypic search strategies [28].

The overexpression of DAT leads to a state which corresponds to the previously described tonic/phasic imbalance. Even considering that the mutant exhibits tics only after pharmacologic induction, the manipulation of the baseline, steady-state dopamine concentration makes the DAT-tg rat an useful model for the exploration of dopamine dependent behavior.

NON-INVASIVE BRAIN STIMULATION

Transcranial direct current stimulation is the application of a constant current non invasevly to the brain. The risks for the patient are heavily reduced as compared to deep brain stimulation, where an electrode is placed within deep brain nuclei. Common risks of this surgical intervention are inflammation and damage of blood vessels, which leads to irreversible damage of neurons. Transcranial Direct Current Stimulation (tDCS) is applied over the cortex and acts through the skull. This chapter will summarize theories about action mechanisms and the potentially useful clinical effects of tDCS.

There is evidence for a network-wide effect of tDCS, which means that cortical stimulation affects distal nuclei which are functionally connected to the stimulated cortical area. Until now, this effect has been studied mostly via EEG and imaging methods. Another intriguing and useful property of tDCS is

that its effect lasts significantly longer than the actual electric stimulation duration.

The terminology widely used is: positive current is entering the body through the anode, positive current is exiting the body through the cathode. The membrane polarization is subthreshold, i.e. it does not lead to action potential generation. The typical field strength is around 1 V/m. The polarization of a membrane segment depends on field magnitude and the tissue specific coupling constant: $V_{tm} = G * E$ where V_{tm} is the polarization, E the field magnitude and G the coupling strength [29].

Physiologic effects

Electric fields polarize the cell membrane during exposure due to the presence of ionic charges. Given that membrane potential is maintained by unequal distribution of ions, any additional electric field will interact with this polarization, and shift the electrochemical equilibrium of ion concentration. Given the constance of charge within closed spaces (as charge does not disappear), a part of the membrane will be slightly hyperpolarized, while another part will be slightly depolarized with respect to the initial state. Being a closed space, cells will show, depending on their shape and the spatial orientation of the somatodendritic axis within the field, a polarization gradient, i.e. the soma might have an opposed polarization than the dendritic tree. A radial constant electric field created by a positively charged electrode on the apical side for instance, will hyperpolarize apical dendrites and depolarize the soma in cortical neurons [30]. Polarisation occurs both in intra- and extracellular spaces.

Although stimulation clearly affects neural functioning, it is hard to predict its effects. One reason lies in the many places of action and the little control we have over many properties of tissue. The consequence is that a hypothesis based approach does not always show the expected results and therefore, the clinical effect often has to studied in a trial-and-error way.

Electric stimulation modulates several compartments of the cell, from synapse to soma, axon and axon terminal. Its effect is a possibly nonlinear combination of all this effects [30] [29]. Until now, prediction or exhaustive simulation have therefore proved to be difficult [29].

The stimulation effects are very diverse and last longer than the effective stimulation interval. The mechanisms involved are spanning a large range: non-neuronal like glial cells [31], blood-brain barrier function, action potential thresholding and timing, network level activity, plasticity changes, morphologic and molecular changes [29].

Several distinct effects can be discussed: immediate, during stimulation and long lasting effects, after stimulation ceases.

During stimulation, only a low, sub-threshold shift in membrane polarisation occurs. While this effect cannot explain large amplitude changes in neural activity, it can nevertheless cause significant shifts in spike timing. Assuming that the variable sub-threshold potential is close to the threshold in the active cell state (not to be confounded with the activated state during anesthesia), any potential shift up or down will lead to earlier or later threshold crossing, changing significantly the timing and probability of firing and by this, allowing for precise temporal modulation [32] [33].

The stimulation effects are lasting even after ceasing the stimulation. In one study, tDCS modulated the excitability of the motor system when applied over the motor cortex. The excitability is proportional to the magnitude of motor-evoked potentials after transcranial magnetic stimulation of the correspondent part of the motor "homunculus". Anodal stimulation increased, while cathodal stimulation decreased excitability [34].

The synapse is also affected by tDCS [35] [36]. Anodal stimulation increased a form of long-term potentiation (LTP) when seconded by low frequency synaptic activation. Usually, LTP can be induced in brain slice by high frequency stimulation or by simultaneous presynaptic stimulation and postsynaptic depolarization. The tDCS induced LTP mechanism seems to be of different nature but is still lacking a description [36].

On the network level, weak electric fields can interfere with endogenous fields [37] [38] and also change, as shown before, spike timing. Small changes in excitability, and thus in firing rate, can propagate and amplify in a network as a result of positive feedback loops [39] [40]. We can therefore expect tDCS effects in deep nuclei, otherwise little or not directly affected by the applied electric field.

The axon orientation and action potential propagation direction determine in certain geometries, whether the tDCS effect is inhibitory or excitatory. Transmission of action potentials com-

ing from opposite directions are modulated in opposite ways by an external field when its vector is parallel to the axon direction [41].

Finally, synaptic terminals (presynapse) can be affected by tDCS, even if the direction of the applied tDCS field is tangential and thus not expected to produce somatic polarization [29].

As of 2018, no other study dealt with the functional connectivity after tDCS by using invasively measured local field potential (LFP) signals. This study aims to be the first to elucidate tDCS effects on LFPs of deep nuclei and the motor cortex.

CLINICAL RESULTS

Human studies

This section summarizes evidence for the involvement of deep brain regions in TS. Deep brain stimulation allows to measure brain activity from patients via the implanted stimulation electrodes. Such studies are not possible in healthy humans.

The main deep brain stimulation (DBS) targets for TS in humans are globus pallidus pars interna (GPi, corresponds to entopeduncular nucleus (EP) in rodents) and the thalamus, especially the centro-medial and parafascicular nucleus of the thalamus [42] [43] [44] [45] [46] [47] [48]. During and after electrode implantation, both LFP and single unit measurements are possible, allowing to compare previous recordings in humans with results from our animal model. Several studies come to the conclusion that the LFP power spectrum is shifted towards low frequencies (theta and alpha waves) in the centro-medial parafascicular nucleus (cmPF) of TS patients and other hyperkinetic disorders [46] [49] [50]. Anyway, the human intracranial recordings performed in [46] or [45], while offering unique insights in human pathophysiology, are less suitable for predictions because data from healthy controls does not exist.

The thalamo-cortical connection plays a role in the pathophysiology of tics. In humans with implanted deep brain stimulation electrodes, coherent activity between this regions preceded tics by 800 to 1500 ms and coherency vanished after tic onset [42]. Also, single unit firing in human EP is correlated to tics [51].

Other studies on TS on functional imaging data find enhanced connectivity of striatum and thalamus with sensorymotor cortex [52] and between basal ganglia and primary motor cortex [53].

Cortical stimulation affects deep regions

Imaging studies found that tDCS over cortical areas modulates deep brain regions [58] [59] [60]. Regarding the stimulation polarity (anodal or cathodal), this results are not consistent, showing that the exact action mechanisms are yet to be illuminated, as sometimes anodal and sometimes cathodal stimulation are providing a measurable effect.

In TS, there are reports about the therapeutic effect of cathodal tDCS over motor and supplementary motor areas, with only a part of patients responding to the treatment. Just as the cellular effect, the clinical effect remains hard to predict, yet it is undeniable [61]. Other studies in healthy test persons are showing that anodal tDCS over the primary motor cortex in humans increases the connectivity between thalamus and ipsilateral primary motor cortex [62].

Electrophysiological clinical markers

The beta frequency range has been found to be related to symptom severity in Parkinson's as well as in TS disorder. In Parkinson's, synchronization between cortex and deep nuclei is inversely correlated to bradykinesia and rigidity severity. Dopaminergic treatment suppresses mostly the lower beta band oscillation [63] [64]. In TS patients, decreased thalamic beta oscillations are supposed to contribute to the tic pathophysiology [46].

During spontaneous tics in TS patients, [55] found changes in connectivity between primary motor cortex and putamen. The primary motor cortex showed a decreased activity during motor tasks and also a decreased co-activation between primary motor cortex and other distributed brain areas [56]. During active suppression of tics, undirected coherence between several cortical areas was increased in TS patients as compared to controls. This shows that coherence is rather an adaptive response and not a clinical TS marker. Due to the EEG paradigm, only cortical areas were tested [57].

Animal studies

Brain stimulation triggers a change in neurotransmitter levels, which lasts long after the end of the stimulation. When stimulating a large prefrontal area, one study found tDCS to increase the extracellular dopamine level of caudate putamen (cPu) tissue, but not the serotonine [65]. Similar experiments performed in our research group however, did not find similar effects, neither in wt nor in DAT-tg [66].

During active states, connectivity was found to be stronger around 20Hz and 50Hz. The frontal cortex, recorded by electrocorticogram, had mostly outward functional connectivity and less inward connections from the basal ganglia. [67]. This findings are another starting point of this study.

AIMS OF THIS STUDY

Here, we study electrophysiological characteristics of the DAT-tg in several settings. The first setting is the natural state without pharmacological treatment. The second one is the stereotypy interval, induced by low doses of amphetamine. The third one is the effect of transcranial electric stimulation. We are also exploring the genotype specific effect of electric stimulation.

The specific goals are: (i) to characterize the power spectrum of relevant nuclei in DAT-tg during baseline and (ii) during the stereotypy interval, (iii) to find markers of stereotypy and compare them to existent findings from human patients, (iv) to find an electrophysiological correlate of the known effect of tDCS treatment on reducing stereotypy.

2 METHODS

HARDWARE AND SURGERY

This study consists of three experiments. Surgery and measurement in Experiment 1 were performed by the lab colleagues Dr. Yoseph Avchalumov, Mareike Anka Voget and Henriette Edemann Callesen. Analysis was performed by the author of this thesis. Experiments 2 and 3 were done entirely by the author of this thesis.

Recording system

Electrophysiological recordings for experiments 2 and 3 were performed using the RHD2000 recording system from Intantech (Los Angeles, California, USA) with an aqcuisition board from the OpenEphys community and the OpenEphys GUI recording software [68]. The headstage was the RHD2132, a 32 channel monopolar amplifier chip.

The Intantech recording device is different in several respects from classical systems which are better rooted in the electrophysiology community. The most noteworthy innovation is that all relevant circuitry is embedded onto the headstage chip. Analogous low-pass and high-pass filters, an additional high-pass digital signal processing (DSP) filter, multiplexer and digital to analog converter (DAC) are on-chip, along with other elements like protective circuitry. The output of this amplifier chip is therefore already digitized. The acquisition board is the interface between one or more headstages and a PC. Its heart consists of a field programmable gate array (FPGA) board which reads data from the headstages, processes it and sends it via USB to a PC.

The filters have the following characteristics: the analog low-pass filter is a 3rd order Butterworth filter with an attenuation of 18 dB/octave, the analog high-pass filter is a 1st order Butterworth filter with an attenuation of 6 dB/octave, the optional DSP is set to 1st order high-pass infinite impulse response (IIR)

filter for additional direct current (DC) offset removal. The cut-off frequencies are set via software to 0.1 Hz and 500 Hz. The amplifier gain is 192 and is constant, acquisition rate is 2 kHz. The alternating current (AC) input voltage range is ± 5 mV with an input noise level of ±2,5 µV [69]. The DC component is discarded by the built-in high-pass filter, as this is customary in most current electrophysiological research. Anyway, this very slow component might be also informative in understanding the field potentials. When filtered out, a given polarity arising from sustained activity is lost and reduced to baseline, also transients can produce spurious correlations with other measured activity [70].

Given the limited input voltage, the Intantech RHD2000 amplifier hardware is only appropriate for extracellular measurements. The lightweight chip can be used for both anesthesia and freely moving paradigms with a high number of recording channels. [71] has already shown a high-density recording in the freely moving rat with up to 512 LFP and single unit channels.

Experiment 1 was performed with an Omniplex (Plexon, TX, USA) recording system, data was bandpass filtered (0.05 to 350 Hz), amplified (1750×) and sampled at 1 kHz.

Electrodes

This section gives an overview on electrode types which have been under consideration before deciding which one is most appropriate for the given task. The criteria are use case (LFP or single units or both), reusability, ease of use, price, size and similarity to electrodes for human usage. The last criterion is particularly important in the lab's context of translational research.

Pure LFP electrodes are usually the easiest to build and handle. Their impedance (measured at 1 kHz) is usually well below 500 kΩ. With a higher impedance at around 500 kΩ it is possible to also measure multiunit activity. This electrodes can measure several single units situated close to the electrode tip, but the signal to noise ratio does not allow identification of individual units.

The Microprobes (Gaithersburg, Maryland, USA) CEA 200 electrode consists of a single wire core with a second outer concentric electrode. The impedance of the inner electrode at 1kHz

is around 50 kΩ, the impedance of the outer electrode is lower due to larger size, but is not specified by the producer. This electrode is suitable for LFP recordings. The great advantage is the presence of the additional concentric electrode which is similar to the circular electrodes used in human brain stimulation devices. This would allow a better comparison of data from animal studies with data recorded from human patients via stimulation electrodes, either intra-operatively or in longitudinal studies. Anyway, this electrode is with a diameter of 0.4 to 0.5 mm very large and might damage much tissue in rodents.

Silicon probes are thin rigid printed silicon boards which allow a wide range of geometries, from tetrode-like to 1D or 2D shapes. They can record both LFP and single units. When used in awake animals, they need to be mounted on microdrives for depth adjustment. If cemented, it is possible that neurons in immediate proximity get damaged and no single unit signal will be recorded. This electrode type is expensive (600$ for a 16 channel linear probe from Cambridge Neurotec, as of 2017) and easy to break. It is reusable only in anesthetized or head fixed awake measurements. Linear silicon probes can be used for spatial mapping of target brain regions along the electrode axis. They can be also used in decoding distributed information within a mapped region. This approach is based on the observation that many brain regions show rhythmicity and sparse coding and that sometimes information is spatially distributed across a region. It has been shown that demodulation of LFP signals from linear silicon probes implanted in rat hippocampus allows decoding the animal's position with a similar accuracy as by using the firing activity of place cells [72].

Thomas Recording GmbH (Giessen, Germany) offers glass coated tetrodes and single electrodes. The glass coating results in similar disadvantages as silicone probes with regard to usability and long-term price. The core diameter of single electrodes is around 25 µm and the outer diameter around 80 µm [1]. They can record both LFP and single units.

FHC Inc. (Bowdoin, Maine, USA) [2] are offering customizable single channel electrodes at competitive prices (around 25 USD per single channel, as of 2017). For 1 MΩ electrodes, the maximal outer diameter is 200 µm while the electrode shape

1 https://www.thomasrecording.com/products/neuroscience-products/microelectrodes.html

2 http://www.fh-co.com/category/metal-microelectrodes

is becoming thinner towards the tip. The 1 MΩ impedance allows LFP and single unit recordings, and it can be assumed that single cell signals are easy to find without extensive search. Electrodes with 2 MΩ impedance allow for a better signal to noise ratio but given the narrower measurement volume, units might need to be searched first and lost easier on setup vibrations (Prof. Dr. Klaus Funke, personal communication, 2017).

The lab decided to use the concentric Microprobes CEA 200 electrodes for all experiments performed in this thesis.

Camera

The cameras are required to be usable for both day and night recordings. Therefore, a large CMOS chip with a higher light sensitive surface is a more important criterion than resolution. The objectives need to be permissive to infrared light, which excludes coated, infrared-reflective lenses. Video and electrophysiological recordings might need to be synchronized in order to link specific behaviors to the corresponding electrophysiological activity. This would allow finding LFP markers during repetitive episodes and predictive markers before onset of repetitive movements. The camera needs therefore input/output pins for acquisition control. For maximal flexibility, it should provide an input pin to trigger frame acquisition and an output pin for reporting frames when used with internal trigger. The OpenEphys acquisition box supports both methods. It has transistor–transistor logic (TTL) input channels which can be recorded along with the physiological signals. In this case, the camera output would change voltage level for each acquired frame. The acquisition box is also able to set an TTL output pin at a desired frequency in order to trigger image acquisition. When selecting the right objective, one of the most important parameters is the depth of field (depth of field (DOF)). The DOF is the range of distances from the objective in which objects are imaged without blur. A narrow DOF means than objects in the focal plane are sharp while the immediate background and foreground are increasingly blurred. The wider the aperture is, the narrower the DOF. During night recordings, we expect to use rather large apertures. The image will be sharp if the circle of confusion is not significantly larger than the size of a pixel on the camera chip. The DOF limits can be calculated depending on the circle of confusion, focal length, aperture and

working distance. Together with lab colleague Carolin Gehr, several night recording sessions have been performed with this camera system.

$$\mathrm{DOF} \approx \frac{2Hs^2}{H^2 - s^2} \text{ for } s < H \tag{2.1}$$

where H is the hyperfocal distance:

$$H = f + \frac{f^2}{Nc} \approx \frac{f^2}{Nc} \tag{2.2}$$

and f the focal length, N the aperture, c the circle of confusion, and s the distance from object to camera lens. The best suited camera is acA1920-40uc from Basler AG (Ahrensburg, Germany) with a LM8HC 8mm objective from KOWA. The DOF corresponds in low light conditions roughly to the width of a rat cage and is enough for tic assessment. After having used the camera, it became clear that a longer focal length would result in slightly better DOF and working distances for our specific use case.

A software for video acquisition and compression had to be developed based on the provided examples in the Pylon library.

Recording procedure

Surgery

The surgery for electrode implantation follows the procedure previously established in the lab [73] [25].

In experiment 1, electrodes are inserted into the medial prefrontal cortex (medial prefrontal cortex (mPFC)), nucleus accumbens (nucleus accumbens (nAcc)), entopeduncular nucleus (EP; corresponding to the globus pallidus internus in primates), caudate putamen (cPu), dorsomedial thalamic nucleus (dorso-medial thalamus (DM)).

In experiments 2 and 3, electrodes are inserted into the motor cortex (motor cortex (mC)), caudate putamen (cPu), entopeduncular nucleus (EP; corresponding to the globus pallidus internus in primates) and centromedial parafascicular nucleus (cmPF) of the thalamus. The following coordinates with respect to bregma were used (in mm): mC : AP = 1.5, ML = 2.7, DV = -1.5; cPu: AP =0.5, ML = 1.8, DV = -5.4; EP: AP= -2.6, ML = 2.6, DV = -7.4; cmPF: AP = -4.1, ML = 1.3, DV = -6.4, according

to [74]. AP = anterio-posterior axis, ML = medio-lateral, DV = dorso-ventral.

The rats are housed in a temperature- and humidity-controlled vivarium with a 12 h light/dark cycle (lights on at 06:00 a.m.). Prior to surgery, rats are anesthetized with 1,2 mg urethane/kg body weight (1,4 mg/kg in experiment 1) (Sigma–Aldrich, Germany) by two intraperitoneal injections, the first delivering 60% of the urethane and the second, which is given 20 to 30 min later, the remaining urethane. Anesthesia depth is assessed by checking reflexes like eyelid reflex and reaction to tail and paw pinch. If necessary, additional urethane is delivered until the desired depth of anesthesia is reached. The surgery starts when the rat is anesthetized at the desired level. The rat is placed in a stereotaxic device model 902 or model 1430 from David Kopf Instruments, California, USA. The head is fixed with ear bars and a teeth holder. After shaving the fur and cutting the skin on top of the head, the remaining tissue is removed with a diluted H_2O_2 solution. The critical step for precise electrode placement is the correct identification of the marker point bregma. Bregma is situated at the intersection of the best fit of the midline and labdoid sutures. The teeth holder is set to $-3{,}3$ mm for most animals.

In some few cases, when rats are much older than the reference group used for constructing the Paxinos and Watson atlas [74], or when the skull shape is more irregular than in other animals and doubts about the correct placement are justified, another method was applied. In these cases, the surface of the skull was scanned, and profile lines were drawn on paper. Scanning was done by moving an electrode and measuring the position of the tip of the electrode when touching the bone. The long axis defined by lambda and bregma gives the rotation angle around the vertical z axis (yaw). The curvature in lateral x direction allows estimating the roll, given the symmetry of the skull. Finally, the pitch is determined, which is the rotation along the interaural (earbar) axis, therefore changing the standard -3.3 mm of the teeth holder [75].

After drilling holes in the skull with a spherical drill, which is slightly blunt in order not to damage the dura mater, electrodes were inserted to the target location. The electrodes were cemented with two-component embedding resin based on methyl methacrylate (Technovit 5071, Heraeus Kulzer GmbH, Wehrheim, Germany).

Correct electrode tip placements were histologically verified, following the procedure previously established in the lab [73] [25].

Experimental timeline

Recordings were conducted over a period between one and three hours for the baseline condition without any pharmacological or stimulation intervention. The baseline recording ends when long enough intervals of stable activated states (AS) were recorded. Typically, this means a minimum of 30 min of stable AS. After baseline, the rats receive an intraperitoneal injection of 2.0 mg/kg body weight of amphetamine dissolved in 0.9% saline at a volume of 1.0 ml/kg (Sigma Aldrich, Germany). Recordings continue until 120 min after injection, including the relevant interval of stereotypic movements shown in awake animals, from 80 to 120 min [27] [66].

A.1 is showing the experimental timeline for all 3 experiments performed in this study.

Transcranial direct current stimulation

If tDCS is applied, an additional wet electrode is mounted. The wet electrode consists of a plastic cylinder filled with saline solution, whose bottom is sealed with instant adhesive and resin. A graphite electrode from the core of a soft pencil is inserted into the saline for tDCS application. A second electrode is applied on the shaved chest with conductive EEG gel. The current is constantly measured with a multimeter and if it drops below the set value, the saline solution needs to be replaced. This effect occurs in saline solutions when NaCl is removed by electrolysis, leading to an increased resistivity. tDCS is delivered by the STG4000 stimulator and the software MC_stimulus II (Multi Channel Systems MCS GmbH, Reutlingen, Germany). The application mode is constant current, anodal stimulation, at 200 µA. The coordinates are (in mm): AP 3.2, ML 1.5.

ANALYSIS

Power spectral analysis

The frequency spectrum was divided into seven bands: 0.4-4 Hz delta, 4-8 Hz theta, 8-15 Hz mu (or alpha), 15-20 Hz lower beta, 20-35 Hz higher beta, 35-48 Hz lower gamma. Power spectra were normalized to total power of the 1 Hz to 100 Hz range for the group comparisons. The comparison of genotypes requires normalization on total signal power due to the measurement in distinct animals. The longitudinal statistics was performed without normalization. For the analysis of power spectral density we used the Welch stFT (short time Fourier transform), 8192 data point windows corresponding to roughly 4 s, linear detrending, Hanning windowing, 50% overlap.

Detection of activated states

Brain activity in this experiments was recorded during "cortical activation" under urethane anesthesia. This activated states are activity patterns which resemble those measured during awake states, as opposed to the slow wave states which resemble deep sleep [76] [77]. We determined the stages of anesthesia by using the stages found in [78]. The most common way of detecting AS is by determining the maximal power of the slow wave states (SW) and defining AS when the power in the SW band falls by at least 70%. The SW frequency band mostly observed is around 1Hz. In rodents, several studies are using 0.4Hz - 1.6Hz [77], 0.5Hz - 1.5Hz [79], around 1Hz and around 4Hz for AS in a metastudy [80], around 1Hz [81], 0.2Hz - 1.2Hz and 3Hz-4Hz for AS [82]. [83] attempted an automation of AS detection by training a linear support vector machine on data labeled by several independent raters. In this study, global activation was elicited by pinching the tail or hindpaw with a forceps, if it did not occur spontaneously, as described in [84].

We developed a method for semi-automatic AS detection. Our method of state classification takes into account both power change in the SW frequency band as well as the spectral characteristics of the different cortical states. The AS detection consists in several steps, as follows: First, we plot the short time Fourier transform (Welch method stFT, 8192 data point windows corresponding to roughly 4 s, linear detrending, Hanning window-

ing, 50% overlap) and plot the spectrogram for all frequencies between 0.1 and 10 Hz. Using the raw signal shape and the spectrogram, we manually define a slow wave (SW) reference period for each animal. The spectrogram renders visible the different spectral characteristics of SW, AS and mixed states. Typical SW intervals show a maximum power in the frequency band below 1.6 Hz and a smooth power decay towards the higher frequencies. Typical AS show a generally lower signal power and several clearly defined oscillation peaks above the 1.6 Hz. The power ratio of the SW band for each stFT window with respect to the reference SW is plotted beneath the spectrogram. The transitions from one state to another are visible as steep parts of this curve. Within one cortical state, the curve remains roughly on a constant level. Following this step, we define a threshold for SW power. Signal intervals showing lower SW power than this threshold are marked as AS. The threshold is set initially to 0.25 and adapted manually in such a way that we optimize the segregation of states. If the SW reference interval shows in time domain a superposition of slow (f $\leqslant$1.6 Hz) and fast (1.6 Hz $<$ f $\leqslant$ 3 Hz) oscillations, we can assume a mixed state and it is reasonable to select a higher threshold than 0.25.

The AS detection algorithm is running over the entire recording, which contains both baseline and amphetamine conditions. The following figures are showing examples for the functioning of the detection algorithm. A.2 shows clear and easily to separate slow wave and activated intervals for rat WT 1056 from experiment 1. A.3 illustrates a case where rat WT 574 (experiment two) has extended SW episodes during baseline and gets activated only after the amphetamine injection at around 5400s. A.3 is depicting a case where the rat 1162 (experiment two) falls into SW sleep at the end of recording, during the stereotypic phase after around 8100 s. Nevertheless, enough activated intervals are present for analysis. During baseline, there are few activated intervals and longer intermediate states like 1800 s to 2700 s, those are excluded from analysis. A.4 is a more ambiguous case (rat 281, experiment 2) with no clear boundaries between cortical states. Based on experience with the other animals, the solution proposed here seems to be reasonable.

Connectivity analysis

Being able to record electrophysiological activity from many brain regions, enables researchers to build models of the neuronal interactions between these regions. Several methods have been developed to this purpose, among those are, for example, cross-correlation in the time domain and coherency in the frequency domain. This measures are symmetric, or commutative, which means that the measure applies equally to A $\rightarrow$ B and B $\rightarrow$ A. A useful additional knowledge would be about the directionality of influence from one region to another. Recently, the Granger "causality" has become popular in neuroscience. It is based on a model which allows the prediction of future values of one signal based on past values of another signal [85]. Such a prediction can then be interpreted in terms of directional connectivity or, with caution, as cause and effect.

Autoregressive models

Given two stationary stochastic processes X_t and Y_t, they can be represented as autoregressive processes [85]. This means that, for each signal, the value at time t can be represented as the sum of (1) a linear combination of its own past values and (2) a stochastic term. The stochastic term contains the variance which is not explained by the past values. n is the order of the autoregressive process and denotes the number of past values which are being used.

The general form of the autoregressive representation is:

$$X_t = \sum_{i=1}^{n} a_i X_{t-i} + \epsilon_{1t} \tag{2.3}$$

$$Y_t = \sum_{i=1}^{n} b_i Y_{t-i} + \eta_{1t} \tag{2.4}$$

The prediction of the future value of X(t) will now take into account also the past values of the other process, Y(t). This gives the joint representation:

$$X_t = \sum_{i=1}^{n} c_i X_{t-i} + \sum_{i=1}^{n} d_i Y_{t-i} + \epsilon_{2t} \tag{2.5}$$

$$Y_t = \sum_{i=1}^{n} f_i X_{t-i} + \sum_{i=1}^{n} g_i Y_{t-i} + \eta_{2t} \tag{2.6}$$

The variance and covariance of the noise terms are defined as:

$$A_1 = var(\epsilon_{1t}), B_1 = var(\eta_{1t})$$

$$A_2 = var(\epsilon_{2t}), B_2 = var(\eta_{2t})$$

$$C_2 = cov(\epsilon_{2t}, \eta_{2t})$$

The covariance matrix of the joint system is:

$$\Sigma = \begin{pmatrix} A_2 & C_2 \\ C_2 & B_2 \end{pmatrix} \tag{2.7}$$

If there is no directional influence from either process towards the other, we expect the parameters d and f to be zero. The variance of the noise terms should also remain unchanged: $A_1 = A_2$, $B_1 = B_2$, the covariance $C_2 = 0$.

The total interdependence between X(t) and Y(t) can be decomposed into three parts: the directional components from X(t) to Y(t), the opposite direction Y(t) to X(t), and the instantaneous causality caused by a common driving input:

$$F_{X,Y} = F_{X \to Y} + F_{Y \to X} + F_{X \cdot Y} \tag{2.8}$$

This total interdependence is

$$F_{X,Y} = \ln \frac{A_1 B_1}{|\Sigma|} \tag{2.9}$$

The determinant of the covariance matrix is the generalized variance and represents the volume of space occupied by the residuals (the noise terms) [86] [87].

If there is a directional information flow from Y(t) to X(t), we expect the residual variance A_1 to be larger than A_2, because of the additional explained variance when taking into account the past values of Y(t) via the parameter d. This leads to the definitions:

$$F_{Y \to X} = \ln \frac{A_1}{A_2} \tag{2.10}$$

$$F_{X \to Y} = \ln \frac{B_1}{B_2} \tag{2.11}$$

The interdependence which is not captured by the directed interactions or by the single autoregressive model, the instantaneous causality, is defined as:

$$F_{X \cdot Y} = \ln \frac{A_2 B_2}{|\Sigma|} \tag{2.12}$$

This time domain formulation is supposed to give a rationale for the usage of the Granger connectivity measures. The frequency domain formulation is explained in detail in [85], [86].

When interpreting Granger results, one should be aware about possible misleading conclusions based on the usage of the word "causality". Let's consider a network with the connectivity Y $\rightarrow$ Z $\rightarrow$ X (example 2 from Chapter 17 in [85]). The pairwise, bivariate Granger analysis will output a Y $\rightarrow$ X connectivity, because it is not able to distinguish between direct and indirect connections. The multivariate implementation of the Granger connectivity can take such indirect (mediated) connections into account. But this method assumes that all mediating network nodes are measured and included into the model. In the case of electrophysiological measurements this is not the case. In this study, we are measuring 4-5 brain regions and there is no way to determine mediator regions other than the measured ones. Based on the Granger connectivity graph, we are therefore still not able to discern between true direct connections and mediated indirect connections. Therefore, the term "causality" should be used with caution. In this study, it is replaced by "connectivity".

For this study, the signals recorded at 2 kHz are lowpass filtered and downsampled to 200 Hz for reducing the model order, while reaching the timescale of the expected interaction [88] [89]. Model order could not be inferred by using the Akaike or Bayesian information criterion, because this criteria did not converge in many animals. After comparing connectivity spectra for model orders of 8, 10, 16, 20 and 30, an order of 10 was selected, as results with this or higher orders were consistent and this model order matches research done on similar data [90]. The frequency bands are defined as follows: 1-8 Hz as low, 8-35 Hz as medium, 35-100 Hz as high. This bands have been selected based on the frequencies found by permutation testing in a similar analysis [91].

Statistics

Comparison of independent groups

Comparison of independent groups is done by using the Kruskal-Wallis test.

Longitudinal data

Interaction of genotype and treatment is tested by using a non-parametric repeated measures test (R package "nparLD" [92]).

Permutation testing

Granger connectivity is calculated for a series of 8s windows with 50% overlap ("snips"). The Granger spectrum is the mean value over all snips. We consider only intervals of artifact free activated brain state.

We are using a permutation test for the Granger connectivity results. This allows us to obtain the baseline "noise" of the connectivity algorithm with this specific given data. This baseline represents the null hypothesis distribution. For this, we are shuffling all signal snips, mixing active and slow wave states and also baseline and the post amphetamine conditions. Additionally, we are calculating a surrogate signal for each snip, by shuffling the phase values of the signal in frequency domain using the amplitude adjusted Fourier transform method (AAFT) of the PyUnicorn package [93]. After repeating the Granger test on surrogate data for 500 times, we calculate the 95th percentile of the spectrum distribution and use it as significance threshold. Given the population of measured animals, only median value peaks above the threshold are considered as significant for the estimation of baseline connectivity and for the comparison of genotypes. This method is used for plotting the connectivity graphs.

We are using an additional test for longitudinal (repeated measures) testing. This simple approach excludes some cases in which the longitudinal test finds a significant difference, while both populations are below their respective thresholds. Here, we are using not the maximum connectivity value in a frequency band, but the median, and compare it to the mean threshold. We consider the connectivity as significant when the

median value is above the mean threshold for each frequency band. This approach is more conservative than the previous one used for drawing connectivity nets for specific experimental conditions. Here, if a connectivity value is significant in one condition and not significant in the other, we do calculate test statistics. For instance, if the connectivity in a certain frequency range is below the significance threshold in the baseline condition, but rises above it after amphetamine injection, we perform the test statistics.

3 EXPERIMENTAL RESULTS

POWER SPECTRAL CHARACTERISTICS

The following animal numbers were used in the analysis.

Experiment 1: DAT-tg: 7 for mPFC, cPu, nAcc, 6 for DM and EP. WT: 10 for mPFC, cPu, nAcc, DM, 7 for EP.

Experiment 2 (amphetamine challenge): DAT-tg: 9 for mC, 10 for cPu, EP, cmPF. wt: 12 for all regions.

Experiment 3 (tDCS): DAT-tg: 11 for all regions, wt: 9 for all regions.

We first consider the power spectrum in the recorded regions in the baseline condition, without any pharmacological treatment. Given the identical paradigm in experiments 2 and 3, baseline data from this experiments is merged and analyzed as one group. In the baseline condition, DAT-tg rats show no stereotypic behavior, but impaired learning and motivation [25] [28].

There are differences in the power spectrum of wt and DAT-tg in all recorded regions, excepting the motor cortex, as figures A.5 and A.6 are showing. Tables 3.2 and 3.1 are showing the test statistics for the regions and frequency bands found to be different between the genotypes on a level of significance of .05. Group differences are found mostly in the theta and alpha band. In this frequency bands, DAT-tg shows a drop in signal power as compared to wt. The mPFC higher beta power is also decreased, in addition to theta and alpha. In contrast, the cmPF is the only region where LFP signal power is higher in DAT-tg, this occurs here in the high beta band.

Two regions were measured in both experiments 1 and 2, namely cPu and EP. The power spectrum shown here is consistent between experiments 1 and 2 for this two common regions.

region	frequency band	H at 1 df	P
cPu	theta	8.0	.005
	alpha	4.0	.046
EP	theta	6.1	.01
cmPF	high beta	8.9	.003

Table 3.1: Levels of evidence for the difference in LFP power between wt and DAT-tg. Combined baselines of experiments 2 and 3. The test used is Kruskal-Wallis (non-parametric).

region	frequency band	H at 1 df	P
mPFC	theta	6.9	.008
	alpha	7.5	.006
	high beta	4.6	.03
cPu	theta	7.5	.006
	alpha	4.6	.03
EP	theta	4.0	.04
nAcc	theta	6.4	.01
DM	theta	4.7	.03

Table 3.2: Levels of evidence for the difference in LFP power between wt and DAT-tg. Baselines of experiment 1. The test used is Kruskal-Wallis (non-parametric).

SPECTRAL CHARACTERISTICS OF THE STEREOTYPY PHASE

In experiment 1 there is no evidence for an interaction between genotype and treatment in the power spectrum (Figure A.7). This means that wt and DAT-tg animals react in similar ways after the stereotypic phase is initiated by the amphetamine injection.

Experiment 2 is showing evidence for interaction in all four measured brain areas, mostly in the beta frequency range (Figure A.8, Table 3.3). wt and DAT-tg animals are reacting differently after induction of stereotypical movements by amphetamine. Anyway, two regions were measured in both experiments 1 and 2, namely cPu and EP. Only experiment 2 shows significant interactions, contradicting the results of experiment 1 and unlike the power spectrum, which was consistent. This can be explained by the differences in experimental procedures, mostly due to deeper anesthesia in experiment 1, as will be discussed in section 4.

	frequency band	Stat at 1 df	P
MC	lower beta	4.0	.046
cPu	lower beta	7.1	.008
	higher beta	7.1	.008
EP	higher beta	9.5	.002
	gamma	6.6	.01
cmPF	higher beta	6.0	.01

Table 3.3: Levels of evidence for the interaction between genotype and treatment. The test used is nparLD (non-parametric test of interaction).

Now we are looking at the simple effects of stereotypy induction on the genotypes, taken separately. In all regions and frequency bands where there is evidence for an interaction between genotype and treatment, DAT-tg does generally not change power. The only exception is cPu in the lower beta band, as shown in Figure A.9.

The genotypes react differently in spectral power after induction of stereotypy. DAT-tg remains close to the baseline values, with exception of cPu in lower beta. wt tends to increase signal power in most cases. A very similar effect occurs after tDCS.

EFFECT OF TDCS TREATMENT

Experiment 3 used the same paradigm as experiments 1 and 2 for inducing the stereotypic phase, but introduces the tDCS treatment for 20 min immediately after amphetamine injection. We are regarding again only baseline and stereotypy intervals. Any effect of tDCS will therefore be a delayed effect, as tDCS treatment occurs at amphetamine injection and does not last until the stereotypic phase is starting (Figure A.1).

wt and DAT-tg are behaving clearly different after tDCS in cmPF. There is evidence for an interaction of genotype and treatment in frequency bands from delta to high beta in the cmPF. In this frequency bands, signal power of wt animals is higher after treatment than that of DAT-tg animals (Figure A.10, Table 3.4). This result is surprising, given that tDCS was previously shown to reduce repetitive behavior in awake rats [66] and we were therefore expecting a stronger tDCS effect in DAT-tg than in wt.

	frequency band	Stat at 1 df	P
	delta	11.2	.0008
	theta	8.4	.004
cmPF	alpha	6.5	.01
	lower beta	22.3	2,4e-06
	higher beta	8.6	.003

Table 3.4: Levels of evidence for the interaction between genotype and treatment after tDCS. The test used is nparLD (non-parametric test of interaction).

	frequency band	Stat at 1 df	P
cmPF	delta	12.4	.0004
	lower beta	4.8	.03

Table 3.5: Levels of evidence for the tDCS effect in wt only. The test used is nparLD (non-parametric test of interaction).

When looking at the simple effects of tDCS on both genotypes, we see again that DAT-tg tends not to change signal power as compared to the baseline condition. Only wt animals show significantly increased signal power in cmPF as shown in figure A.11.

Given this result, we are now assessing the tDCS effect within each genotype individually. For this purpose, we are comparing the groups without and with tDCS, respectively. The group without tDCS comes from experiment 2, the group with tDCS from experiment 3. Comparisons are made during the stereotypy intervals only. This also means that the tDCS effect was assessed only under amphetamine.

wt animals show a higher power in delta and lower beta in the cmPF in the tDCS condition (Figure A.12, Table 3.5). DAT-tg shows a higher power in the alpha and beta bands in mC and cPu (Figure A.13, Table 3.6). In conclusion, tDCS affects signal power in a genotype dependent way. After manipulation of the DAT transporter, tDCS long-term effects are affecting different brain regions. In wt tDCS affects the cmPF, in DAT-tg it affects mC and cPu.

	frequency band	Stat at 1 df	P
mC	alpha	4.5	.03
	lower beta	4.9	.03
cPu	lower beta	8.2	.004

Table 3.6: Levels of evidence for the tDCS effect in DAT-tg only. The test used is nparLD (non-parametric test of interaction).

FUNCTIONAL CONNECTIVITY

Functional connectivity during baseline

Experiment 1

Figures A.14 and A.15 are showing the connectivity matrix for wt and DAT-tg during the baseline condition of experiment 1. The connectivity graph has to be read as "row causes column". The upper right red half is showing the feedforward direction, the lower left green part the feedback direction. The first left-most red box is the influence of mPFC on nAcc. The first green box, symmetric with respect to the matrix diagonal, is the influence of nAcc on mPFC. The significance threshold resulting from the permutation test is shown as dotted line.

Data from Figures A.14 and A.15 is used to create network graphs. Any median value above threshold is considered significant and plotted as graph edge. We therefore take into consideration even narrow connectivity peaks as long as they are above the threshold. This allows for a qualitative assessment of connectivity as shown in Figure A.19 for wt and A.20 for DAT-tg. Figures A.19 (a) and A.20 (a) are showing that wt animals have a higher number of statistically significant edges than DAT-tg, leading to more interconnected nodes. Figure A.16 is showing the quantitative comparison of both genotypes during baseline. The statistically significant differences are in mPFC $\rightarrow$ nAcc in the low frequency band and mPFC $\leftarrow$ nAcc in the high band. Further differences are cPu $\rightarrow$ nAcc and EP $\rightarrow$ DM.

Experiments 2 and 3

This section describes the connectivity of both genotypes during the baseline condition of experiments 2 and 3. Given the identical paradigm during baseline, both data sets are merged.

The wt shows the following pronounced connections: mC → cmPF and mC → cPu in lower frequencies and mC ← cPu as well as mC ← EP in the middle frequencies. The strongest edges in the higher band are EP ↔ cmPF (Figure A.21 and Figure A.24 (a)).

The DAT-tg shows the same sparseness of connectivity as found in experiment 1. They have less significant edges in the lower frequencies as compared to wt (Figure A.22 and A.24 (b)). The outward connections of mC are all below the significance threshold in DAT-tg, while wt shows two such edges. Figure A.23 is showing the quantitative comparison of both genotypes during baseline. The statistically significant differences are in cPu → cmPF and EP → cmPF in the middle frequency band and EP ← cmPF in the high band. The main difference between the genotypes during baseline are located thus the cmPF.

Functional connectivity after induction of stereotypy

Experiment 1

After amphetamine injection and during the stereotypy interval, wt rats show an increased connectivity in the low frequency band and a reduced connectivity in the high band. The only significant effect in the middle band (cPu → nAcc) is ambiguous due to the overlap with the wide low frequency peak. Figure A.17 is showing this effects. Connectivity in DAT-tg develops similarly, but in different regions (Figure A.18).

The connectivity graph remains sparse for DAT-tg during the stereotypy interval, when compared to WT, especially in the lower frequency band. (Figures A.19 (b) and A.20 (b)). A striking difference between wt and DAT-tg lies in the role of the mPFC in the connectivity graph. In DAT-tg, it's weights are higher and especially during stereotypy they are pointing outwards. This is valid for the lower frequencies, no such effect is visible in the other bands.

The test used is the repeated measures, non-parametric nparLD due to the longitudinal measurement.

Experiment 2

This section deals with the connectivity changes after inducing the stereotypy with amphetamine.

During the stereotypy interval, wt rats show an increased connectivity in the low frequency band and a reduced connectivity in the middle and high band (Figure A.25 and Figure A.29 (a) (b)). Figure A.25 is showing the repeated measures statistics on WT. All connectivity edges in the lower band pointing to cmPF increase strongly, as well as towards EP. In contrast, edges pointing to mC from all other regions are reduced in the middle band.

The connectivity graph remains sparse for DAT-tg during the stereotypy interval, when compared to wt in the lower frequency band. In the high band we observe a denser connection graph (Figures A.22 and A.30 (a) (b)). The most notable difference is the increase in connectivity in the lower band, which is weaker than in wt. Especially the edges pointing to cmPF and EP are not responding after induction of stereotypy as they do in wt.

This finding goes in line with previous results from the power spectral analysis. Both LFP power spectrum and functional connectivity of DAT-tg react - with little exceptions - less to the amphetamine treatment than wt rats.

Given that two regions, cPu and EP, have been measured in all experiments, a consistency check can be done despite all methodical differences. During baseline, the cPu $\rightarrow$ EP connection is present in experiment 1 but missing in experiments 2 and 3. However, after amphetamine treatment, connectivity becomes more consistent, showing in both experiments a two-way connection: a stronger cPu $\rightarrow$ EP and a weaker cPu $\leftarrow$ EP (Figures A.19 and A.29).

EFFECT OF TDCS ON FUNCTIONAL CONNECTIVITY

This section deals with the connectivity changes induced by tDCS during the stereotypy interval. Comparisons were done for each genotype between the stereotypy intervals from experiments 2 and 3. The statistical test used was therefore Kruskal Wallis, for non-parametric comparison of independent groups.

The main effect of tDCS in wt occured in the cmPF (Figure A.27). The edge mC $\rightarrow$ cmPF increases after tDCS in the middle and upper frequency bands, while EP $\rightarrow$ cmPF decreases in the lower band. This is the only region which also showed a

change in LFP power after tDCS (Figure A.12). Interestingly, signal power in both delta and lower beta was increased while connectivity behaves differently, and seems not to depend on increased or decreased signal power. Figure A.29 (b) and (c) is illustrating the tDCS induced lower connectivity in low frequencies and the increased connectivity towards cmPF in the high frequency.

The main effect of tDCS in DAT-tg is located in the cmPF too, but here, all outgoing connections are reduced in the higher frequencies. Also, the connection cPu $\rightarrow$ EP is stronger (Figure A.28). DAT-tg shows no change in power spectrum in cmPF, which is the region with the most robust effect of tDCS. Figure A.30 (b) and (c) is illustrating the tDCS induced generally lower connectivity from cmPF to all others regions in the high frequency band.

4 DISCUSSION

This is the first study to show the effect of non-invasive electric brain stimulation on LFP power spectrum and functional connectivity of both cortical and deep brain regions. Additionally, this study discusses the genotype-specific effect in a model with manipulated dopaminergic tonic/phasic equilibrium (DAT-tg rat), relevant to stereotypic movement disorders.

BASELINE CONDITION

During the baseline condition, the DAT-tg rats do not receive any treatment and do not show any stereotypic behavior, but do show learning deficits [28]. Overexpression of DAT leads to a consistent drop in the power spectrum mostly in the theta (4Hz - 8Hz) and alpha (8Hz - 15Hz) frequency bands. Exceptions are the mC, without any relevant difference between genotypes, and the cmPF, with a higher power in DAT-tg thanwt in high beta (20Hz - 35Hz).

The functional connectivity network in DAT-tg is sparse when compared towt. This can be interpreted as a lack of communication between brain regions, as defined by the Granger connectivity. This finding fits the non-motor characteristics of the DAT-tg behavior, which are less motivation and/or less learning thanwt [27] [28]. This confirms similar studies which linked a lower Granger connectivity to clinical symptoms of Autism Spectrum Disorder [94] and an unbalanced local vs. global connectivity to Childhood Onset Schizophrenia [95].

Here, we found that the motor cortex is driving deep nuclei inwt, as also observed by [67]. In DAT-tg, the opposite is the case, with the mC being rather driven by incoming edges from deep nuclei. This effect is most clearly seen in the low connectivity frequency band.

STEREOTYPY INTERVAL

All regions measured in experiments 2 and 3 show significant statistical interactions between genotype and amphetamine treatment. This interactions are correlated to the motor stereotypies. LFP power in DAT-tg is less modulated by the induction of stereotypy than inwt.

The only significant change in the power spectrum in DAT-tg after inducing stereotypy is in the lower beta (15Hz - 20Hz) in the cPu.

The beta frequency range is known to be related to hypokinesia and inversely correlated to the amplitude of pathologic movement [64] [46]. This study can replicate this finding. We found a decrease in low beta power during stereotypy in the cPu of DAT-tg. tDCS lead to an increased power in low beta in the cPu and in the mC which is correlated to the reduced stereotypy.

DISEASE AS NETWORK MALFUNCTION

The functioning of the brain, as a complex system, is thought to be supported by modular network elements, which are dynamically changing according to the state or task being performed [96]. These networks are found across different temporal and spatial scales and create a hierarchical system of "networks within networks". In the temporal domain, short- and long-term memory formation can form temporal modules. Spatial modules can be, for example, cortical columns. Elements within a module are having more connections to each other that to other modules. This organizational principle renders the system robust and specific [97]. But this principle also ensures a flexibility which allows the same brain region to perform multiple tasks. This is thought to be done by integrating modules over large scales and recruiting neuronal populations "on the fly", in a dynamic and flexible way. Such dynamic changes of network structure correlate with the ability to learn [98] [99]. The lack of such flexible network dynamic will, therefore, be detrimental to learning and adaptive behavior.

In 3.2 we have seen that power spectrum in DAT-tg remains unchanged after induction of stereotypy, with the exception of low beta in cPu. This lack of reaction to amphetamine treat-

ment is also visible in the functional connectivity graphs. We conclude that in DAT-tg, signal power and connectivity react generally less to an amphetamine challenge than inwt. This behavior is surprising, as the expectation was for a more pronounced effect in DAT-tg, linked to the positive symptoms of stereotypic movements.

A possible interpretation of this effects is that DAT-tg animals adapt less to external or internal perturbations. We can hypothesize that stereotypic behavior is caused by a lack of adaptability in the relevant networks. The brain is therefore less able to compensate the effects of even small amounts of amphetamine. This effect runs parallel to the observation that amphetamine increases tic severity in TS patients [7]. Further support for this interpretation comes from a functional imaging study, which showed that TS patients show a lower co-activation of motor cortex and other brain regions involved in motor processing [56].

We can therefore regard both the stereotypy and the cognitive impairments of DAT-tg animals as an expression of non-flexible large scale, inter-regional networks. Irrespective of the hypothesis which will be proven to best explain motor disorders (be it the tonic-phasic imbalance, the hyperinnervation hypothesis or any other approach), we conclude that the tonic and phasic dopamine levels are essential for the proper building and flexible reconfiguration of large-scale networks.

TDCS

Stimulation affects deep areas

Our results show that tDCS affects deep regions of the brain and not only the cortical area where the electrical field is directly acting. This corresponds to our expectations. Many imaging studies have shown that tDCS affects distal brain areas and acts on both LFP power spectrum and functional connectivity. This has been shown previously with imaging techniques in humans [62] [58] [59] [60] [100]. This study found the same effect with a higher temporal resolution in rat LFP. Anyway, current experimental results are very diverse with respect to the polarity specific effect. For example [58] found effects of cathodal but no effects of anodal tDCS, contradicting other studies as well as

the results of this work. These discrepancies display our lack of understanding of brain stimulation mechanisms. For this reason, clinical studies will still have to be conducted in a trial and error mode, to improve our understanding of tDCS.

We have seen here a very different effect of tDCS on both genotypes: electrical stimulation acts onwt in a different way than on DAT-tg. A possible interpretation is that the long term effects of tDCS are mediated by processes which are impaired in the DAT-tg rat, most likely of dopaminergic nature.

Most differences between the genotypes are in the cmPF. tDCS increases significantly the functional connectivity in the high frequency range inwt. EP $\rightarrow$ cmPF is decreased. Both effects are not seen in DAT-tg. This fits the observation that thalamic deep brain stimulation is an efficient treatment for TS patients [46] [45] [42].

Specific stimulation effects

The only increase in functional connectivity in DAT-tg is in the cPu $\rightarrow$ EP connection. This data does not allow to identify whether stimulation acts on the direct (cPu $\rightarrow$ EP) or indirect pathway (via GPe and STN), leaving the question open, which system we manipulated: the Go or the NoGo pathway.

In DAT-tg, outgoing edges from the cmPF are suppressed by stimulation in the higher frequency band.

The cmPF is particularly important in the context of this work. It represents the main source of striatal input from the thalamus [101]. In primates, the centromedial and the parafascicular nucleus receive sensorimotor, associative and limbic input from the basal ganglia, mainly via the globus pallidus (GPi or EP) and substantia nigra pars reticulata (SNr). The cmPF projects to the nucleus accumbens, putamen and to the primary motor cortex (mC). Rodents show a similar organization. There is some evidence that the cmPF is regulating striatal interneurons which are responding on salient stimuli. cmPF neurons are sensitive to visual, auditory and somatosensory stimuli which are relevant to behavior (behaviorally salient stimuli). Therefore, some cognitive and attentional deficits observed in parkinsonian patients might be linked to the partial loss of cmPF - striatal connections ([102], Chapter 24).

Inwt, tDCS modulates Granger connectivity edges pointing towards cmPF, in DAT-tg it modulates those originating from the

cmPF. This effect occurs mostly at frequencies between 30 and 100 Hz. Similar studies found functional Granger connectivity linking thalamic nuclei to the somatosensory cortex in the same frequency band in monkeys performing a motor task [103]. The gamma frequency seems therefore to be involved in linking distant modules during motor tasks. This result is also in line with the observed increase of thalamus $\leftrightarrow$ motor cortex connectivity after anodal tDCS treatment in humans [62].

The functional link mC $\rightarrow$ cmPF shows in both genotypes a clear peak around 50 Hz, a frequency observed in a similar assessment of cortical to basal ganglia connectivity [67].

Potential clinical usage

The effect of tDCS on the cmPF functional connectivity leads to the hypothesis that also the cognitive deficits of the DAT-tg animal might be improved, additionally to the reduction of stereotypic behavior. For now, only the motor component has been studied in this work. Deep brain stimulation in TS patients has already shown improvements in some patients in other symptomatic areas than tics, such as depressive mood, emotional hypersensitivity, anxiety, impulsiveness [104], and subjective calmness [48]. Our finding, that non invasive stimulation modulates the cmPF, opens promising perspectives for the treatment of those non motor symptoms.

The intralaminar thalamic nuclei (to which cmPF belongs) are also part of a disynaptic direct path from the cerebellum to the basal ganglia, allowing for a short-latency connection between those areas [105]. Being able to modulate uninvasively the thalamic hub may open several possible clinical applications, targeting motor as well as non-motor, cognitive functions.

The described effect on power spectrum in cPu and mC as well as on functional connectivity on the cmPF correlates with the behavioral effect of tDCS. Previous work in the lab found that both tDCS and deep brain stimulation reduce stereotypy in DAT-tg [66]. We therefore found evidence that functional pathways originating in the cmPF and targeting cortical and subcortical areas are causal to stereotypy. This functional links can be targeted in future stimulation based therapies for TS or related tic disorders. tDCS treatment could replace the invasive dbs in patients which might benefit from a manipulation of the cmPF, but for whom dbs is not indicated due to its risks.

A FIGURES

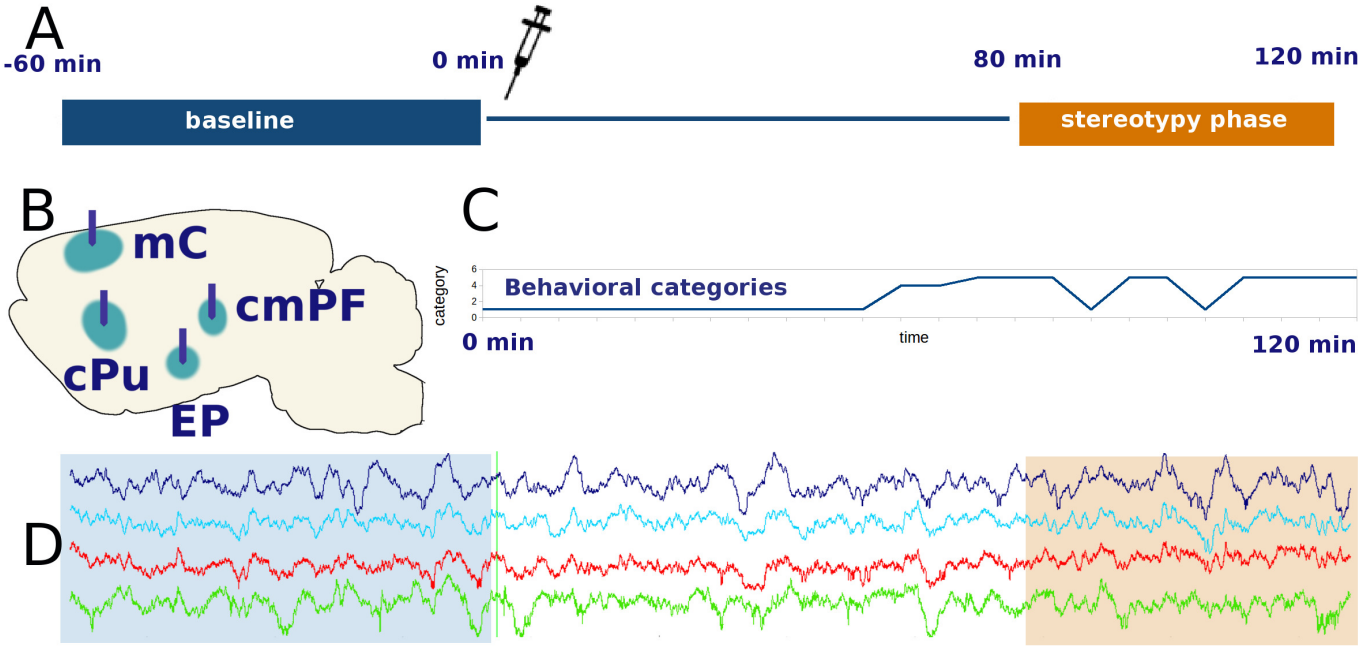

Figure A.1: **Experimental timeline**
A: the baseline was recorded for at least 60 min before amphetamine injection. The stereotypy phase has been found previously to be from 80 to 120 min after amphetamine injection
B: motor cortex (mC), caudate putamen (cPu), entopeduncular nu. (EP in rat corresponds to GPi in primates), centromedial parafascicular nu. (cmPF)
C: significant increase in repetitive behavior in one single DAT-tg rat as previously shown in [25] , [66]
D: electrophysiological recordings under urethane anesthesia. The baseline and the stereotypy phases are marked with blue and orange backgrounds

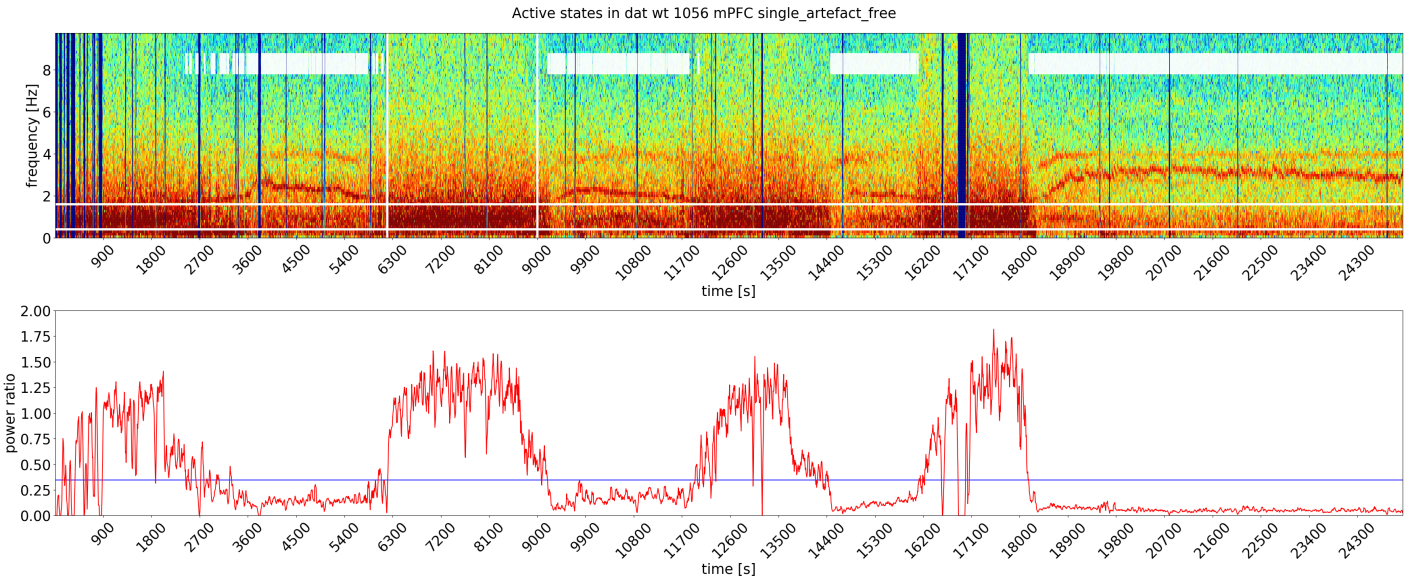

Figure A.2: Activated state detection

Upper panel: Spectrogram comprising both baseline and treatment. The white vertical lines delineate the slow wave reference area. The white horizontal lines are showing the frequency range of slow waves. The blue vertical lines are artifacts which occur after a tailpinch or on external EM noise. Those artifacts are excluded from analysis. The horizontal white bars mark the detected active state. X axis is time, y axis is frequency from 0 to 10 Hz.

Lower panel: The function describing the spectral power ratio for each spectrogram time window in the 0.4 – 1.6 Hz with respect to the SW reference area. The blue horizontal line is the threshold which separates SW from AS.

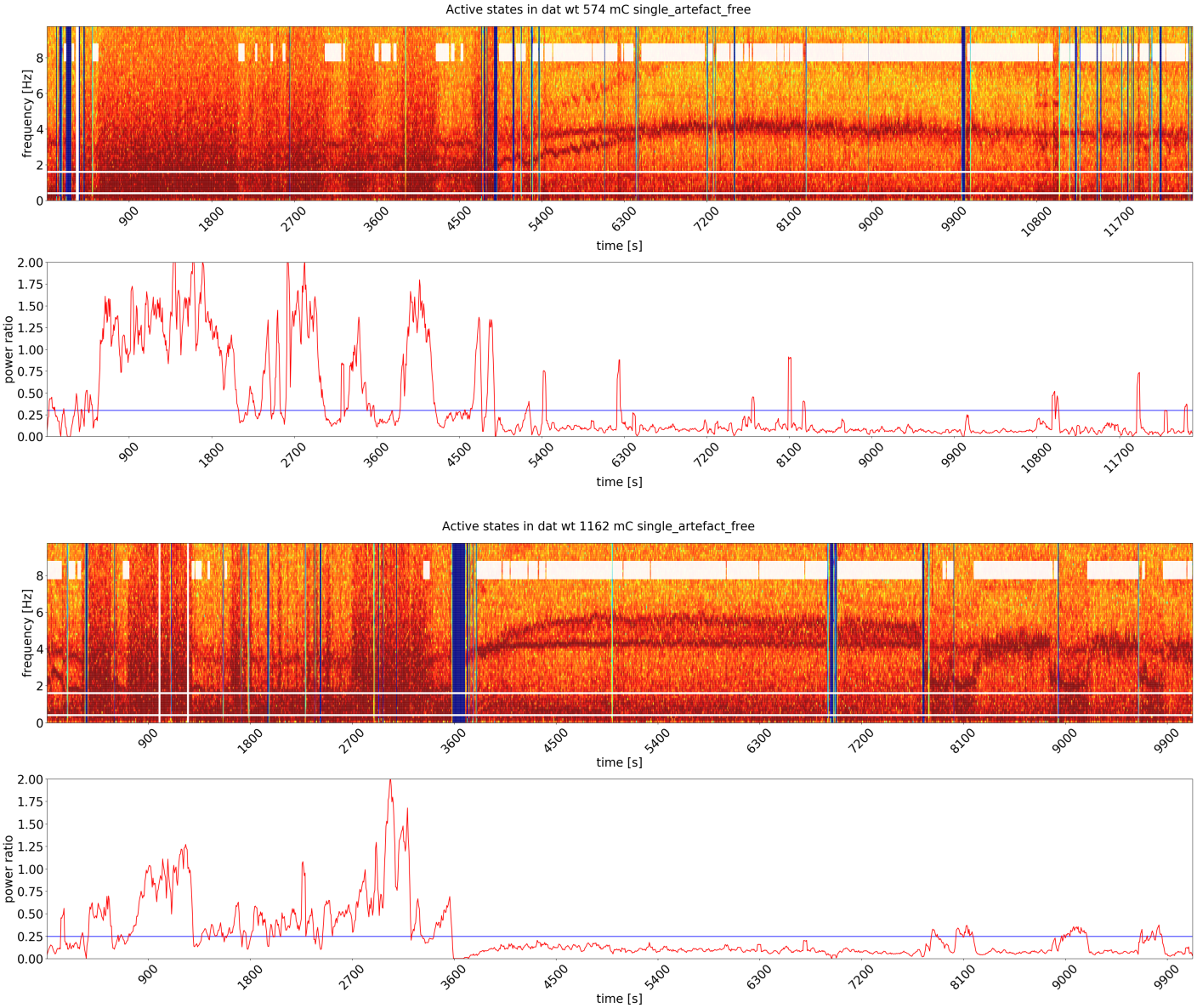

Figure A.3: Acitvated state detection Panels as in A.2

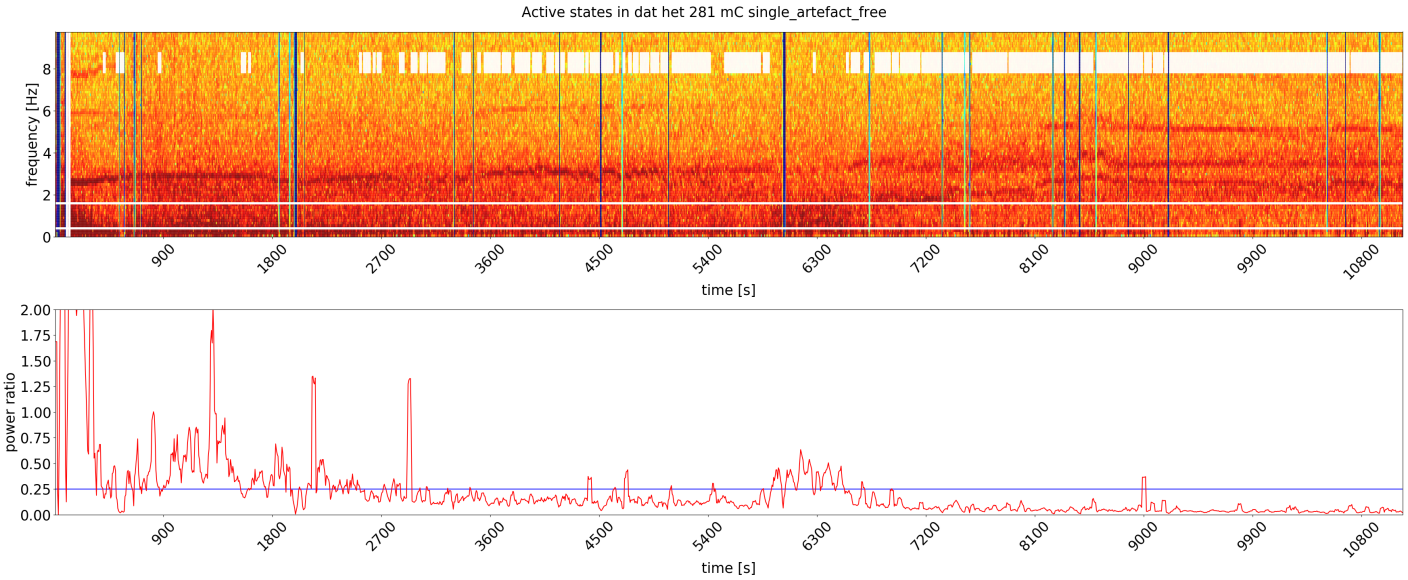

Figure A.4: Acitvated state detection Panels as in A.2

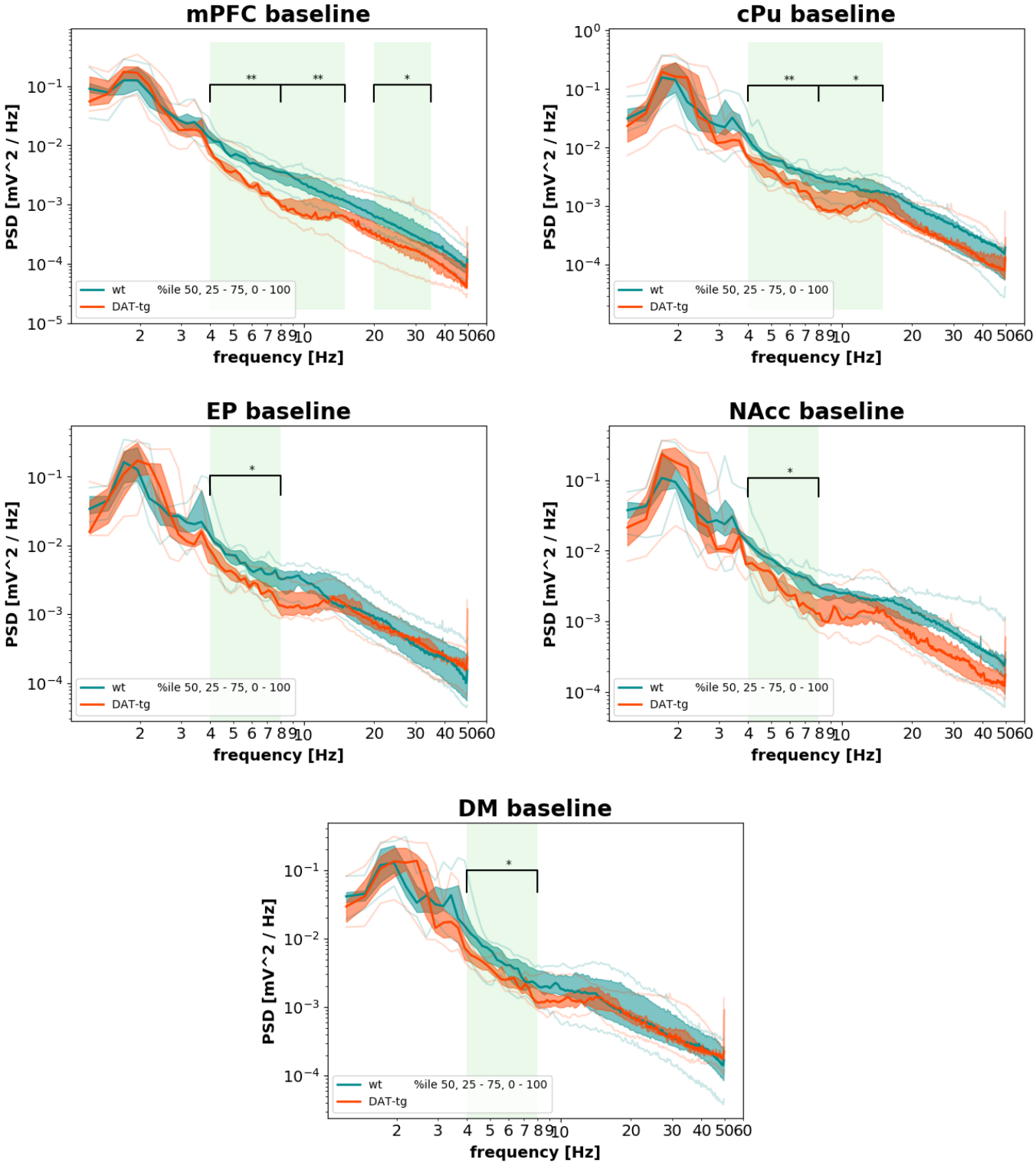

Figure A.5: **PSD of wt and DAT-tg in the baseline condition in experiment 1** Significant differences in the baseline condition were found between DAT-tg and its respective controls in all recorded regions. * denotes P < .05, ** denotes P < .01, *** denotes P < .001.

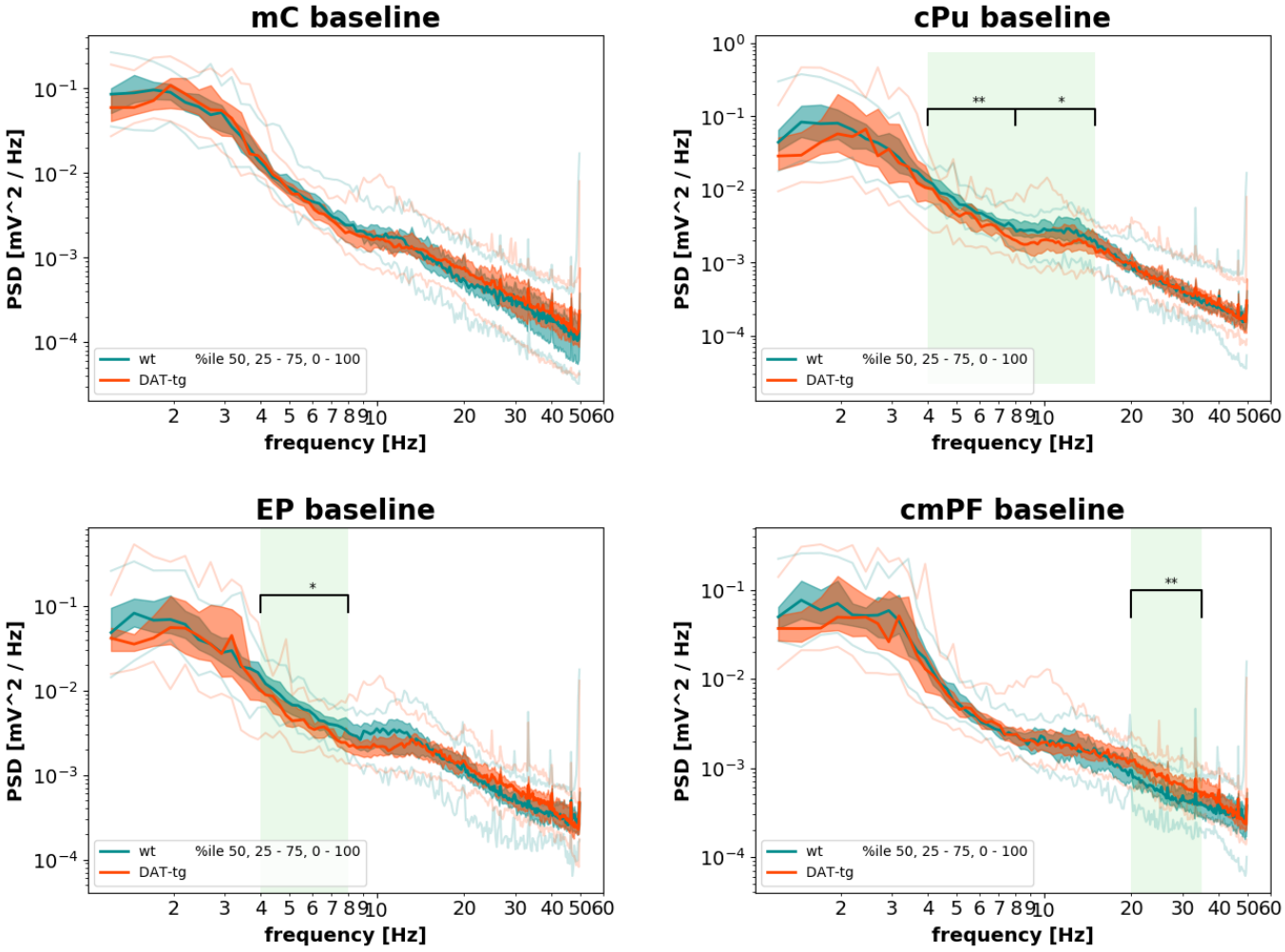

Figure A.6: **PSD of wt and DAT-tg in the baseline conditions of experiments 2 and 3 combined** Significant differences in the baseline condition were found between DAT-tg and its respective controls in cPu, EP and cmPF. * denotes P < .05, ** denotes P < .01, *** denotes P < .001.

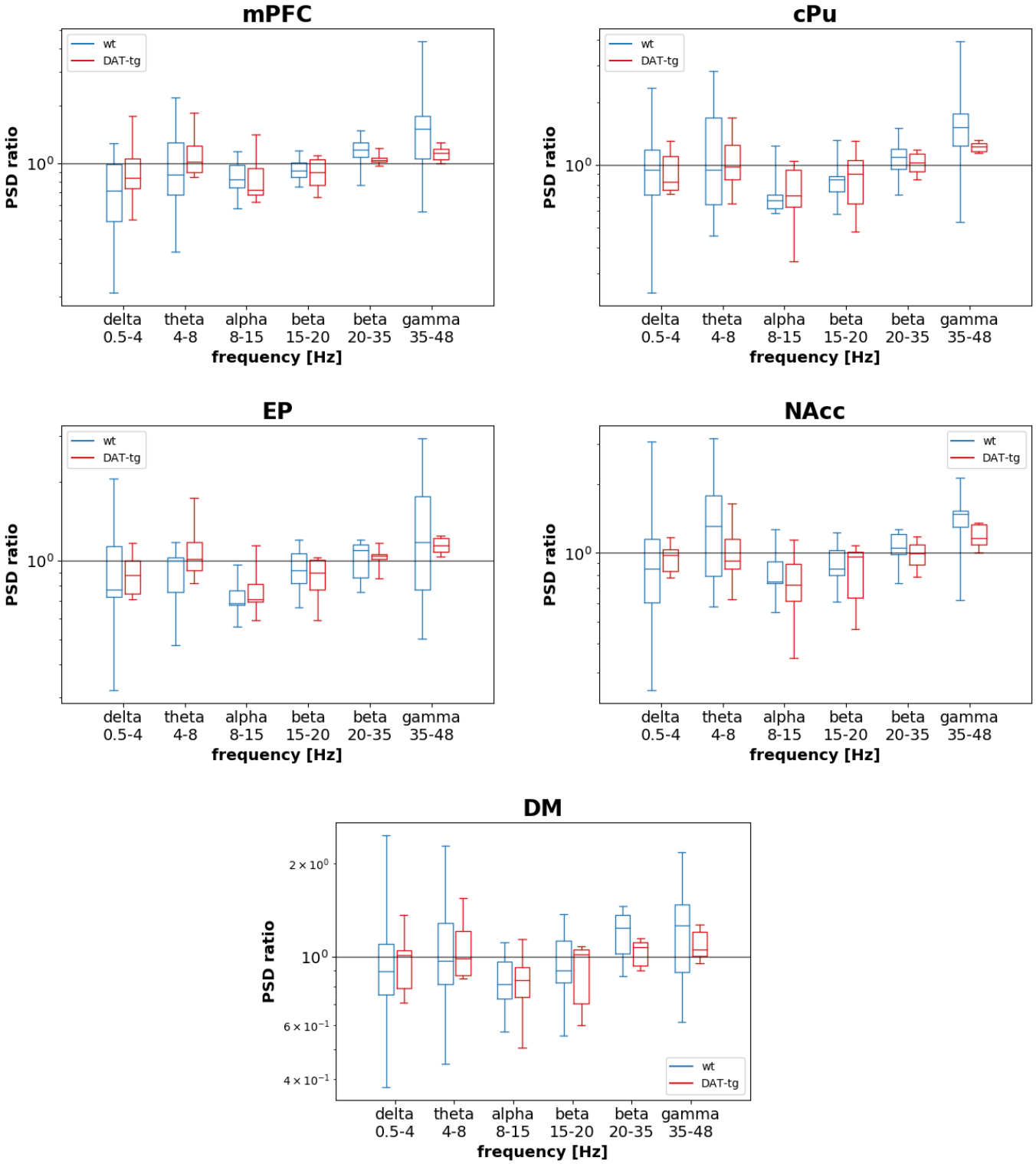

Figure A.7: **Interaction of genotype and treatment in experiment 1.** Treatment is amphetamine, which induces stereotypic behavior. For each genotype, the ratio of signal power during the stereotypical interval and the baseline interval is calculated. Values around one represent therefore no change in power, values above one indicate increasing power after treatment. There is no evidence for an interaction of genotype and amphetamine treatment during the stereotypical interval regarding oscillation power.

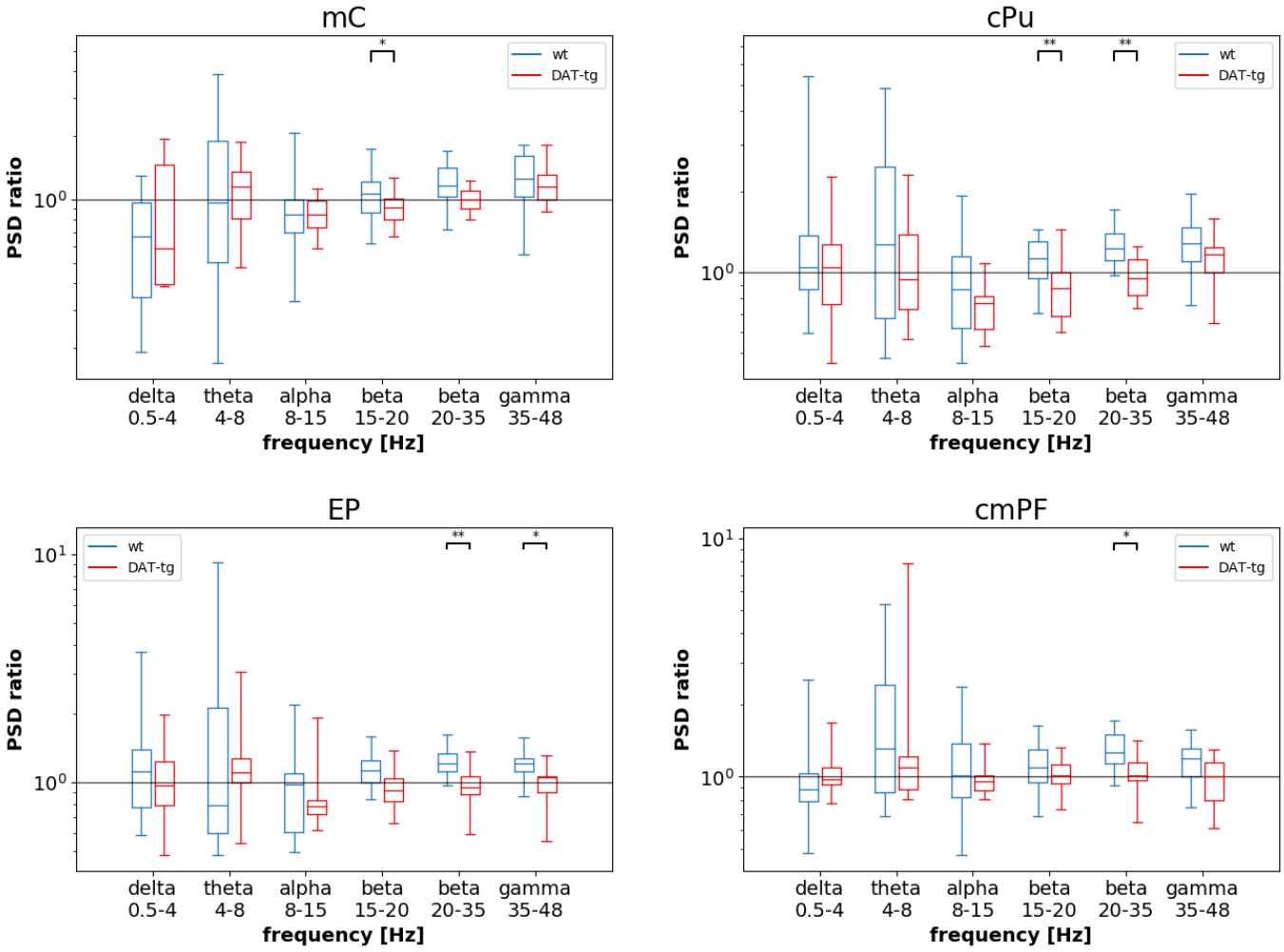

Figure A.8: Interaction of genotype and treatment in experiment 2. Treatment is amphetamine, which induces stereotypic behavior. For each genotype, the ratio of signal power during the stereotypical interval and the baseline interval is calculated. Values around one represent therefore no change in power, values above indicate that power increases after treatment. The box shows the median and spans 25%-75%, the whiskers span 0%-100%. * denotes P < .05, ** denotes P < .01, *** denotes P < .001.

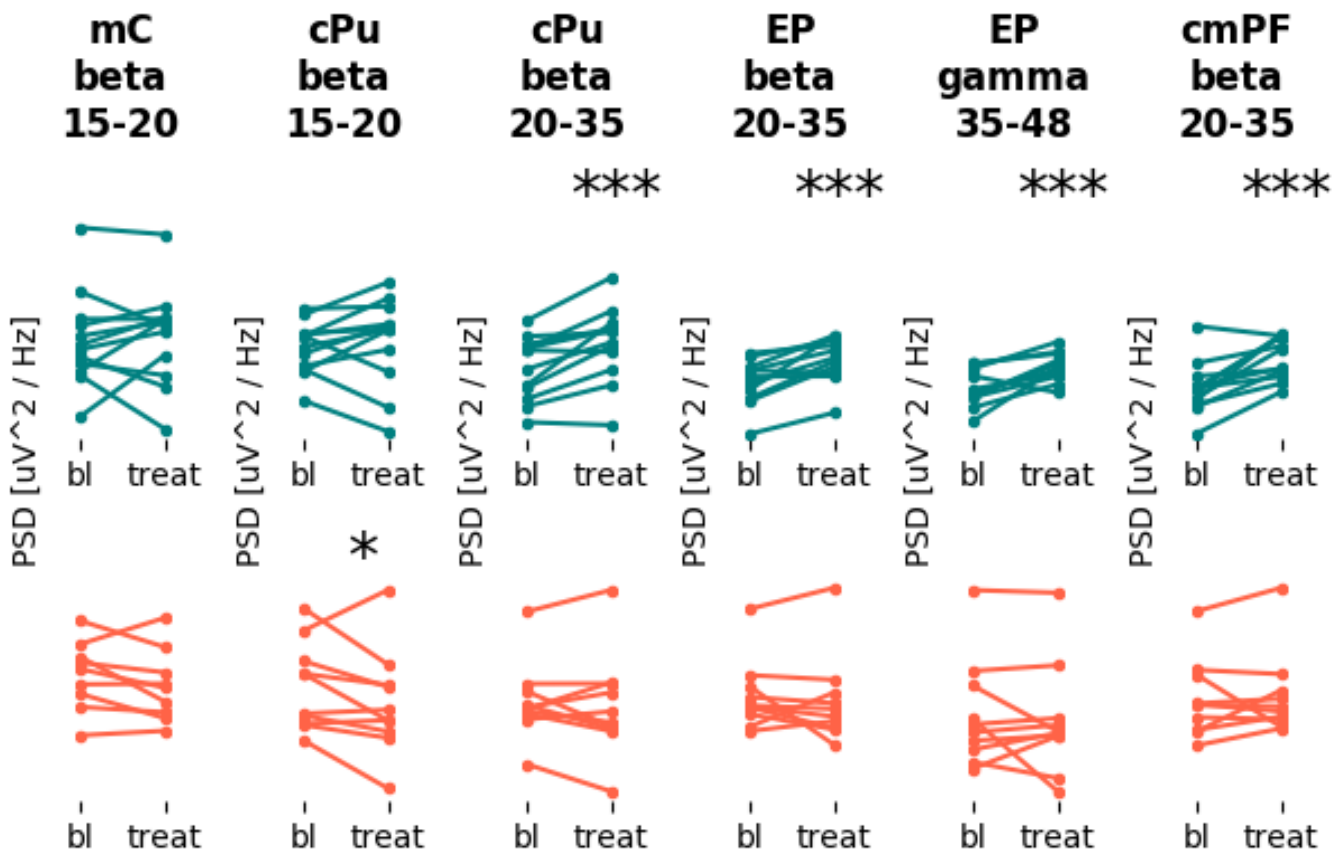

Figure A.9: Simple effects in experiment 2 * denotes P < .05, ** denotes P < .01, *** denotes P < .001.

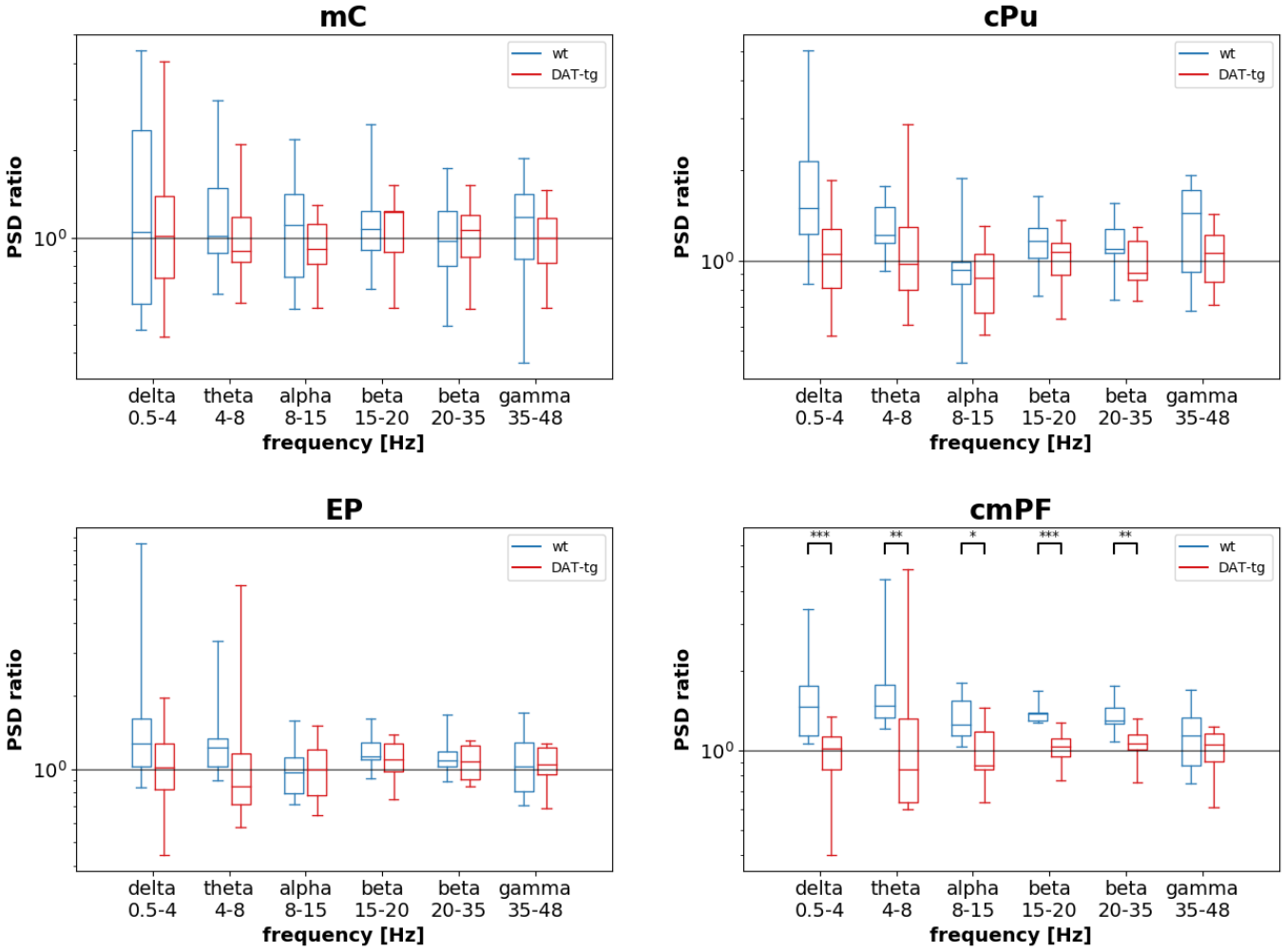

Figure A.10: **Interaction of genotype and treatment in experiment 3.** Treatment is 20 min tDCS after amphetamine injection, which induces stereotypic behavior. For each genotype, the ratio of signal power during the stereotypical interval and the baseline interval is calculated. Values around one represent therefore no change in power, values above one indicate that power increases after treatment. The box shows the median and spans 25%-75%, the whiskers span 0%-100%. * denotes P < .05, ** denotes P < .01, *** denotes P < .001.

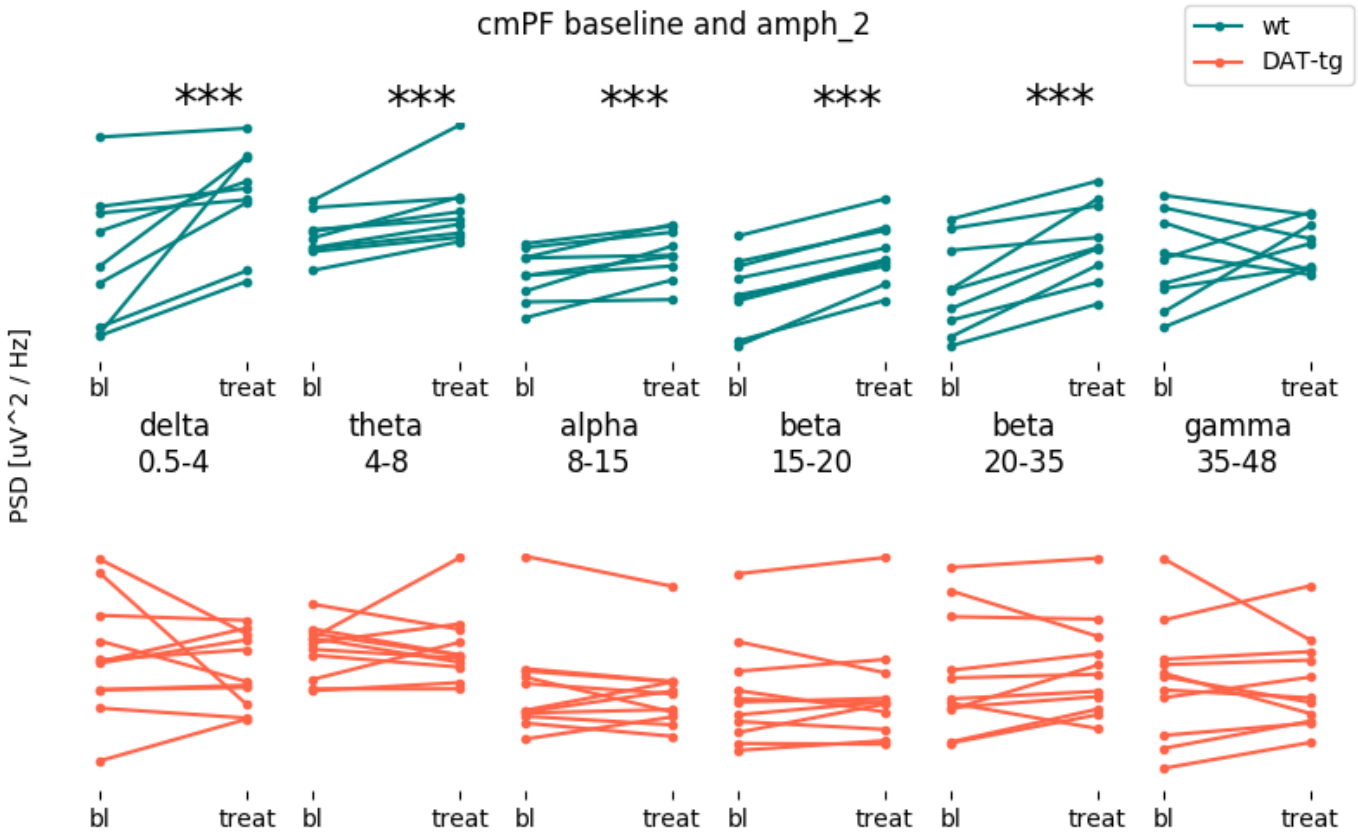

Figure A.11: Simple effects in experiment 3 * denotes P < .05, ** denotes P < .01, *** denotes P < .001.

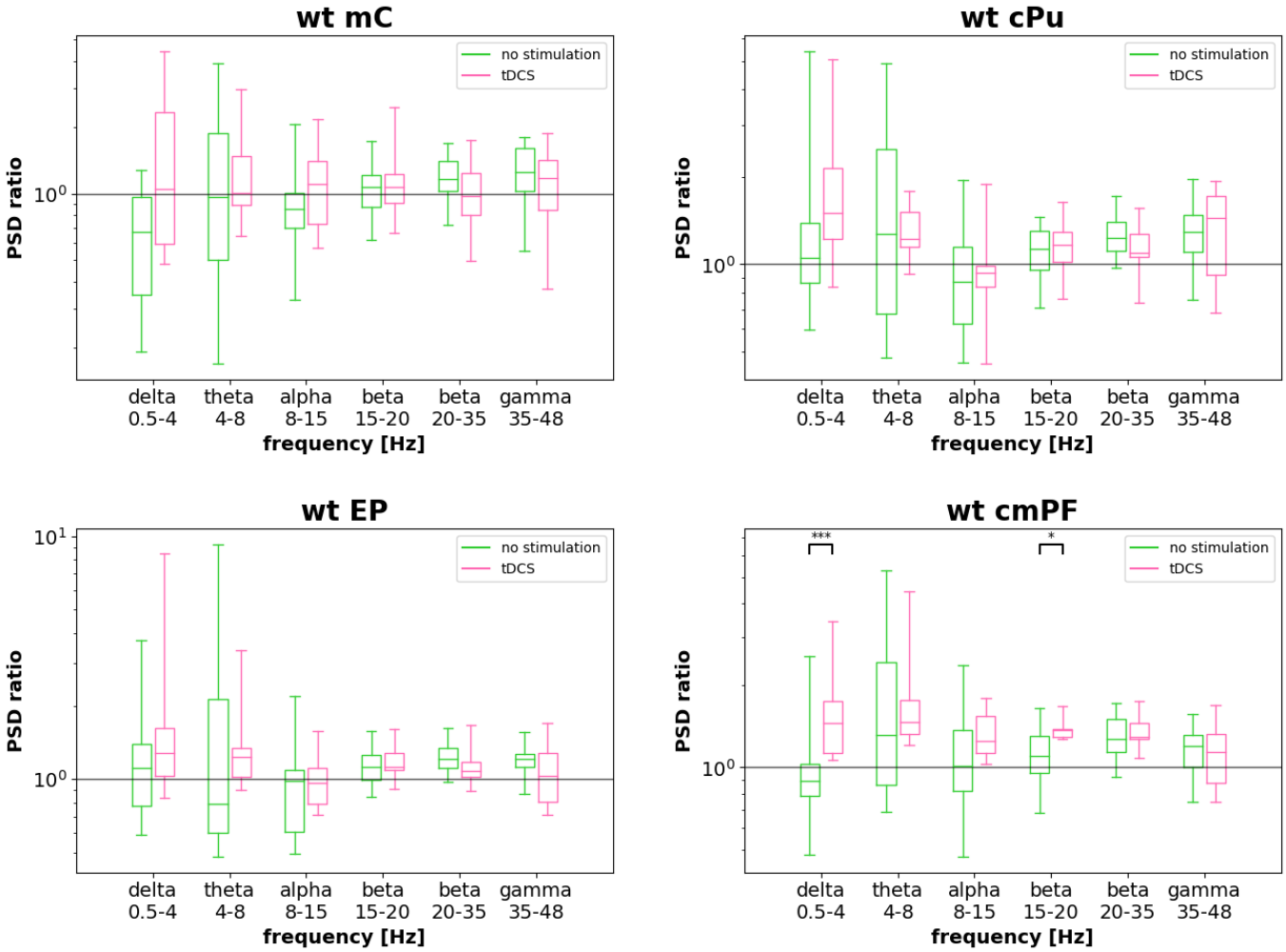

Figure A.12: tDCS effect on wt. Here we compare the PSD of WT without (green) and with tDCS (pink). Data without tDCS is from experiment 2 and data with tDCS from experiment 3. The box shows the median and spans 25%-75%, the whiskers span 0%-100%. * denotes P < .05, ** denotes P < .01, *** denotes P < .001.

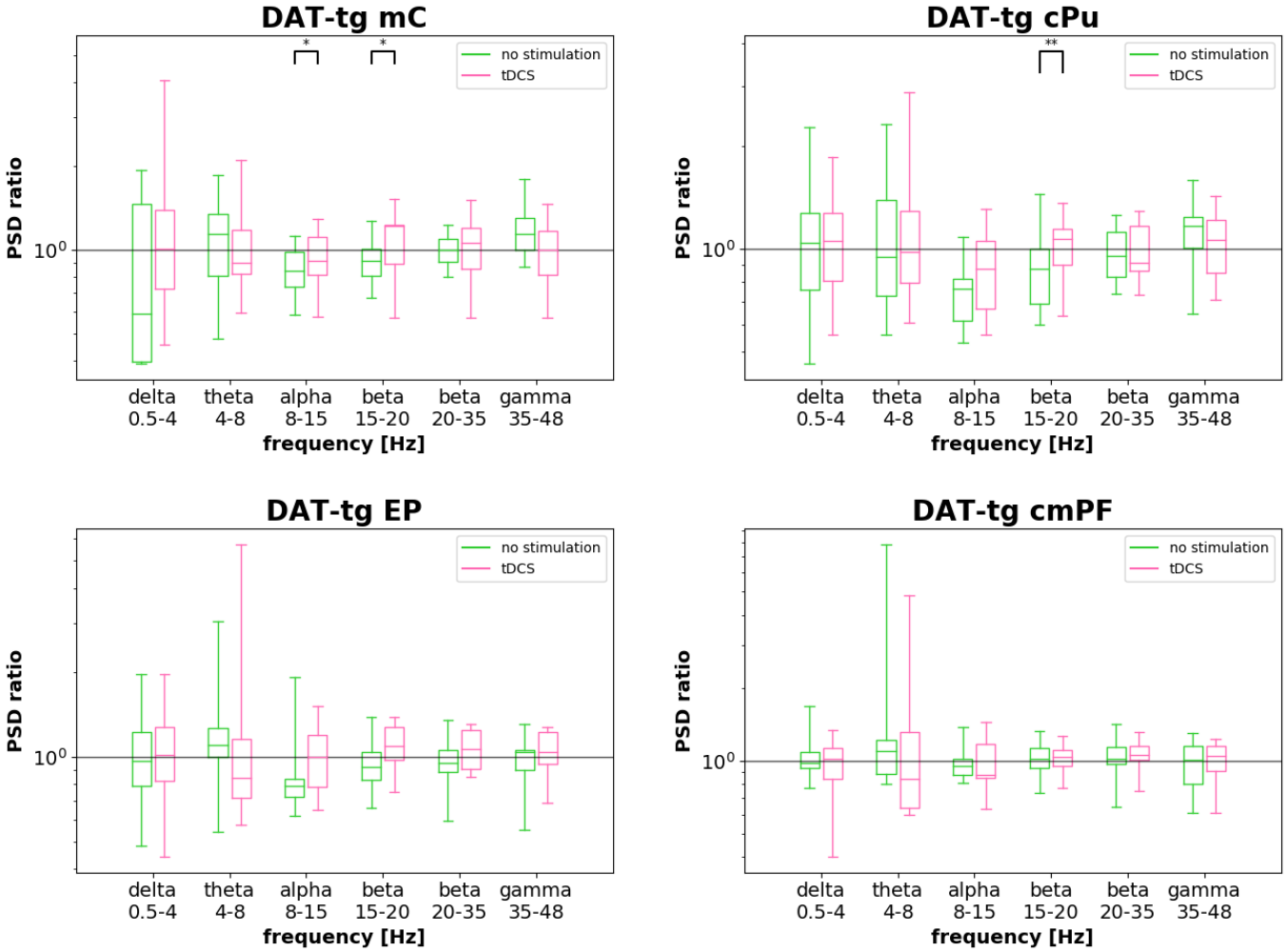

Figure A.13: **Stimulation effect on DAT-tg** Here we compare the PSD of DAT-tg without (green) and with tDCS (pink). Data without tDCS is from experiment 2 and data with tDCS from experiment 3. The box shows the median and spans 25%-75%, the whiskers span 0%-100%. * denotes P < .05, ** denotes P < .01, *** denotes P < .001.

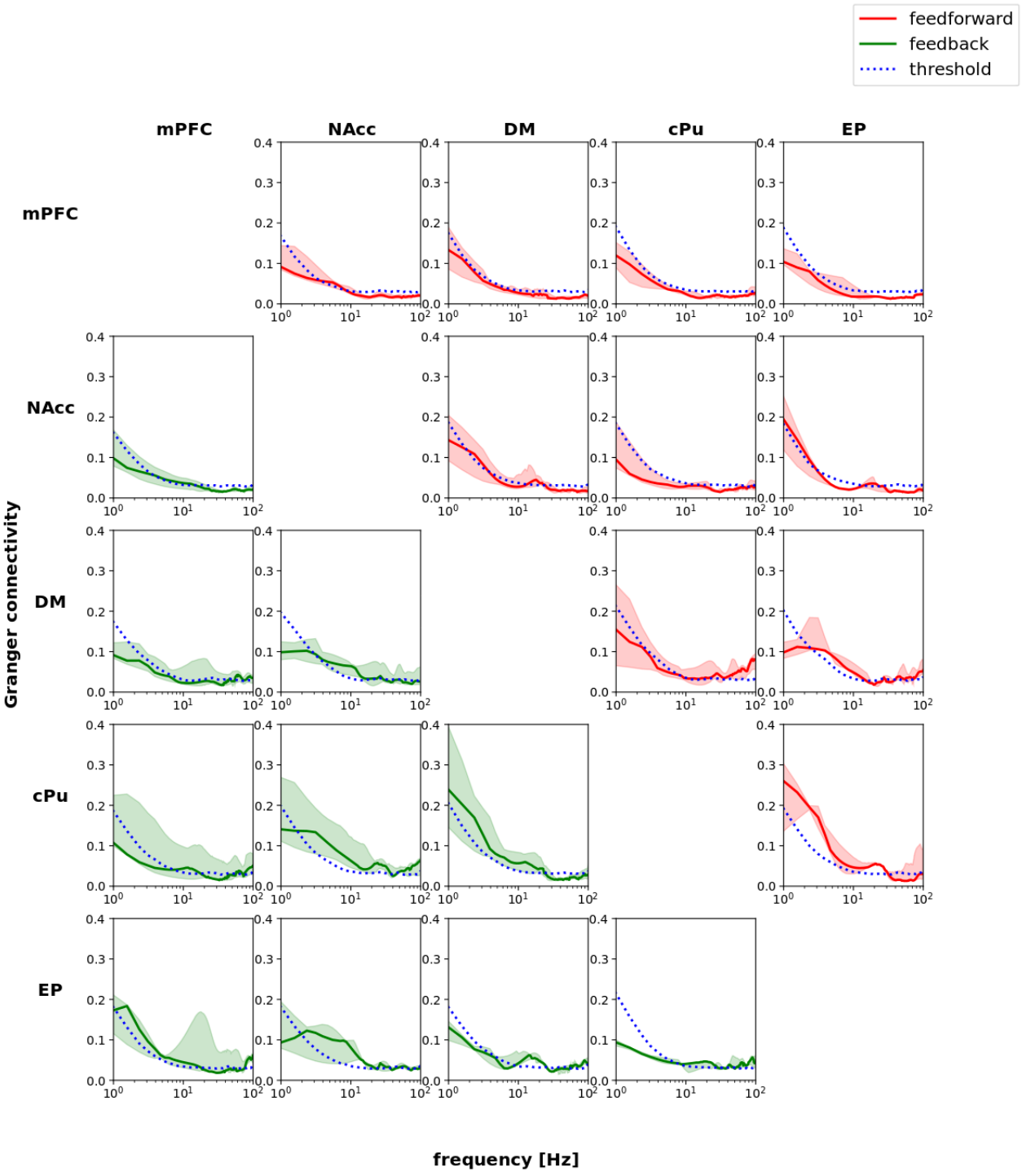

Figure A.14: **Functional connectivity for WT during baseline in experiment 1.** The connectivity graph has to be read as "row causes column". The upper right red half is showing the feedforward direction, the lower left green part the feedback direction. The first leftmost red box is the influence of mPFC on nAcc. The first green box, symmetric with respect to the matrix diagonal, is the influence of nAcc on mPFC. The significance threshold resulting from the permutation test is shown as dotted line.

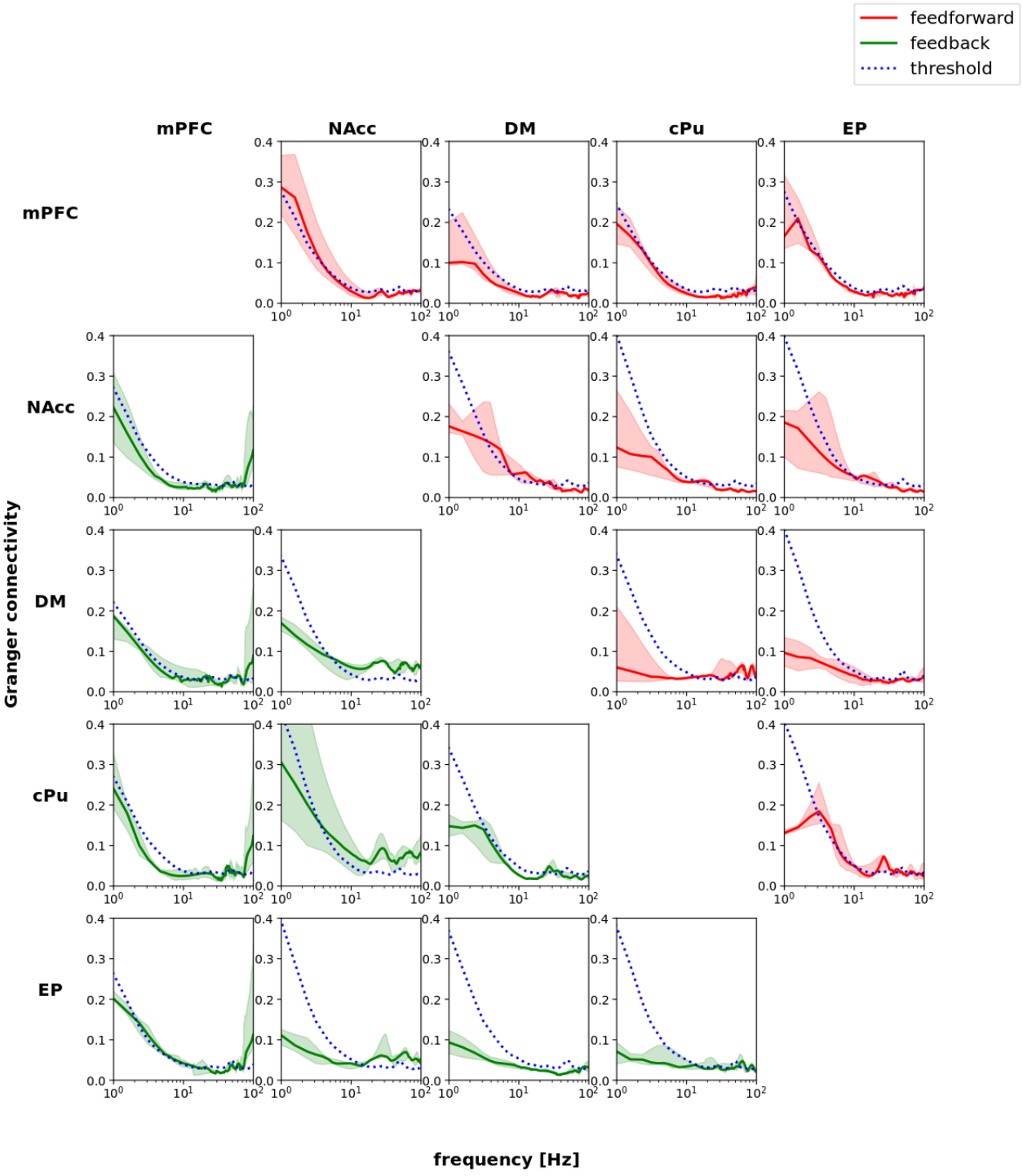

Figure A.15: **Functional connectivity for DAT-tg during baseline in experiment 1** The significance threshold resulting from the permutation test is shown as dotted line. Solid line: median, shaded surface: 25%-75%.

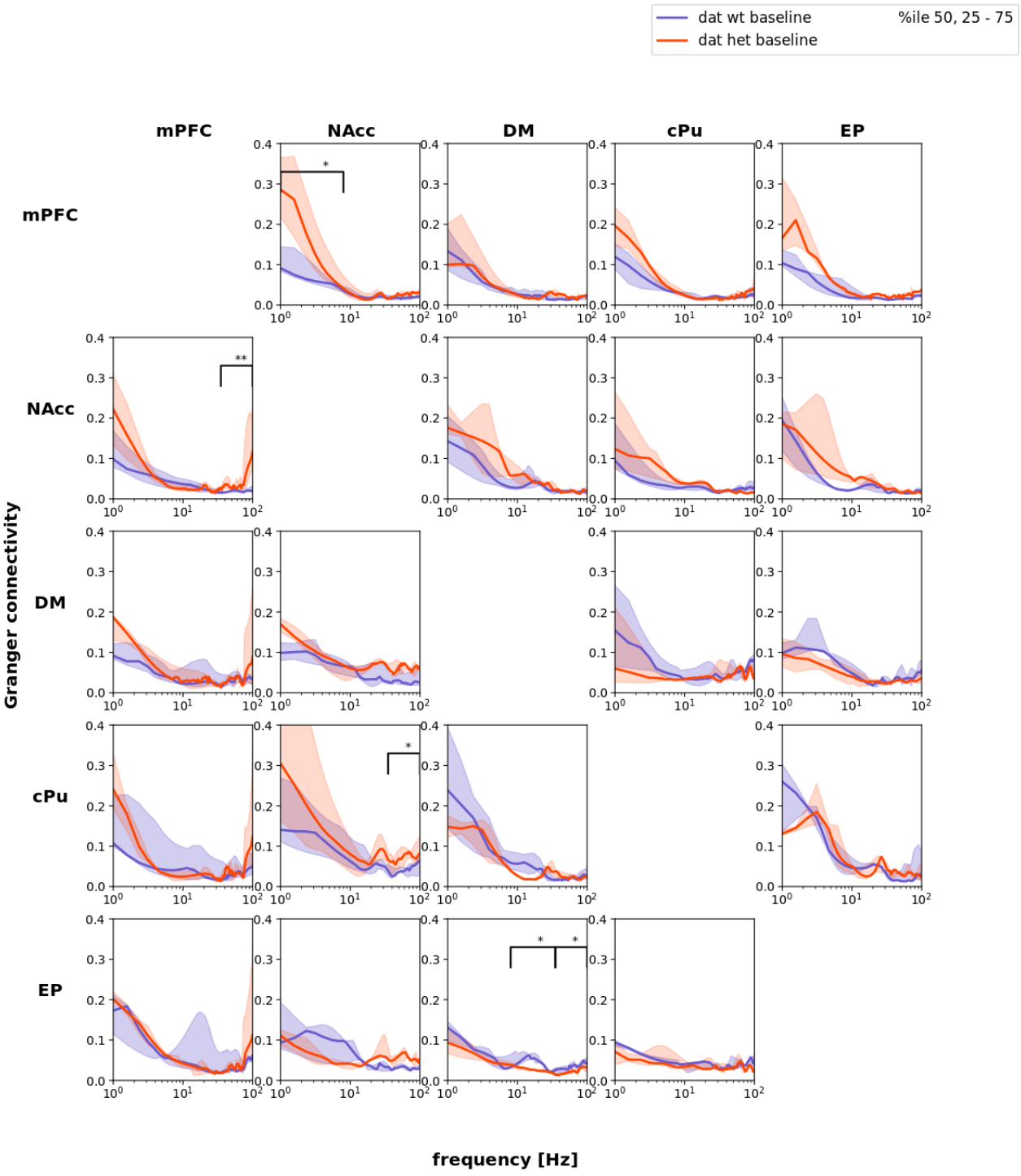

Figure A.16: **Comparison of wt and DAT-tg in the baseline condition in experiment 1** Solid line: median, shaded surface: 25%-75%.

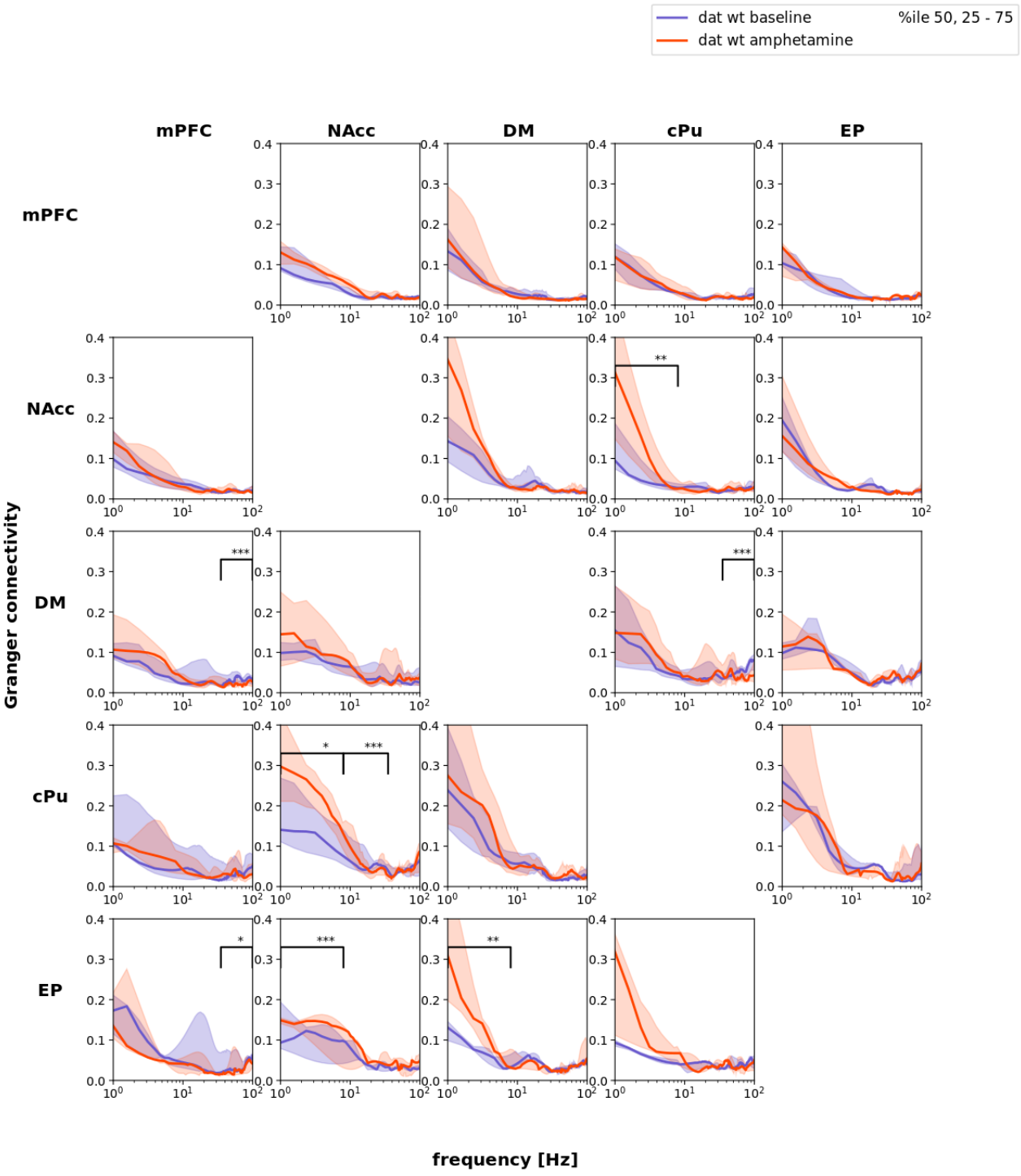

Figure A.17: **Functional connectivity before and during the stereotypic interval in WT in experiment 1** Solid line: median, shaded surface: 25%-75%.

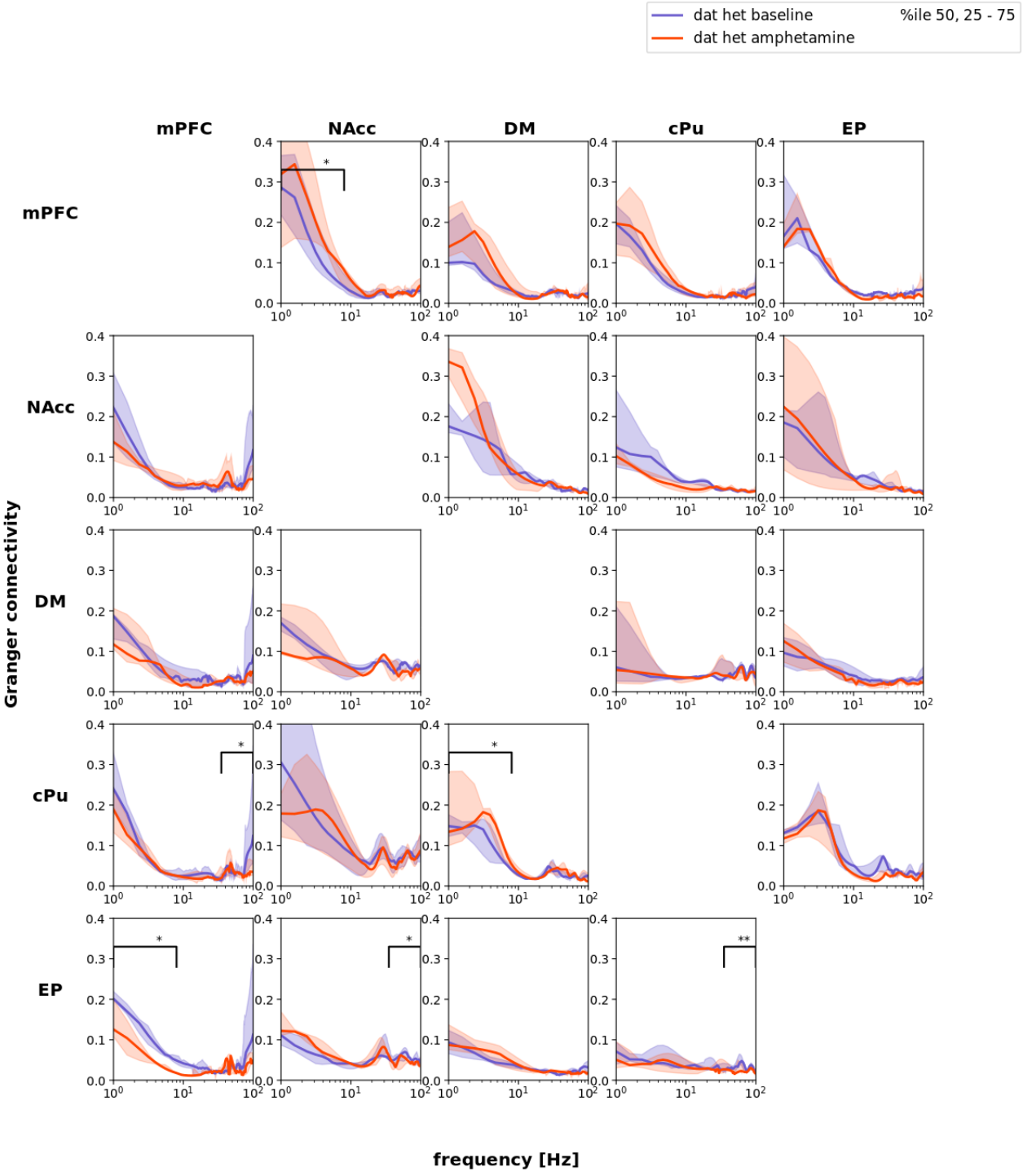

Figure A.18: **Functional connectivity before and during the stereotypic interval in DAT-tg in experiment 1** Solid line: median, shaded surface: 25%-75%.

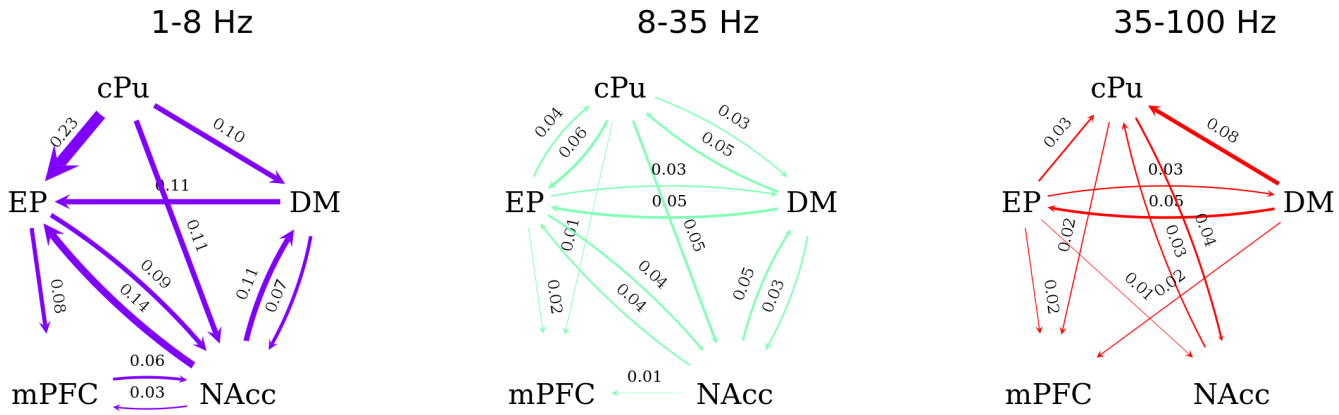

(a)

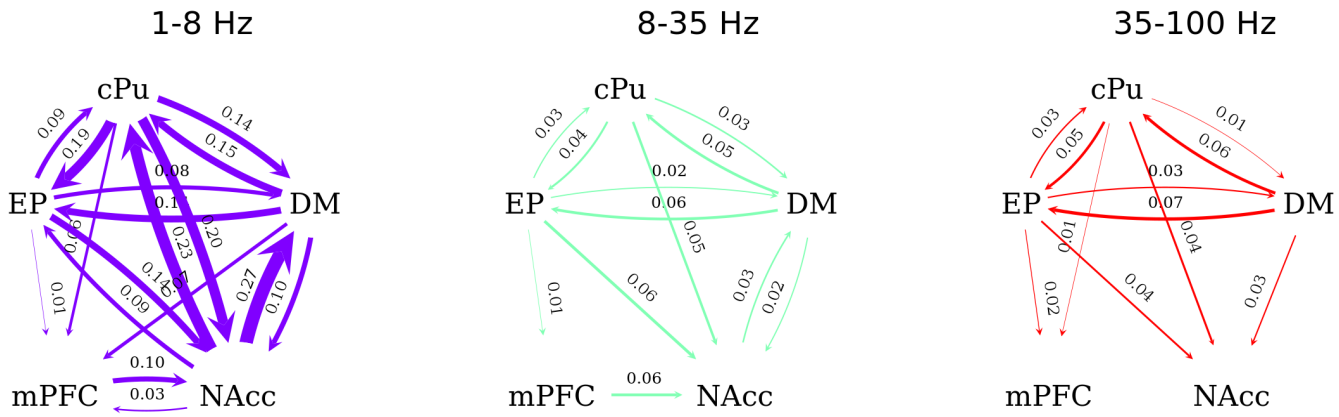

(b)

Figure A.19: Connectivity graph of WT before (a) and during the stereotypy interval (b) in experiment 1

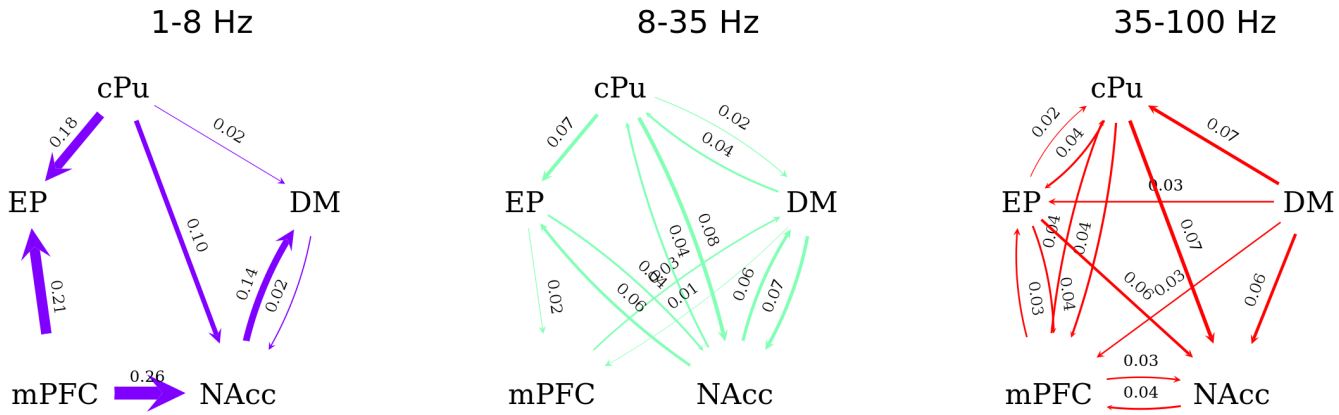

(a)

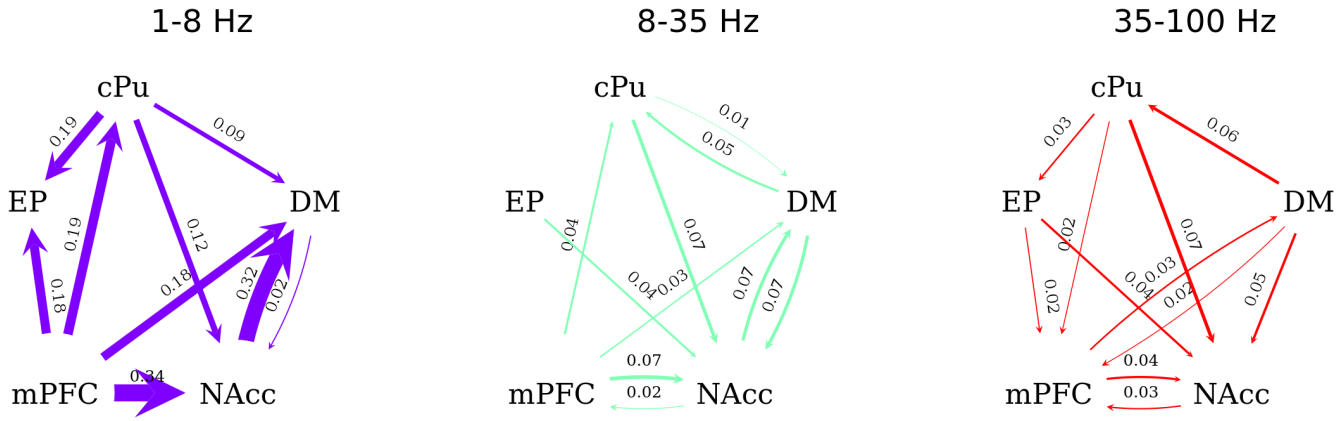

(b)

Figure A.20: Connectivity graph of DAT-tg before (a) and during the stereotypy interval (b) in experiment 1

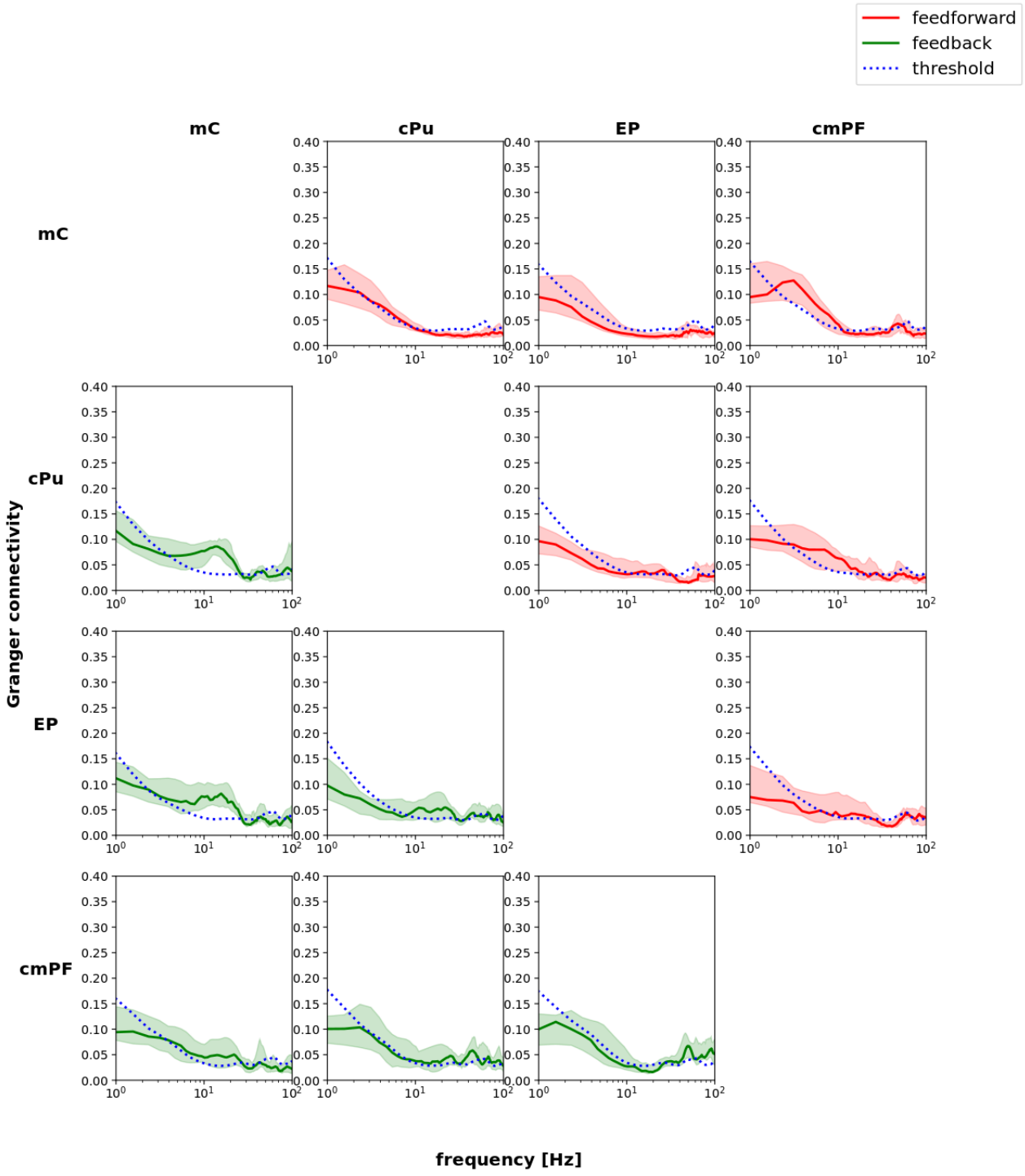

Figure A.21: **Functional connectivity during baseline for WT in experiments 2 and 3 combined** The significance threshold resulting from the permutation test is shown as dotted line. Solid line: median, shaded surface: 25%-75%.

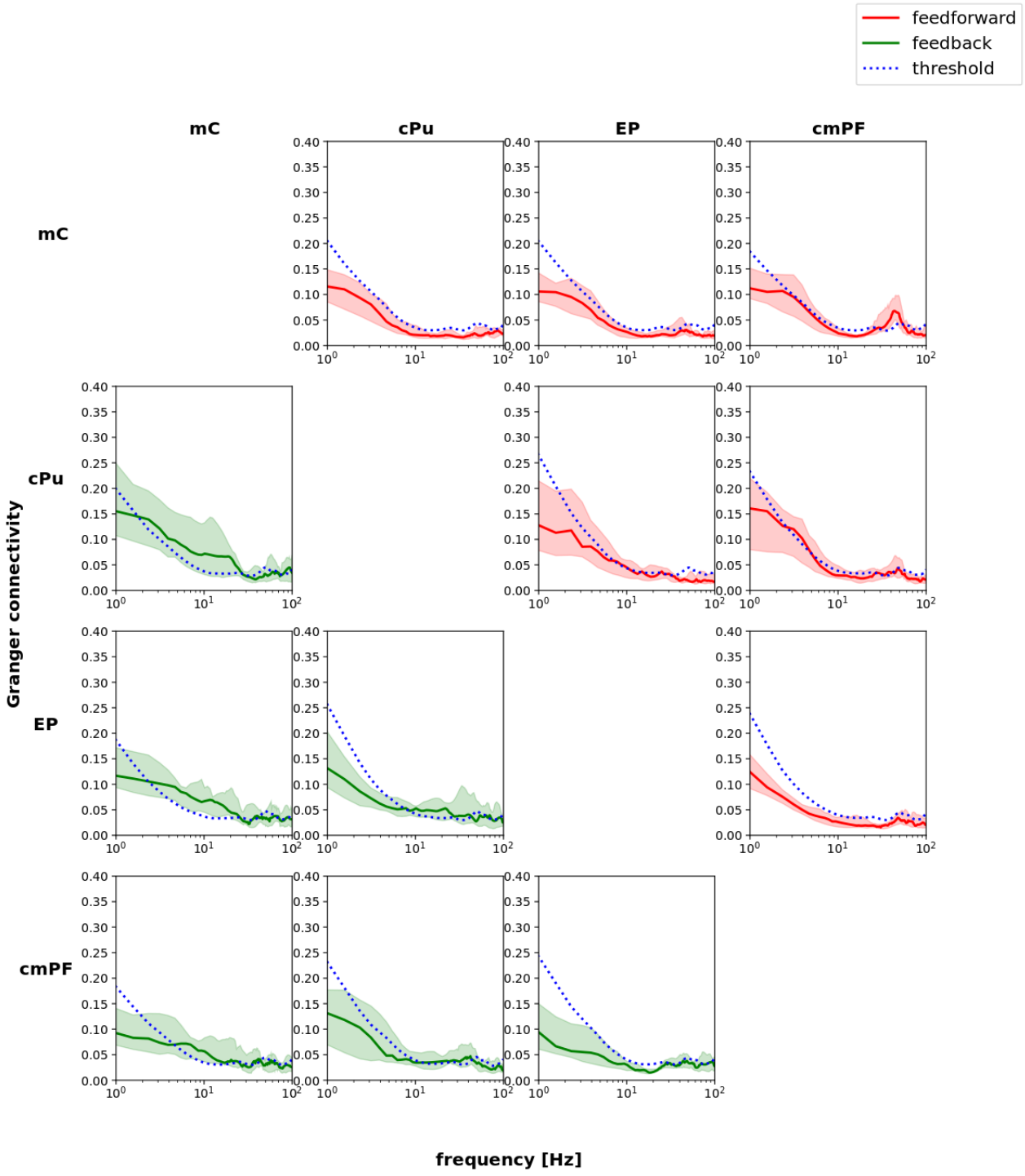

Figure A.22: **Functional connectivity during baseline for DAT-tg in experiments 2 and 3 combined** The significance threshold resulting from the permutation test is shown as dotted line. Solid line: median, shaded surface: 25%-75%.

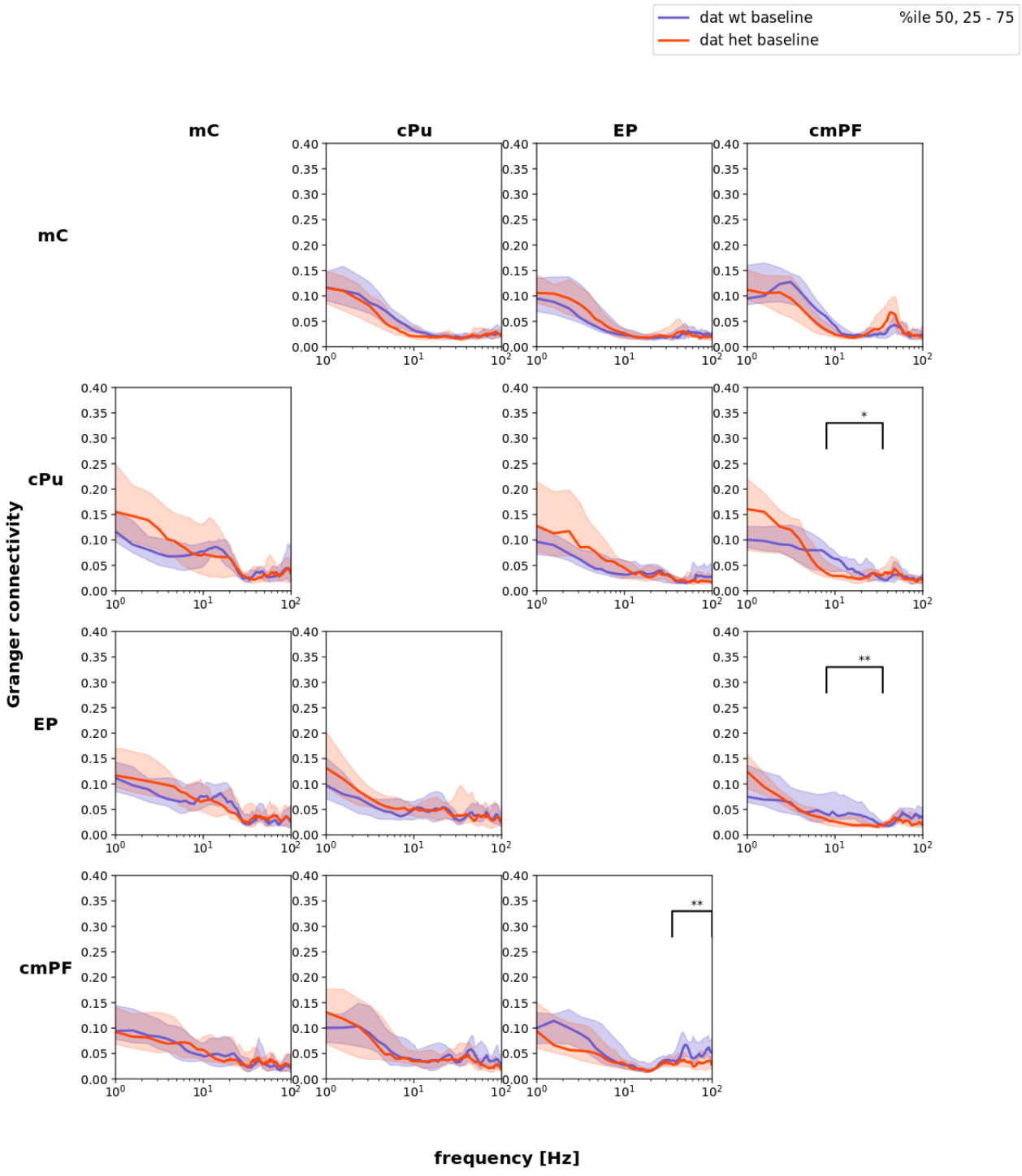

Figure A.23: **Comparison of wt and DAT-tg in the baseline condition in experiments 2 and 3 combined** Solid line: median, shaded surface: 25%-75%.

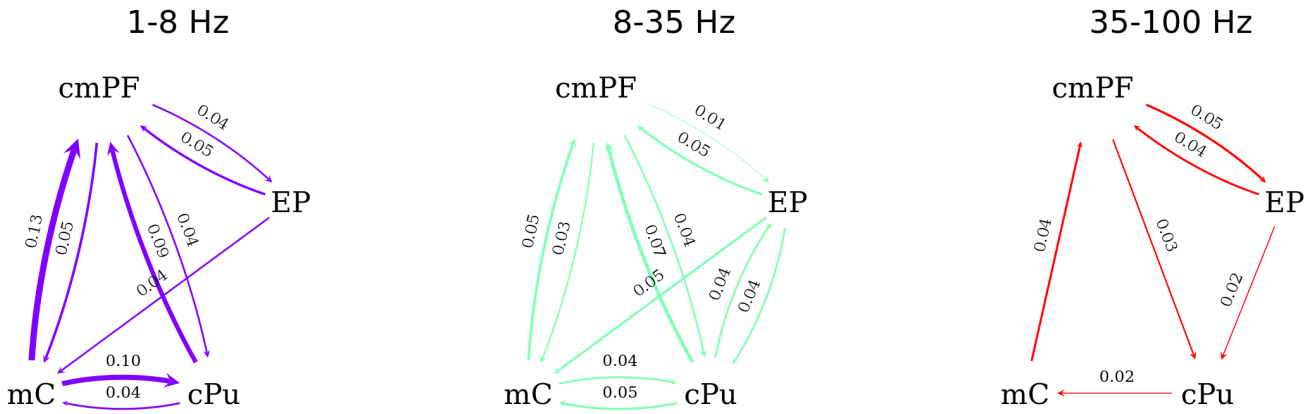

(a)

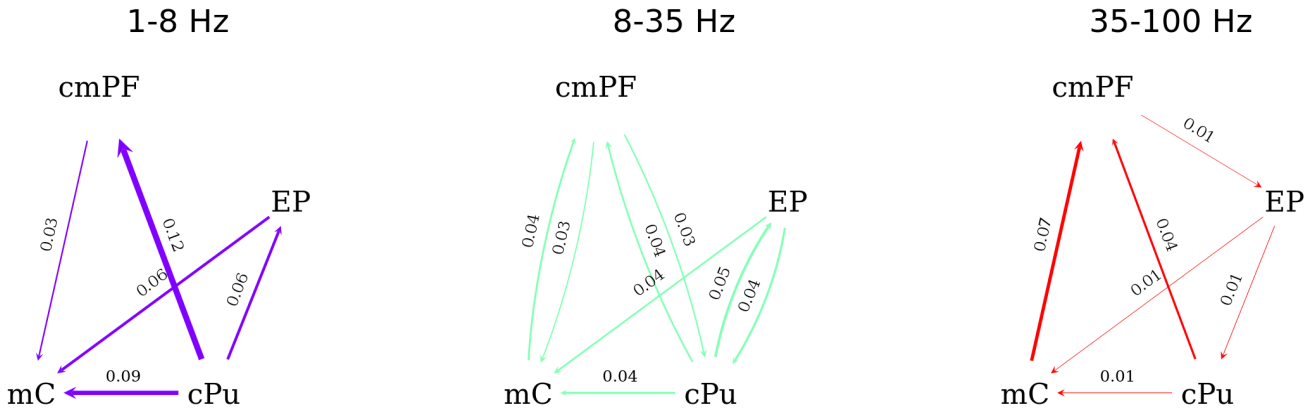

(b)

Figure A.24: Baseline connectivities of WT (a) and DAT-tg (b) in the combined baselines of experiments 2 and 3

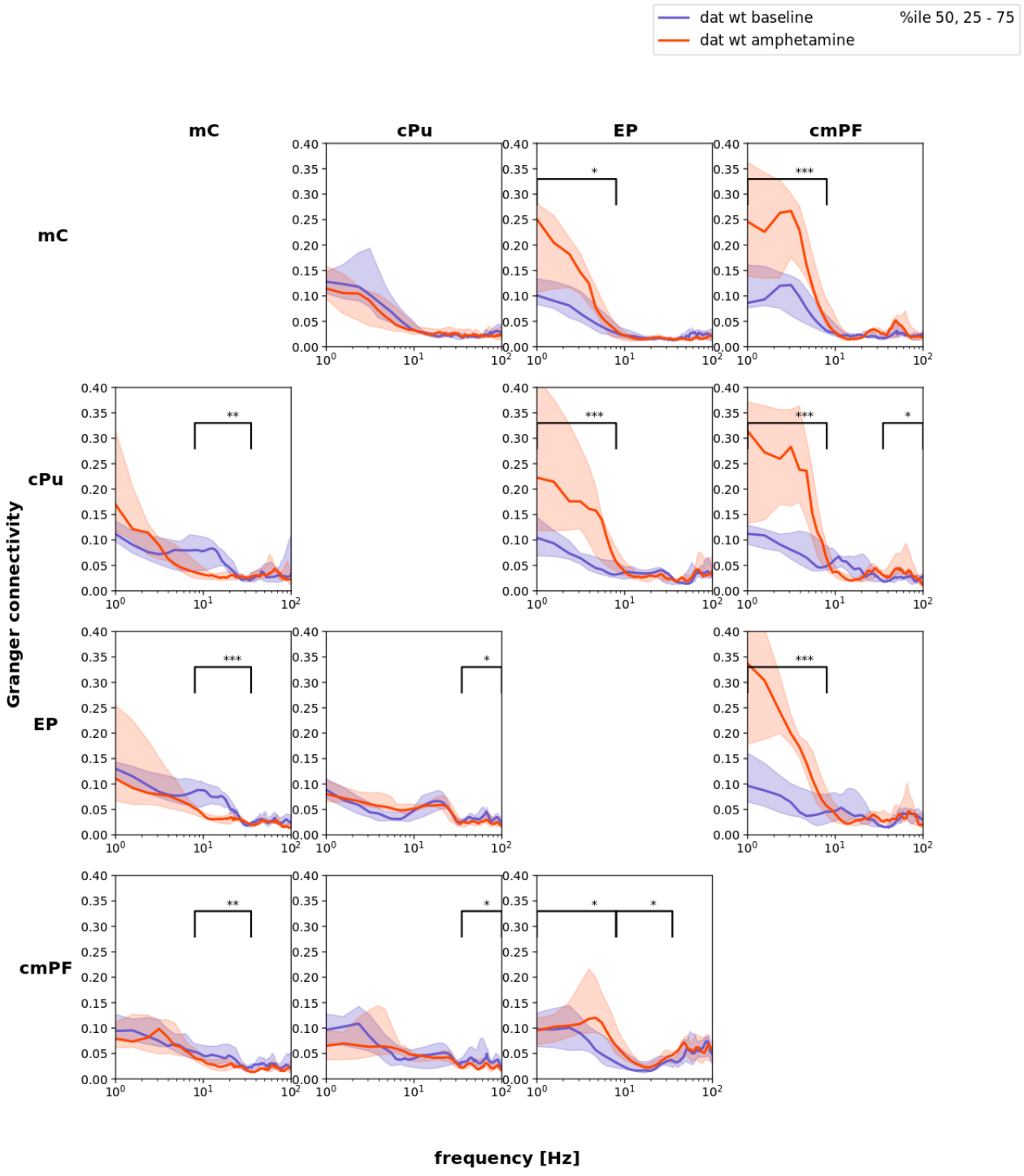

Figure A.25: **Functional connectivity before and during stereotypy interval in WT in experiment 2** Solid line: median, shaded surface: 25%-75%.

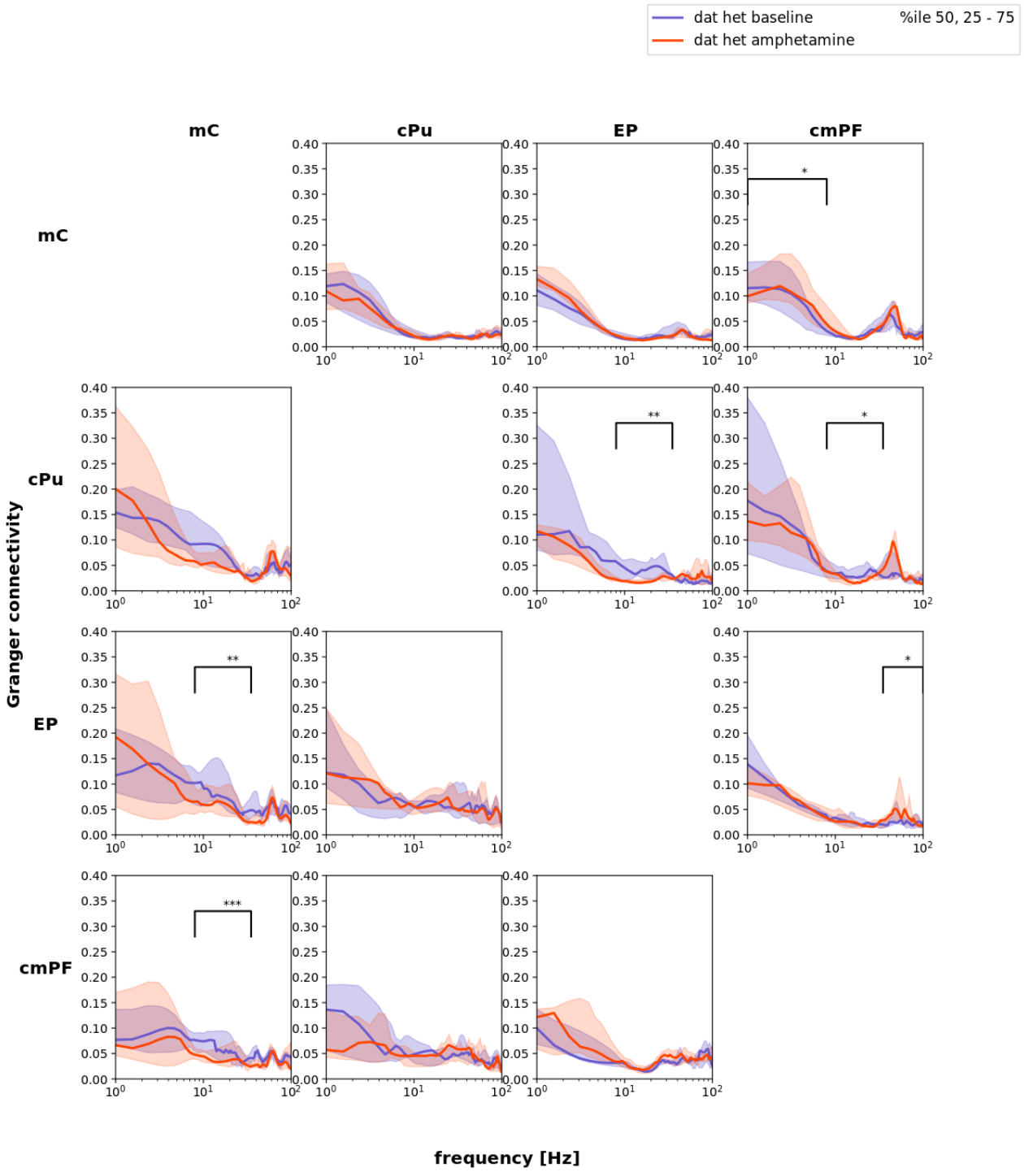

Figure A.26: **Functional connectivity before and during stereotypy interval in DAT-tg in experiment 2** Solid line: median, shaded surface: 25%-75%.

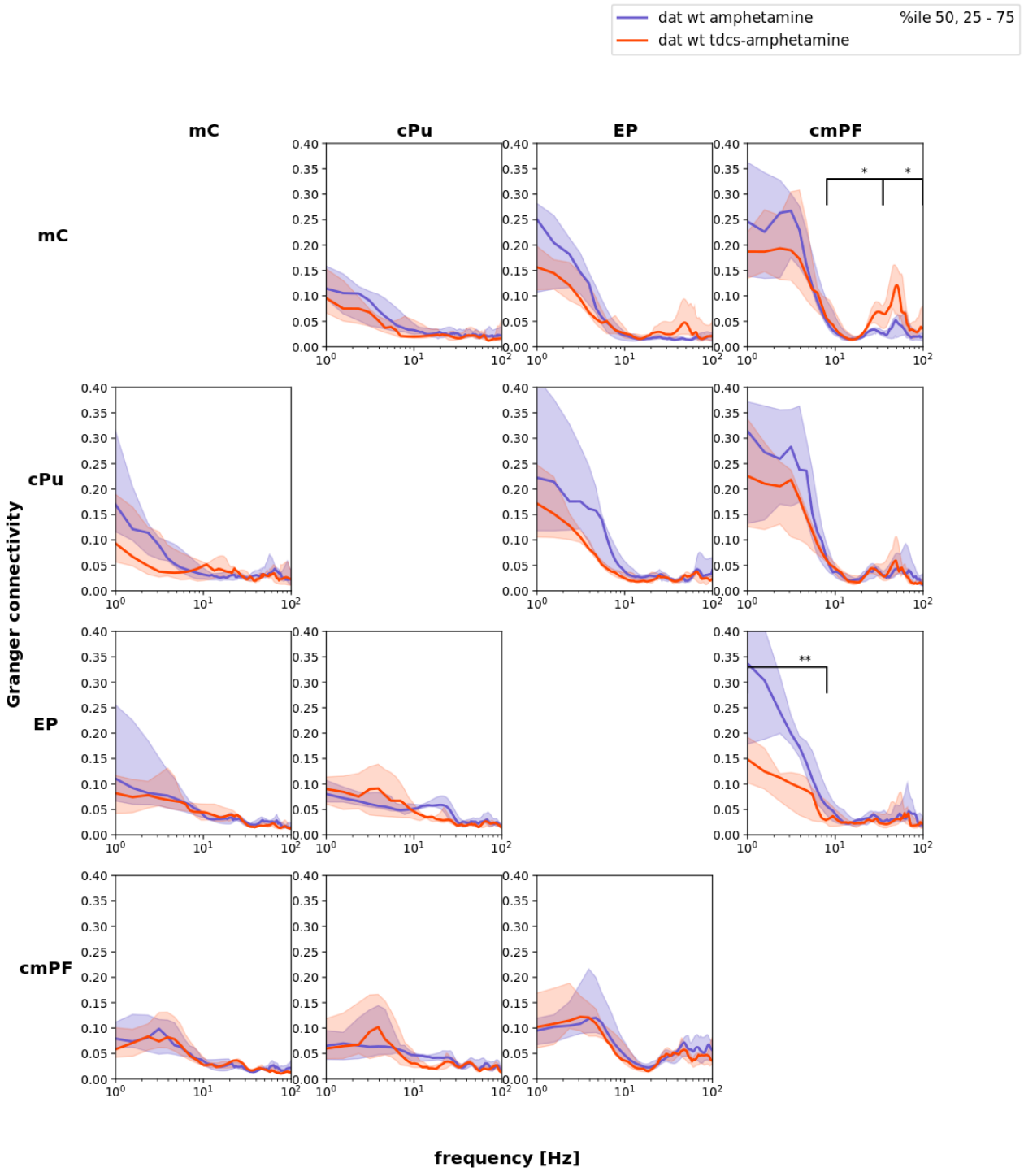

Figure A.27: **Functional connectivity during the stereotypy interval, without (blue) and with (red) tDCS in WT** Solid line: median, shaded surface: 25%-75%.

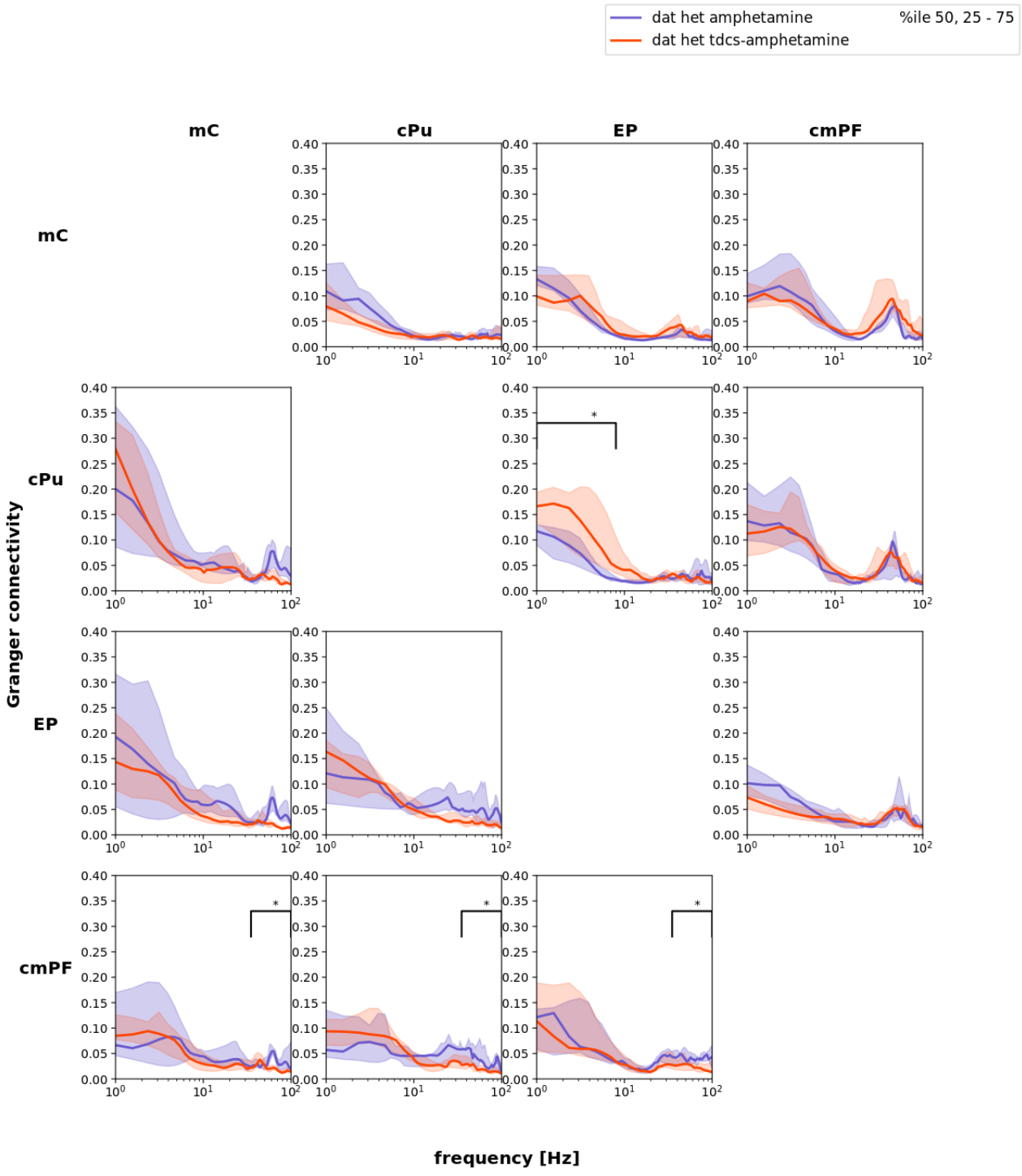

Figure A.28: **Functional connectivity during the stereotypy interval, without (blue) and with (red) tDCS in DAT-tg** Solid line: median, shaded surface: 25%-75%.

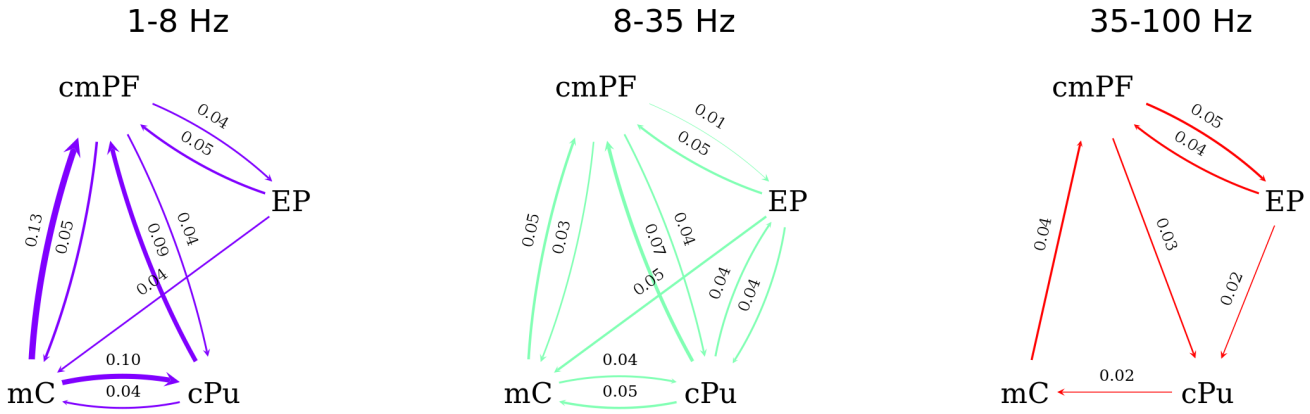

(a)

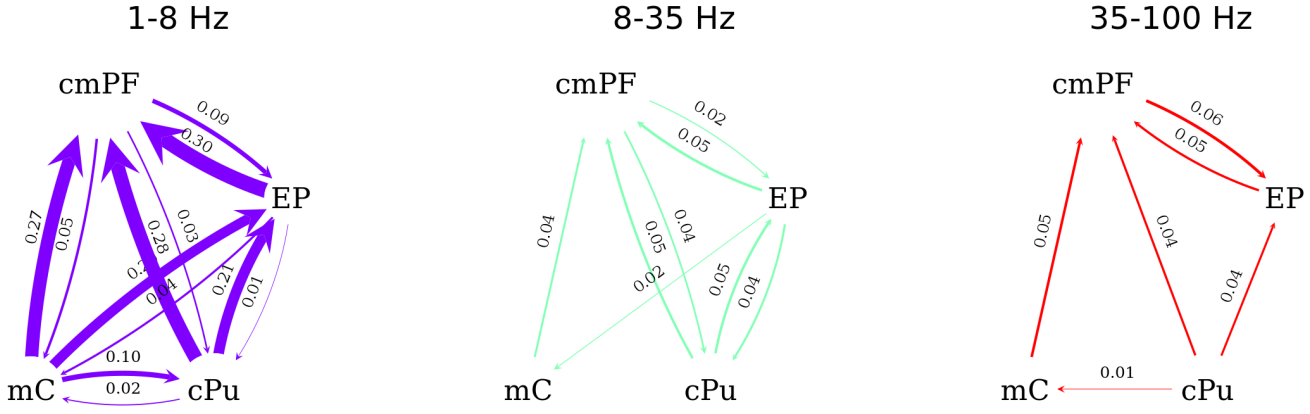

(b)

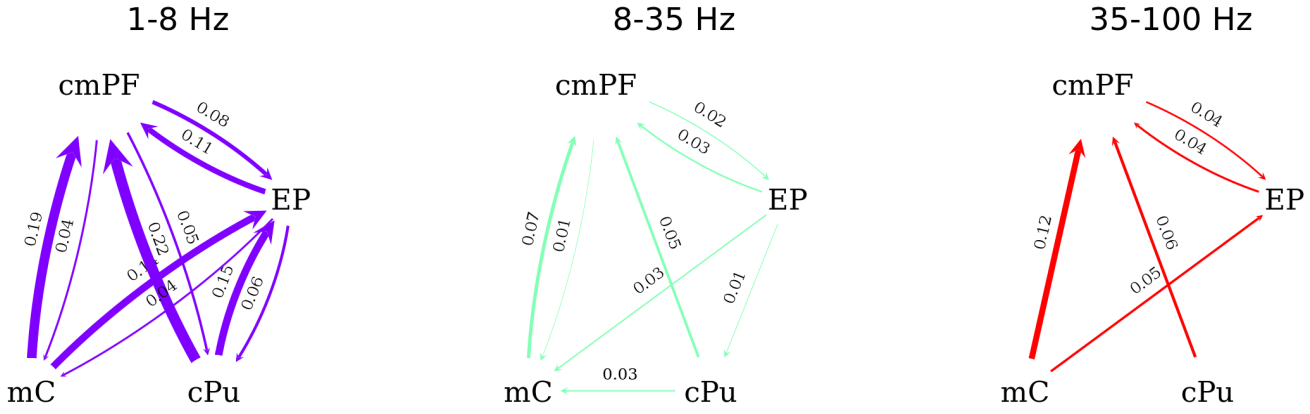

(c)

Figure A.29: **Connectivity graphs for WT during baseline (a), stereotypy interval (b) and stereotypy interval with tDCS (c).**

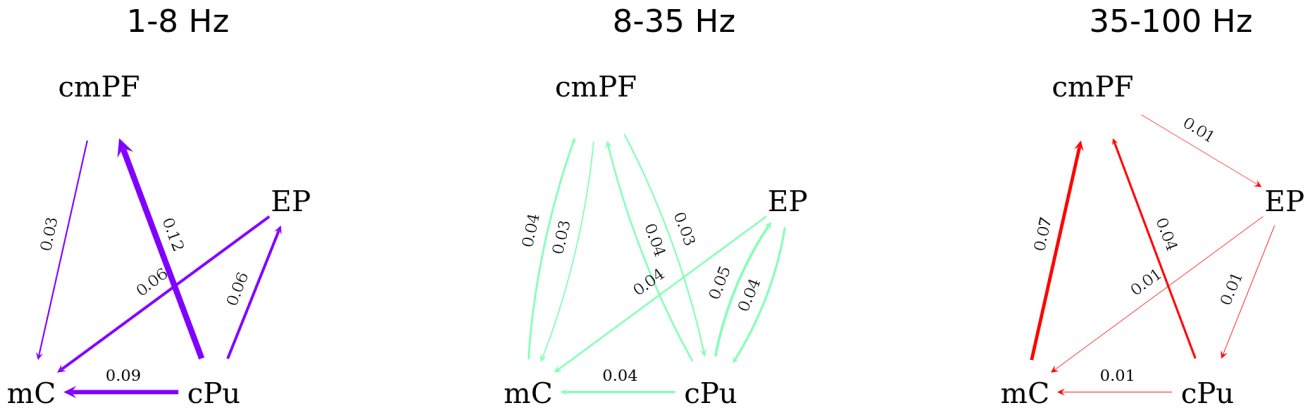

(a)

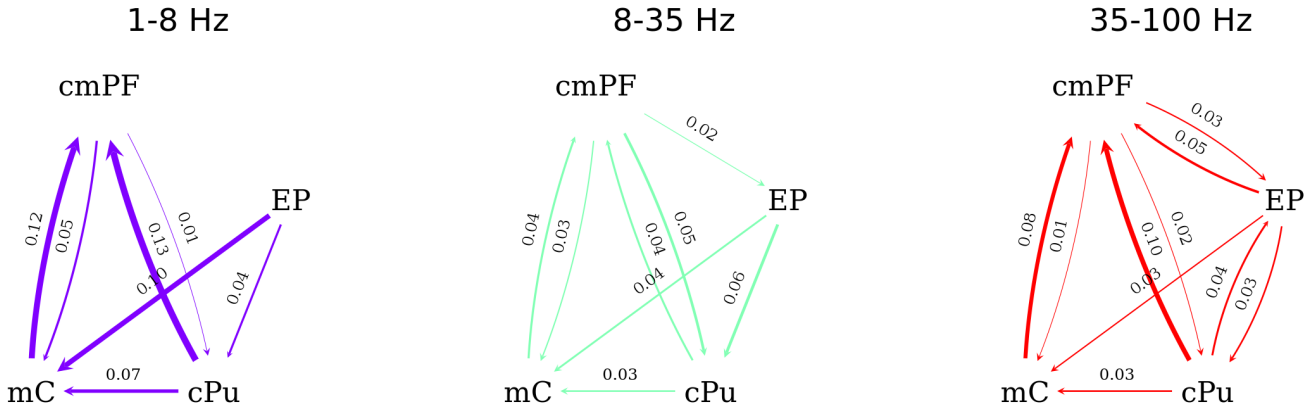

(b)

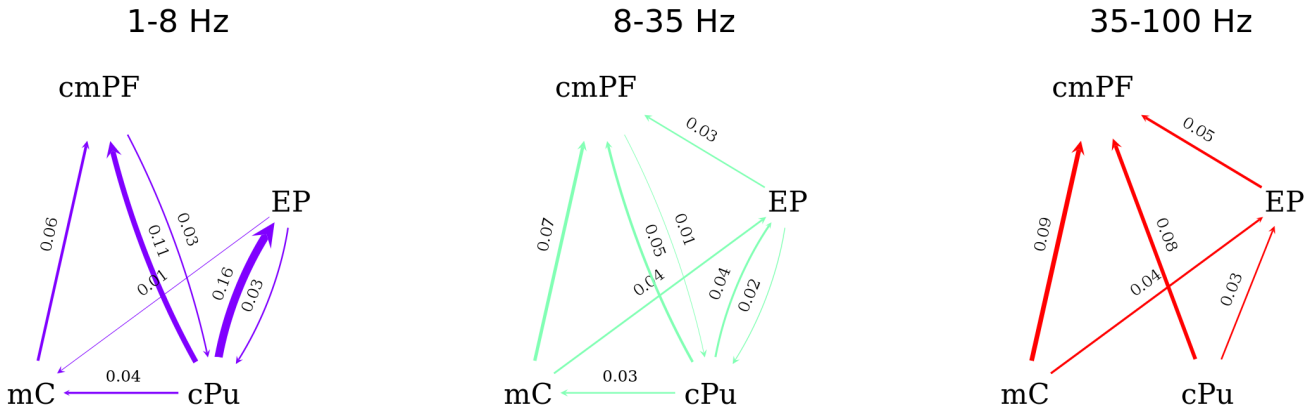

(c)

Figure A.30: Connectivity graphs for DAT-tg during baseline (a), stereotypy interval (b) and stereotypy interval with tDCS (c).

ACRONYMS

DSP digital signal processing 11

DAC digital to analog converter 11

DC direct current 12

AC alternating current 12

FPGA field programmable gate array 11

IIR infinite impulse response 11

LFP local field potential 8

tDCS Transcranial Direct Current Stimulation 5

DOF depth of field 14

TTL transistor–transistor logic 14

AS activated states 17

SW slow wave states 18

DAT dopamine transporter 3

mC motor cortex 15

cPu caudate putamen 10

EP entopeduncular nucleus 8

cmPF centro-medial parafascicular nucleus 8

mPFC medial prefrontal cortex 15

nAcc nucleus accumbens 15

DM dorso-medial thalamus 15

DAT-tg DAT-transgenic viii

LTP long-term potentiation 7

TS Tourette's syndrome 1

wt wild-type 4

BIBLIOGRAPHY

[1] R. J. Felling, and H. S. Singer, "Neurobiology of Tourette Syndrome: Current Status and Need for Further Investigation", Journal of Neuroscience **31**, 12387–12395 (2011) (cit. on pp. 1, 3).

[2] J. L. Taylor, A. K. Rajbhandari, K. C. Berridge, and J. W. Aldridge, "Dopamine receptor modulation of repetitive grooming actions in the rat: Potential relevance for Tourette syndrome", Brain Research **1322**, 92–101 (2010) (cit. on p. 1).

[3] A. P. Association, and A. P. Association, eds., *Diagnostic and statistical manual of mental disorders: DSM-5*, 5th ed (American Psychiatric Association, Washington, D.C, 2013), 947 pp. (cit. on p. 1).

[4] S. Rajagopal, S. Seri, and A. E. Cavanna, "Premonitory Urges and Sensorimotor Processing in Tourette Syndrome", Behavioural Neurology **27**, 65–73 (2013) (cit. on p. 1).

[5] H. S. Singer, "Motor control, habits, complex motor stereotypies, and Tourette syndrome: Motor control, habits, CMS, and TS", Annals of the New York Academy of Sciences **1304**, 22–31 (2013) (cit. on pp. 1–3).

[6] F. Augustine, and H. S. Singer, "Merging the Pathophysiology and Pharmacotherapy of Tics", 18 (2019) (cit. on p. 2).

[7] K. S. P. McNaught, and J. W. Mink, "Advances in understanding and treatment of Tourette syndrome", Nature Reviews Neurology **7**, 667–676 (2011) (cit. on pp. 2, 35).

[8] A. J. D. Nelson, and S. Killcross, "Accelerated habit formation following amphetamine exposure is reversed by D1, but enhanced by D2, receptor antagonists", Frontiers in Neuroscience **7** (2013) 10.3389/fnins.2013.00076 (cit. on p. 2).

[9] K. J. Black, and J. W. Mink, "Response to levodopa challenge in Tourette syndrome", Movement Disorders **15**, 1194–1198 (2000) (cit. on p. 2).

[10]L. Lykouras, B. Alevizos, P. Michalopoulou, and A. Rabavilas, "Obsessive–compulsive symptoms induced by atypical antipsychotics. A review of the reported cases", Progress in Neuro-Psychopharmacology and Biological Psychiatry **27**, 333–346 (2003) (cit. on p. 2).

[11]S. B. Floresco, A. R. West, B. Ash, H. Moore, and A. A. Grace, "Afferent modulation of dopamine neuron firing differentially regulates tonic and phasic dopamine transmission", Nature Neuroscience **6**, 968–973 (2003) (cit. on p. 3).

[12]A. Grace, "Phasic versus tonic dopamine release and the modulation of dopamine system responsivity: A hypothesis for the etiology of schizophrenia", Neuroscience **41**, 1–24 (1991) (cit. on p. 3).

[13]W. Schultz, "Multiple Dopamine Functions at Different Time Courses", Annual Review of Neuroscience **30**, 259–288 (2007) (cit. on p. 3).

[14]D. F. Wong, J. R. Brašić, H. S. Singer, D. J. Schretlen, H. Kuwabara, Y. Zhou, A. Nandi, M. A. Maris, M. Alexander, W. Ye, O. Rousset, A. Kumar, Z. Szabo, A. Gjedde, and A. A. Grace, "Mechanisms of Dopaminergic and Serotonergic Neurotransmission in Tourette Syndrome: Clues from an In Vivo Neurochemistry Study with PET", Neuropsychopharmacology **33**, 1239–1251 (2008) (cit. on p. 3).

[15]T. V. Maia, and V. A. Conceição, "Dopaminergic Disturbances in Tourette Syndrome: An Integrative Account", Biological Psychiatry **84**, 332–344 (2018) (cit. on p. 3).

[16]A. S. Hart, R. B. Rutledge, P. W. Glimcher, and P. E. M. Phillips, "Phasic Dopamine Release in the Rat Nucleus Accumbens Symmetrically Encodes a Reward Prediction Error Term", The Journal of Neuroscience **34**, 698–704 (2014) (cit. on p. 3).

[17]W. Schultz, P. Dayan, and P. R. Montague, "A Neural Substrate of Prediction and Reward", Science, 8 (1997) (cit. on p. 3).

[18]T. V. Maia, and V. A. Conceição, "The Roles of Phasic and Tonic Dopamine in Tic Learning and Expression", Biological Psychiatry **82**, 401–412 (2017) (cit. on p. 3).

[19]D. J. Surmeier, J. Ding, M. Day, Z. Wang, and W. Shen, "D1 and D2 dopamine-receptor modulation of striatal glutamatergic signaling in striatal medium spiny neurons", Trends in Neurosciences **30**, 228–235 (2007) (cit. on p. 3).

[20]M. S. Sonders, S.-J. Zhu, N. R. Zahniser, M. P. Kavanaugh, and S. G. Amara, "Multiple Ionic Conductances of the Human Dopamine Transporter: The Actions of Dopamine and Psychostimulants", The Journal of Neuroscience **17**, 960–974 (1997) (cit. on p. 3).

[21]B. D. Richardson, K. Saha, D. Krout, E. Cabrera, B. Felts, L. K. Henry, J. Swant, M.-F. Zou, A. H. Newman, and H. Khoshbouei, "Membrane potential shapes regulation of dopamine transporter trafficking at the plasma membrane", Nature Communications **7**, 10423 (2016) (cit. on p. 3).

[22]K. C. Berridge, J. W. Aldridge, K. R. Houchard, and X. Zhuang, "Sequential super-stereotypy of an instinctive fixed action pattern in hyper-dopaminergic mutant mice: a model of obsessive compulsive disorder and Tourette's", BMC Biology, 16 (2005) (cit. on p. 4).

[23]A. Salahpour, A. J. Ramsey, I. O. Medvedev, B. Kile, T. D. Sotnikova, E. Holmstrand, V. Ghisi, P. J. Nicholls, L. Wong, K. Murphy, S. R. Sesack, R. M. Wightman, R. R. Gainetdinov, and M. G. Caron, "Increased amphetamine-induced hyperactivity and reward in mice overexpressing the dopamine transporter", Proceedings of the National Academy of Sciences **105**, 4405–4410 (2008) (cit. on p. 4).

[24]D. Sulzer, M. S. Sonders, N. W. Poulsen, and A. Galli, "Mechanisms of neurotransmitter release by amphetamines: A review", Progress in Neurobiology **75**, 406–433 (2005) (cit. on p. 4).

[25]R. Hadar, H. Edemann-Callesen, C. Reinel, F. Wieske, M. Voget, E. Popova, R. Sohr, Y. Avchalumov, J. Priller, C. van Riesen, I. Puls, M. Bader, and C. Winter, "Rats overexpressing the dopamine transporter display behavioral and neurobiological abnormalities with relevance to repetitive disorders", Scientific Reports **6** (2016) 10.1038/srep39145 (cit. on pp. 4, 15, 17, 25, 38).

[26]K. Antoniou, E. Kafetzopoulos, Z. Papadopoulou-Daifoti, T. Hyphantis, and M. Marselos, "D-amphetamine, cocaine and caffeine: a comparative study of acute effects on locomotor activity and behavioural patterns in rats", Neuroscience & Biobehavioral Reviews **23**, 189–196 (1998) (cit. on p. 4).

[27] R. Hadar, H. Edemann-Callesen, C. Reinel, F. Wieske, M. Voget, E. Popova, R. Sohr, Y. Avchalumov, J. Priller, and C. Van Riesen, "Rats overexpressing the dopamine transporter display behavioral and neurobiological abnormalities with relevance to repetitive disorders", Scientific reports **6**, 39145 (2016) (cit. on pp. 5, 17, 33).

[28] N. Bernhardt, M. K. Lieser, E.-B. Hlusicka, B. Habelt, F. Wieske, H. Edemann-Callesen, A. Garthe, and C. Winter, "Learning deficits in rats overexpressing the dopamine transporter", Scientific Reports **8** (2018) 10.1038/s41598-018-32608-7 (cit. on pp. 5, 25, 33).

[29] M. P. Jackson, A. Rahman, B. Lafon, G. Kronberg, D. Ling, L. C. Parra, and M. Bikson, "Animal models of transcranial direct current stimulation: Methods and mechanisms", Clinical Neurophysiology **127**, 3425–3454 (2016) (cit. on pp. 6–8).

[30] A. Rahman, D. Reato, M. Arlotti, F. Gasca, A. Datta, L. C. Parra, and M. Bikson, "Cellular effects of acute direct current stimulation: somatic and synaptic terminal effects: Somatic and terminal origin of DCS effects", The Journal of Physiology **591**, 2563–2578 (2013) (cit. on p. 6).

[31] A.-K. Gellner, J. Reis, and B. Fritsch, "Glia: A Neglected Player in Non-invasive Direct Current Brain Stimulation", Frontiers in Cellular Neuroscience **10** (2016) 10.3389/fncel.2016.00188 (cit. on p. 7).

[32] T. Radman, Y. Su, J. H. An, L. C. Parra, and M. Bikson, "Spike Timing Amplifies the Effect of Electric Fields on Neurons: Implications for Endogenous Field Effects", Journal of Neuroscience **27**, 3030–3036 (2007) (cit. on p. 7).

[33] D. Desmaisons, J.-D. Vincent, and P.-M. Lledo, "Control of action potential timing by intrinsic subthreshold oscillations in olfactory bulb output neurons", The Journal of Neuroscience **19**, 10727–10737 (1999) (cit. on p. 7).

[34] M. A. Nitsche, and W. Paulus, "Excitability changes induced in the human motor cortex by weak transcranial direct current stimulation", The Journal of Physiology **527**, 633–639 (2000) (cit. on p. 7).

[35]J. Marquez-Ruiz, R. Leal-Campanario, R. Sanchez-Campusano, B. Molaee-Ardekani, F. Wendling, P. C. Miranda, G. Ruffini, A. Gruart, and J. M. Delgado-Garcia, "Transcranial direct-current stimulation modulates synaptic mechanisms involved in associative learning in behaving rabbits", Proceedings of the National Academy of Sciences **109**, 6710–6715 (2012) (cit. on p. 7).

[36]B. Fritsch, J. Reis, K. Martinowich, H. M. Schambra, Y. Ji, L. G. Cohen, and B. Lu, "Direct Current Stimulation Promotes BDNF-Dependent Synaptic Plasticity: Potential Implications for Motor Learning", Neuron **66**, 198–204 (2010) (cit. on p. 7).

[37]C. A. Anastassiou, and C. Koch, "Ephaptic coupling to endogenous electric field activity: why bother?", Current Opinion in Neurobiology **31**, 95–103 (2015) (cit. on p. 7).

[38]C. A. Anastassiou, R. Perin, H. Markram, and C. Koch, "Ephaptic coupling of cortical neurons", Nature Neuroscience **14**, 217–223 (2011) (cit. on p. 7).

[39]D. Reato, A. Rahman, M. Bikson, and L. C. Parra, "Low-Intensity Electrical Stimulation Affects Network Dynamics by Modulating Population Rate and Spike Timing", Journal of Neuroscience **30**, 15067–15079 (2010) (cit. on p. 7).

[40]D. Reato, A. Rahman, M. Bikson, and L. C. Parra, "Effects of weak transcranial alternating current stimulation on brain activity—a review of known mechanisms from animal studies", Frontiers in Human Neuroscience **7** (2013) 10.3389/fnhum.2013.00687 (cit. on p. 7).

[41]A. Y. Kabakov, P. A. Muller, A. Pascual-Leone, F. E. Jensen, and A. Rotenberg, "Contribution of axonal orientation to pathway-dependent modulation of excitatory transmission by direct current stimulation in isolated rat hippocampus", Journal of Neurophysiology **107**, 1881–1889 (2012) (cit. on p. 8).

[42]L. Bour, L. Ackermans, E. Foncke, D. Cath, C. van der Linden, V. Visser Vandewalle, and M. Tijssen, "Tic related local field potentials in the thalamus and the effect of deep brain stimulation in Tourette syndrome: Report of three cases", Clinical Neurophysiology **126**, 1578–1588 (2015) (cit. on pp. 8, 36).

[43]J. Jimenez-Shahed, I. Telkes, A. Viswanathan, and N. F. Ince, "GPi Oscillatory Activity Differentiates Tics from the Resting State, Voluntary Movements, and the Unmedicated Parkinsonian State", Frontiers in Neuroscience **10** (2016) 10.3389/fnins.2016.00436 (cit. on p. 8).

[44]G.-J. Ji, W. Liao, Y. Yu, H.-H. Miao, Y.-X. Feng, K. Wang, J.-H. Feng, and Y.-F. Zang, "Globus Pallidus Interna in Tourette Syndrome: Decreased Local Activity and Disrupted Functional Connectivtiy", Frontiers in Neuroanatomy **10** (2016) 10.3389/fnana.2016.00093 (cit. on p. 8).

[45]S. Marceglia, D. Servello, G. Foffani, M. Porta, M. Sassi, S. Mrakic-Sposta, M. Rosa, S. Barbieri, and A. Priori, "Thalamic single-unit and local field potential activity in Tourette syndrome: Thalamic Activity in TS", Movement Disorders **25**, 300–308 (2010) (cit. on pp. 8, 36).

[46]A. Priori, G. Giannicola, M. Rosa, S. Marceglia, D. Servello, M. Sassi, and M. Porta, "Deep brain electrophysiological recordings provide clues to the pathophysiology of Tourette syndrome", Neuroscience & Biobehavioral Reviews **37**, 1063–1068 (2013) (cit. on pp. 8, 9, 34, 36).

[47]J. L. Houeto, "Tourette's syndrome and deep brain stimulation", Journal of Neurology, Neurosurgery & Psychiatry **76**, 992–995 (2005) (cit. on p. 8).

[48]M. S. Okun, K. D. Foote, S. S. Wu, H. E. Ward, D. Bowers, R. L. Rodriguez, I. A. Malaty, W. K. Goodman, D. M. Gilbert, H. C. Walker, J. W. Mink, S. Merritt, T. Morishita, and J. C. Sanchez, "A Trial of Scheduled Deep Brain Stimulation for Tourette Syndrome: Moving Away From Continuous Deep Brain Stimulation Paradigms", JAMA Neurology **70**, 85–94 (2013) (cit. on pp. 8, 37).

[49]J. B. Shute, M. S. Okun, E. Opri, R. Molina, P. J. Rossi, D. Martinez-Ramirez, K. D. Foote, and A. Gunduz, "Thalamocortical network activity enables chronic tic detection in humans with Tourette syndrome", NeuroImage: Clinical **12**, 165–172 (2016) (cit. on p. 8).

[50]S. Marceglia, M. Rosa, D. Servello, M. Porta, S. Barbieri, E. Moro, and A. Priori, "Adaptive Deep Brain Stimulation (aDBS) for Tourette Syndrome", Brain Sciences **8**, 4 (2017) (cit. on p. 8).

[51]P. Zhuang, M. Hallett, X. Zhang, J. Li, Y. Zhang, and Y. Li, "Neuronal activity in the globus pallidus internus in patients with tics", Journal of Neurology, Neurosurgery & Psychiatry **80**, 1075–1081 (2009) (cit. on p. 8).

[52]Y. Worbe, L. Marrakchi-Kacem, S. Lecomte, R. Valabregue, F. Poupon, P. Guevara, A. Tucholka, J.-F. Mangin, M. Vidailhet, S. Lehericy, A. Hartmann, and C. Poupon, "Altered structural connectivity of cortico-striato-pallido-thalamic networks in Gilles de la Tourette syndrome", Brain **138**, 472–482 (2015) (cit. on p. 9).

[53]L. Zapparoli, M. Tettamanti, M. Porta, A. Zerbi, D. Servello, G. Banfi, and E. Paulesu, "A tug of war: antagonistic effective connectivity patterns over the motor cortex and the severity of motor symptoms in Gilles de la Tourette syndrome", European Journal of Neuroscience **46**, 2203–2213 (2017) (cit. on p. 9).

[54]A. Antal, R. Polania, C. Schmidt-Samoa, P. Dechent, and W. Paulus, "Transcranial direct current stimulation over the primary motor cortex during fMRI", NeuroImage **55**, 590–596 (2011).

[55]Z. Wang, T. V. Maia, R. Marsh, T. Colibazzi, A. Gerber, and B. S. Peterson, "The Neural Circuits That Generate Tics in Tourette's Syndrome", American Journal of Psychiatry **168**, 1326–1337 (2011) (cit. on p. 9).

[56]G. Thomalla, M. Jonas, T. Bäumer, H. R. Siebner, K. Biermann-Ruben, C. Ganos, M. Orth, F. C. Hummel, C. Gerloff, K. Müller-Vahl, A. Schnitzler, and A. Münchau, "Costs of control: decreased motor cortex engagement during a Go/NoGo task in Tourette's syndrome", Brain **137**, 122–136 (2014) (cit. on pp. 9, 35).

[57]D. J. Serrien, "Motor inhibition in patients with Gilles de la Tourette syndrome: functional activation patterns as revealed by EEG coherence", Brain **128**, 116–125 (2004) (cit. on p. 9).

[58]U. Amadi, A. Ilie, H. Johansen-Berg, and C. J. Stagg, "Polarity-specific effects of motor transcranial direct current stimulation on fMRI resting state networks", NeuroImage **88**, 155–161 (2014) (cit. on pp. 9, 35).

[59]D. Keeser, T. Meindl, J. Bor, U. Palm, O. Pogarell, C. Mulert, J. Brunelin, H.-J. Moller, M. Reiser, and F. Padberg, "Prefrontal Transcranial Direct Current Stimulation Changes Connectivity of Resting-State Networks during fMRI", Journal of Neuroscience **31**, 15284–15293 (2011) (cit. on pp. 9, 35).

[60]M. A. Hunter, B. A. Coffman, C. Gasparovic, V. D. Calhoun, M. C. Trumbo, and V. P. Clark, "Baseline effects of transcranial direct current stimulation on glutamatergic neurotransmission and large-scale network connectivity", Brain Research **1594**, 92–107 (2015) (cit. on pp. 9, 35).

[61]N. Behler, B. Leitner, E. Mezger, E. Weidinger, R. Musil, B. Blum, B. Kirsch, L. Wulf, L. Löhrs, C. Winter, F. Padberg, and U. Palm, "Cathodal tDCS Over Motor Cortex Does Not Improve Tourette Syndrome: Lessons Learned From a Case Series", Frontiers in Behavioral Neuroscience **12** (2018) 10.3389/fnbeh.2018.00194 (cit. on p. 9).

[62]R. Polanía, W. Paulus, and M. A. Nitsche, "Modulating cortico-striatal and thalamo-cortical functional connectivity with transcranial direct current stimulation", Human Brain Mapping **33**, 2499–2508 (2012) (cit. on pp. 9, 35, 37).

[63]A. Priori, G. Foffani, A. Pesenti, F. Tamma, A. Bianchi, M. Pellegrini, M. Locatelli, K. Moxon, and R. Villani, "Rhythm-specific pharmacological modulation of subthalamic activity in Parkinson's disease", Experimental Neurology **189**, 369–379 (2004) (cit. on p. 9).

[64]P. Brown, and A. Eusebio, "Paradoxes of functional neurosurgery: Clues from basal ganglia recordings", Movement Disorders **23**, 12–20 (2008) (cit. on pp. 9, 34).

[65]T. Tanaka, Y. Takano, S. Tanaka, N. Hironaka, K. Kobayashi, T. Hanakawa, K. Watanabe, and M. Honda, "Transcranial direct-current stimulation increases extracellular dopamine levels in the rat striatum", Frontiers in Systems Neuroscience **7** (2013) 10.3389/fnsys.2013.00006 (cit. on p. 10).

[66]H. Edemann-Callesen, B. Habelt, F. Wieske, M. Jackson, N. Khadka, D. Mattei, N. Bernhardt, A. Heinz, D. Liebetanz, M. Bikson, F. Padberg, R. Hadar, M. A. Nitsche, and C. Winter, "Non-invasive modulation reduces repetitive behavior in a rat model through the sensorimotor cortico-striatal circuit", Translational Psychiatry **8** (2018) 10.1038/s41398-017-0059-5 (cit. on pp. 10, 17, 27, 37, 38).

[67] A. Sharott, P. J. Magill, J. P. Bolam, and P. Brown, "Directional analysis of coherent oscillatory field potentials in the cerebral cortex and basal ganglia of the rat: Directional analysis of activity in cortico-basal ganglia circuits", The Journal of Physiology **562**, 951–963 (2005) (cit. on pp. 10, 33, 37).

[68] J. H. Siegle, A. C. López, Y. A. Patel, K. Abramov, S. Ohayon, and J. Voigts, "Open Ephys: an open-source, plugin-based platform for multichannel electrophysiology", Journal of Neural Engineering **14**, 045003 (2017) (cit. on p. 11).

[69] Intantech, *Downloads | Intan Technologies*, (2013) http://www.intantech.com/downloads.html (visited on 10/09/2018) (cit. on p. 12).

[70] O. Herreras, "Local Field Potentials: Myths and Misunderstandings", Frontiers in Neural Circuits **10** (2016) 10.3389/fncir.2016.00101 (cit. on p. 12).

[71] A. Berenyi, Z. Somogyvari, A. J. Nagy, L. Roux, J. D. Long, S. Fujisawa, E. Stark, A. Leonardo, T. D. Harris, and G. Buzsaki, "Large-scale, high-density (up to 512 channels) recording of local circuits in behaving animals", Journal of Neurophysiology **111**, 1132–1149 (2014) (cit. on p. 12).

[72] G. Agarwal, I. H. Stevenson, A. Berenyi, K. Mizuseki, G. Buzsaki, and F. T. Sommer, "Spatially Distributed Local Fields in the Hippocampus Encode Rat Position", Science **344**, 626–630 (2014) (cit. on p. 13).

[73] M. Voget, J. Rummel, Y. Avchalumov, R. Sohr, J. K. Haumesser, E. Rea, A. A. Mathé, R. Hadar, C. van Riesen, and C. Winter, "Altered local field potential activity and serotonergic neurotransmission are further characteristics of the Flinders sensitive line rat model of depression", Behavioural Brain Research **291**, 299–305 (2015) (cit. on pp. 15, 17).

[74] G. Paxinos, and C. Watson, *The Rat Brain in Stereotaxic Coordinates* (Academic Press, Oct. 24, 2013) (cit. on p. 16).

[75] G. Schuller, S. Radtke-Schuller, and M. Betz, "A stereotaxic method for small animals using experimentally determined reference profiles", Journal of Neuroscience Methods **18**, 339–350 (1986) (cit. on p. 16).

[76] M. Steriade, "Corticothalamic resonance, states of vigilance and mentation", Neuroscience **101**, 243–276 (2000) (cit. on p. 18).

[77] A. Sharott, F. Vinciati, K. C. Nakamura, and P. J. Magill, "A Population of Indirect Pathway Striatal Projection Neurons Is Selectively Entrained to Parkinsonian Beta Oscillations", The Journal of Neuroscience **37**, 9977–9998 (2017) (cit. on p. 18).

[78] M. H. Friedberg, S. M. Lee, and F. F. Ebner, "Modulation of Receptive Field Properties of Thalamic Somatosensory Neurons by the Depth of Anesthesia", Journal of Neurophysiology **81**, 2243–2252 (1999) (cit. on p. 18).

[79] J. Crook, and T. Lovick, "Urodynamic function during sleep-like brain states in urethane anesthetized rats", Neuroscience **313**, 73–82 (2016) (cit. on p. 18).

[80] S. Pagliardini, G. D. Funk, and C. T. Dickson, "Breathing and brain state: Urethane anesthesia as a model for natural sleep", Respiratory Physiology & Neurobiology **188**, 324–332 (2013) (cit. on p. 18).

[81] J. Kühn, J. K. Haumesser, M. H. Beck, J. Altschüler, A. A. Kühn, V. V. Nikulin, and C. van Riesen, "Differential effects of levodopa and apomorphine on neuronal population oscillations in the cortico-basal ganglia loop circuit in vivo in experimental parkinsonism", Experimental Neurology **298**, 122–133 (2017) (cit. on p. 18).

[82] S. Pagliardini, S. Gosgnach, and C. T. Dickson, "Spontaneous Sleep-Like Brain State Alternations and Breathing Characteristics in Urethane Anesthetized Mice", PLoS ONE **8**, edited by G. Foffani, e70411 (2013) (cit. on p. 18).

[83] A. Altmann, M. Schröter, V. Spoormaker, S. Kiem, D. Jordan, R. Ilg, E. Bullmore, M. Greicius, M. Czisch, and P. Sämann, "Validation of non-REM sleep stage decoding from resting state fMRI using linear support vector machines", NeuroImage **125**, 544–555 (2016) (cit. on p. 18).

[84] N. Mallet, A. Pogosyan, A. Sharott, J. Csicsvari, J. P. Bolam, P. Brown, and P. J. Magill, "Disrupted Dopamine Transmission and the Emergence of Exaggerated Beta Oscillations in Subthalamic Nucleus and Cerebral Cortex", Journal of Neuroscience **28**, 4795–4806 (2008) (cit. on p. 18).

[85] B. Schelter, M. Winterhalder, and J. Timmer, eds., *Handbook of time series analysis: recent theoretical developments and applications* (Wiley-VCH, Weinheim, 2006), 496 pp. (cit. on pp. 20, 22).

[86] A. B. Barrett, L. Barnett, and A. K. Seth, "Multivariate Granger causality and generalized variance", Physical Review E **81** (2010) 10.1103/PhysRevE.81.041907 (cit. on pp. 21, 22).

[87] A. Sengupta, "Generalized variance", Indian Statistical Institute, Applied Statistics University, Kolkata, India, ashis@isical.ac.in, 11 (cit. on p. 21).

[88] A. B. Barrett, M. Murphy, M.-A. Bruno, Q. Noirhomme, M. Boly, S. Laureys, and A. K. Seth, "Granger Causality Analysis of Steady-State Electroencephalographic Signals during Propofol-Induced Anaesthesia", PLoS ONE **7**, edited by P. A. Valdes-Sosa, e29072 (2012) (cit. on p. 22).

[89] A. K. Seth, A. B. Barrett, and L. Barnett, "Granger Causality Analysis in Neuroscience and Neuroimaging", Journal of Neuroscience **35**, 3293–3297 (2015) (cit. on p. 22).

[90] A. Brovelli, M. Ding, A. Ledberg, Y. Chen, R. Nakamura, and S. L. Bressler, "Beta oscillations in a large-scale sensorimotor cortical network: directional influences revealed by Granger causality", Proceedings of the National Academy of Sciences of the United States of America **101**, 9849–9854 (2004) (cit. on p. 22).

[91] G. Michalareas, J. Vezoli, S. van Pelt, J.-M. Schoffelen, H. Kennedy, and P. Fries, "Alpha-Beta and Gamma Rhythms Subserve Feedback and Feedforward Influences among Human Visual Cortical Areas", Neuron **89**, 384–397 (2016) (cit. on p. 22).

[92] K. Noguchi, Y. R. Gel, E. Brunner, and F. Konietschke, "nparLD: an R software package for the nonparametric analysis of longitudinal data in factorial experiments", Journal of Statistical Software **50** (2012) (cit. on p. 23).

[93] J. F. Donges, J. Heitzig, B. Beronov, M. Wiedermann, J. Runge, Q. Y. Feng, L. Tupikina, V. Stolbova, R. V. Donner, N. Marwan, H. A. Dijkstra, and J. Kurths, "Unified functional network and nonlinear time series analysis for complex systems science: The pyunicorn package", Chaos: An Interdisciplinary Journal of Nonlinear Science **25**, 113101 (2015) (cit. on p. 23).

[94]G. Deshpande, L. E. Libero, K. R. Sreenivasan, H. D. Deshpande, and R. K. Kana, "Identification of neural connectivity signatures of autism using machine learning", Frontiers in Human Neuroscience **7** (2013) 10.3389/fnhum.2013.00670 (cit. on p. 33).

[95]A. F. Alexander-Bloch, N. Gogtay, D. Meunier, R. Birn, L. Clasen, F. Lalonde, R. Lenroot, J. Giedd, and E. T. Bullmore, "Disrupted Modularity and Local Connectivity of Brain Functional Networks in Childhood-Onset Schizophrenia", Frontiers in Systems Neuroscience **4** (2010) 10.3389/fnsys.2010.00147 (cit. on p. 33).

[96]M. W. Cole, J. R. Reynolds, J. D. Power, G. Repovs, A. Anticevic, and T. S. Braver, "Multi-task connectivity reveals flexible hubs for adaptive task control", Nature Neuroscience **16**, 1348–1355 (2013) (cit. on p. 34).

[97]D. S. Bassett, and M. S. Gazzaniga, "Understanding complexity in the human brain", Trends in Cognitive Sciences **15**, 200–209 (2011) (cit. on p. 34).

[98]D. S. Bassett, N. F. Wymbs, M. A. Porter, P. J. Mucha, J. M. Carlson, and S. T. Grafton, "Dynamic reconfiguration of human brain networks during learning", Proceedings of the National Academy of Sciences **108**, 7641–7646 (2011) (cit. on p. 34).

[99]U. Braun, A. Schäfer, H. Walter, S. Erk, N. Romanczuk-Seiferth, L. Haddad, J. I. Schweiger, O. Grimm, A. Heinz, H. Tost, A. Meyer-Lindenberg, and D. S. Bassett, "Dynamic reconfiguration of frontal brain networks during executive cognition in humans", Proceedings of the National Academy of Sciences **112**, 11678–11683 (2015) (cit. on p. 34).

[100]B. M. Hampstead, G. S. Brown, and J. F. Hartley, "Transcranial Direct Current Stimulation Modulates Activation and Effective Connectivity During Spatial Navigation", Brain Stimulation **7**, 314–324 (2014) (cit. on p. 35).

[101]A. F. Sadikot, A. Parent, and C. François, "Efferent connections of the centromedian and parafascicular thalamic nuclei in the squirrel monkey: A PHA-L study of subcortical projections: CM-Pf EFFERENTS TO PRIMATE BASAL GANGLIA", Journal of Comparative Neurology **315**, 137–159 (1992) (cit. on p. 36).

[102]H. Steiner, and K.-Y. Tseng, eds., *Handbook of basal ganglia structure and function*, Second edition, Handbook of Behavioral Neuroscience volume 24, OCLC: ocn949750099 (Elsevier/Academic Press, Amsterdam ; Boston, 2017), 1012 pp. (cit. on p. 36).

[103]W. Song, and J. T. Francis, "Gating of tactile information through gamma band during passive arm movement in awake primates", Frontiers in Neural Circuits **9** (2015) 10.3389/fncir.2015.00064 (cit. on p. 37).

[104]M.-L. Welter, L. Mallet, J.-L. Houeto, C. Karachi, V. Czernecki, P. Cornu, S. Navarro, B. Pidoux, D. Dormont, E. Bardinet, J. Yelnik, P. Damier, and Y. Agid, "Internal Pallidal and Thalamic Stimulation in Patients With Tourette Syndrome", Archives of Neurology **65**, 952–957 (2008) (cit. on p. 37).

[105]C. H. Chen, R. Fremont, E. E. Arteaga-Bracho, and K. Khodakhah, "Short latency cerebellar modulation of the basal ganglia", Nature Neuroscience **17**, 1767–1775 (2014) (cit. on p. 37).

DECLARATION

I hereby declare that the work presented in this thesis has been conducted independently and without inappropriate support. All sources of information are referenced. I hereby declare that this thesis has not been submitted either in the same or a different form to this or any other university for a degree.

Berlin, december 2018

Cristian Alexandru Tătărău